Unidirectional Fibre Reinforced Thermoplastic Composites: A Forming Study

Alexander Fabian Schug

Vollständiger Abdruck der von der Fakultät für Maschinenwesen der Technischen Universität München zur Erlangung des akademischen Grades eines

Doktor-Ingenieurs

genehmigten Dissertation.

Vorsitzender: Prof. Dr.-Ing. Karsten Stahl

Prüfer der Dissertation:

1.   Prof. Dr.-Ing. Klaus Drechsler

2.   Prof. Dr.-Ing. Wolfram Volk

Die Dissertation wurde am 07.01.2019 bei der Technischen Universität München eingereicht und durch die Fakultät für Maschinenwesen am 02.12.2019 angenommen.

Technische Universität München
Fakultät für Maschinenwesen
Lehrstuhl für Carbon Composites
Boltzmannstraße 15
D-85748 Garching bei München

Tel.:   +49 (0) 89 / 289 – 15092
Fax.:   +49 (0) 89 / 289 – 15097
Email: info@lcc.mw.tum.de
Web: www.lcc.mw.tum.de

ACKNOWLEDGEMENTS

KURZFASSUNG

Das Thermoformen von faserverstärkten Thermoplasten bietet die Möglichkeit, Bauteile mit kurzen Zykluszeiten herzustellen. Das Leichtbaupotenzial kann insbesondere durch die Verwendung von unidirektional verstärkten Laminaten voll ausgeschöpft werden. Mit automatisierten Legetechnologien, wie dem Automated Tape Laying, können unidirektional verstärkte Tapes zu ebenen Gelegen verarbeitet werden. Diese lassen sich anschließend in die gewünschte Bauteilgeometrie umformen. Der Thermoformprozess unterliegt dabei vielen Einflussfaktoren, die die erreichbare Bauteilqualität maßgeblich beeinflussen. Diese Dissertation untersucht in mehreren experimentellen Studien die Auswirkungen verschiedener Prozessparameter. Dabei werden sowohl die Komplexität der Geometrien, als auch die verwendeten Materialien variiert. Die Bewertung der umgeformten Bauteile erfolgt anhand verschiedener Qualitätskriterien, um damit die geeignetste Parameterkonfiguration zu ermitteln. Weiterhin werden Optimierungsmöglichkeiten für den Thermoformprozess aufgezeigt. Neben den experimentellen Studien findet eine Betrachtung des Umformverhalten auch mit Hilfe einer Finite-Element-Simulation statt. Dafür wird vorab die Charakterisierung der Materialparameter beschrieben. Diese umfasst neben der Auswahl und Entwicklung geeigneter Charakterisierungsverfahren auch die Versuchsdurchführung und Auswertung. Mit den ermittelten Materialparametern werden Simulationsstudien basierend auf den Umformversuchen durchgeführt. Abschließend werden die Resultate mit den Ergebnissen der experimentellen Studien verglichen und die Möglichkeiten und Grenzen der verwendeten Simulationsmethodik aufgezeigt.

ABSTRACT

The thermoforming of fibre reinforced thermoplastics facilitates the manufacturing of parts within short cycle times. Especially by using unidirectional reinforced laminates the lightweight potential can be fully used. With automated placement technologies, such as the Automated Tape Laying, flat layups of unidirectional reinforced tapes can be produced. These can then be formed into the desired part geometry. Several input parameters influence the thermoforming process and affect the resulting part quality. Within the scope of this thesis the influences of different process parameters are determined in several experimental studies. In the course of this the complexity of the geometry as well as the used materials are varied. Based on different criteria, the quality of the formed parts is evaluated and the most suitable parameter configuration is determined. In addition to that, possibilities to improve the thermoforming process are revealed. Besides the experimental studies, the forming behaviour is analysed using finite element simulations. First, the material parameter characterisation procedure is described. It comprises the selection and development of suitable characterisation methods, the experimental characterisation and the evaluation of the results. With the derived input parameters simulation studies based on the forming experiments are performed. The results are then compared to the outcome of the experimental studies and the possibilities and limits of the used simulation method are presented.

Contents

Nomenclature

Symbol	Unit	Description
Latin letters		
a, b	-	Curve fitting coefficients
D	mm	Diameter of the loading bars on the fixture
d	mm	Initial gap between the compensation ply and the inner specimen
D_m	µm	Displacement at mid span
d_x	mm	Horizontal distance between two adjacent top and bottom loading bars
F	N	Force
F_n	N	Normal force
F_{peak}	N	Peak force
g	m/s^2	Gravitational acceleration constant
G_r	Pa	Shear relaxation modulus
G_∞	Pa	Constant curve fitting factor
L	mm	Free span length
l	mm	Length
l_1	mm	Length of the compensation ply
l_2	mm	Length of the inner specimen under the pressure plate
l_m	mm	Length of pressure plate
m	kg	Mass
M_{mid}	Nm	Torque at the middle of the specimen
P	N	Total force

Symbol	Unit	Description
t	mm	Thickness
u	mm	Displacement
w	mm	Width
Greek letters		
$\dot{\gamma}$	1/s	Shear strain rate
γ_{max}	%	Maximum shear strain
ε	-	Strain
κ_{mid}	1/mm	Curvature at the middle of the specimen
μ_{peak}	-	Peak coefficient of friction
σ	MPa	Stress
ϕ	°	Angle from horizontal of the specimen's legs

List of abbreviations

Abbreviation	Description
2D, 3D	Two-, three-dimensional
AFP	Automated fibre placement
ATL	Automated tape laying
CAD	Computer aided design
CATIA	Computer Aided Three-Dimensional Interactive Application
CBS	Curved beam strength
CF	Carbon fibre
CF/PA6	Carbon fibre reinforced polyamide 6
CF/PEEK	Carbon fibre reinforced polyether ether ketone
CF/PPS	Carbon fibre reinforced polyphenylene sulfide
CFM	Composite Fiber Modeler
CFRP	Carbon fibre reinforced plastics
CFRTP	Carbon fibre reinforced thermoplastic
CO_2	Carbon dioxide
CoF	Coefficient of friction
CPD	Composite design
DIN	German institute for standardisation
DKT	Discrete Kirchhoff Triangle
DMA	Dynamic Mechanical Analysis
EN	European Standard
FE	Finite element

Abbreviation	Description
FRP	Fibre reinforced plastics
FRTP	Fibre reinforced thermoplastics
FVF	Fibre volume fraction
GF	Glass fibre
GF/PP	Glass fibre reinforced polypropylene
IGCV	Fraunhofer Research Institution for Casting, Composite and Processing Technology
IR	Infrared
ISO	International organisation for standardisation
LCC	Chair of Carbon Composites
LTR3D	Three-node membrane element with linear shape functions
LVE	Linear viscoelastic
NCF	Non-crimped fabric
PA6	Polyamide 6
PEEK	Polyether ether ketone
PI	Polyimide
PO	Pull-out
PP	Polypropylene
PPS	Polyphenylene sulfide
Prepreg	Pre-impregnated reinforcement
PT	Pull-through
PTFE	Polytetrafluoroethylene
QI	Quasi-isotropic

Abbreviation	Description
RELAY	Rapid efficient layup
RT	Room temperature
RTM	Resin transfer moulding
TPRC	ThermoPlastic composites Research Center
TUM	Technical University of Munich
UD	Unidirectional
US	Ultrasonic
VAP	Vacuum assisted process
VARI	Vacuum assisted resin infusion
VVC	Void volume content

List of figures

List of tables

1 Introduction

Every year the German Federal Ministry for the Environment, Nature Conservation and Nuclear Safety issues a publication on the climate policy of the Federal Government of Germany. In recent years, the main goal was to reduce greenhouse gas emissions by 55% until 2030 in comparison with 1990 [1, 2]. In 2016 905 million tonnes of CO_2 equivalents were emitted in Germany, of which about 18% were produced by the transport sector, which even increased in 2017 (see Fig. 1-1). This is not only caused by the ongoing demand for larger and heavier cars but also by differences between CO_2 emissions on dynamometers and under realistic conditions. One important aspect with regard to achieving the greenhouse gas emission goals is the further dissemination of electric vehicles. [2]

Lienkamp [3] even believes that only with battery electric vehicles the climate goals can be realized. But also the weight reduction of conventional combustion engine cars is important to decrease CO_2 emissions within the next years [4, 5].
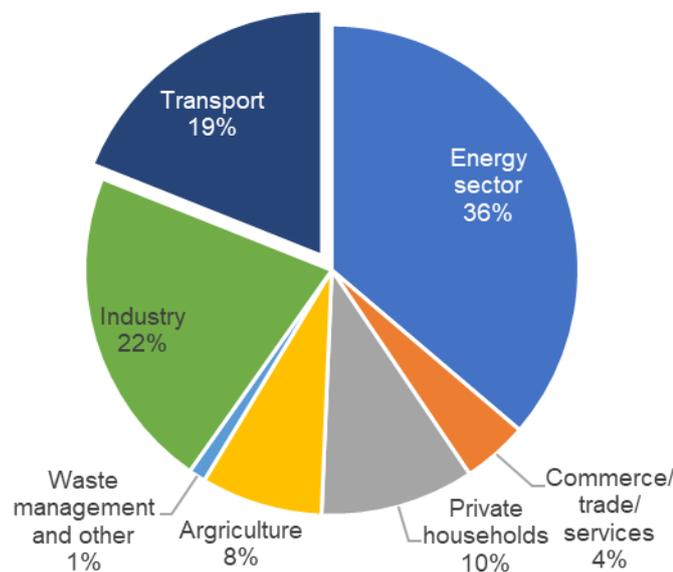
Fig. 1-1.   **Emission distribution by sector in Germany 2017 (numbers from [2])**

It is often stated that the weight of an electric car is less important as energy can be recuperated during deceleration [6], but a weight reduction always has a positive effect on the vehicle dynamics [7, 8] and decreases the desired battery capacity and engine power [5]. One possible solution to achieve weight reduction is the application of glass or carbon fibre reinforced plastics (CFRP). But for a wide application in the

automotive industry robust and fast production processes are necessary [9, 10]. Fibre reinforced thermoplastics (FRTP) offer the potential to achieve these goals. Their advantages over fibre reinforced thermosets include shorter cycle times through the omission of curing times, possibility for integrated processes such as injection moulding and better recyclability [11].

1.1 Motivation

In recent years, the application of carbon fibre reinforced thermoplastics (CFRTP) has increased [12, 13]. Advantages over thermosets imply weldability [14–16], recyclability potential [12, 17] and unlimited storage time. In addition, short cycle times are possible in combination with automated processing technologies [18, 19]. This increased interest in CFRTP especially by the automotive industry [20]. A promising production technology is the automated tape laying (ATL) of unidirectional (UD) tapes. With modern ATL processes like the Fiberforge RELAY2000 (see Fig. 1-2), tailored preforms of UD fibre reinforced thermoplastic tapes can be generated within minutes [21–23].

Fig. 1-2.   **Fiberforge RELAY2000**
                Automated tape laying machine at Fraunhofer IGCV

Applying this technology, scrap and costs can be reduced because the layup shape closely resembles the final shape of the part [21]. Furthermore, the lightweight potential can be utilised more efficiently, as the fibre directions can be chosen as mechanically needed. The Fiberforge RELAY2000 produces ultrasonic (US) spot-welded layups. These two-dimensional (2D) layups are dimensionally stable and easy to handle. But in order to remove the air between the plies and fuse the plies completely a subsequent consolidation step is necessary [24–26]. For the consolidation

the layups have to be heated over melting temperature and then fused and cooled under pressure. Different procedures are available for this process step [27]. In general, continuous, e.g. using a double belt press, and discontinuous, e.g. using a hydraulic heating press, consolidation processes can be distinguished. The consolidated layups can then be formed into the final three-dimensional (3D) shape, which can be realized within some minutes [28]. For that purpose, the material has to be heated above melting temperature again and then formed between two matched metal tools or with a diaphragm [24, 25], whereas the matched metal die forming has the highest potential for application in the industry [29].

As a result of the inextensibility of the reinforcing fibres, forming them into complex shapes is very challenging. Different forming effects could occur that have a negative influence on the mechanical performance of the part [30]: folds, fibre waviness, delaminations, gaps or fibre deviations. Various process parameters influence the final result in combination with the material properties. All these parameters have to be synchronized in order to achieve the best result. Because of this, it is necessary to thoroughly understand all forming mechanisms influencing the part quality and how the process parameters have to be chosen.

Reasons why thermoplastic composites have not yet experienced broader usage are its high material and manufacturing costs [31]. To cope with this challenge, the process routes have to be improved further, especially the energy-intensive process steps must be reconsidered. Another possibility to reduce costs during development and design is the usage of forming simulations. Especially with Finite Element (FE) simulations a detailed and realistic prediction of the forming result is possible, as it allows to include all constitutive equations, boundary conditions and relevant material models [32]. Various publications on the different simulation approaches can be found [33–39]. A benchmark of several FE codes is presented in [40]. But the quality of the simulation results mostly depends on the precision of the material parameters [35, 41]. With that said utmost accuracy during the material characterisation is necessary. As a drawback it has to be stated that no standardised characterisation methods are available for thermoplastic composites so far [32].

1.2 Definition of tasks

Based on the described motivation, the following tasks were defined for this doctoral dissertation:

- To study the forming behaviour of unidirectional reinforced thermoplastics by using different forming tools with increasing geometry complexity.
- To develop and design respective forming tools that cause characteristic forming effects of the thermoplastic materials.

- To identify the influence of different process parameters on the various forming effects and the achievable party quality by structured experimental studies using different materials.
- To improve the thermoforming process and develop new process options to reduce the cycle time and enhance the party quality.
- To develop and apply new characterisation methods for forming simulations that cope with the specific properties of the used materials and are suitable to measure the desired material data for the material models.
- To reveal the performance of forming simulations and improve the results by proper material data fitting and validation.

1.3 Structure of the thesis

Chapter 1 introduces the topic, highlights the motivation and reveals the tasks of the dissertation.

Chapter 2 provides an overview over the current state of the art for the discussed topics. Besides the description of the thermoforming processes and their former developments, also the predominant deformation mechanisms and existing characterisation methods are addressed. Finally, the field of forming simulations of fibre reinforced plastics is presented and the used software tool described.

Chapter 3 contains the conducted experimental forming studies. Two detailed studies are described using different tools and material to gain a thorough understanding of the forming process. Additionally, concepts for the forming of unconsolidated layups are presented.

Chapter 4 covers the corresponding numerical studies. The developed and applied characterisation test is described. Also the used forming simulation software and material models are outlined. Finally, the validation of the simulation is presented. It is based on the experimental investigations and evaluates the quality of the simulation results.

Chapter 5 summarizes the content of the thesis and evaluates the results.

Chapter 6 provides an outlook on potential future studies based on the lessons learned by this doctoral dissertation.

2 State of the art

A composite is a material that consists of two or more base materials, which possess different properties. By combining the materials superior properties can be achieved compared with those of single components [21, 24]. Well-known examples for composite materials are wood or concrete. Special types of composites are fibre reinforced plastics (FRP). They combine the low density of plastic with high mechanical properties of reinforcing fibres. Typical fibre materials used in FRP are glass, carbon, aramid or natural fibres like hemp or flax [27]. Besides the type of the fibre, also its length within the composite influences its mechanical properties. They can be divided into short fibres (<1 mm), long fibres (1 mm – 50 mm) and continuous fibres [21]. Continuous in this context means that the fibres do not end within a part, but extend from one edge to the other. Within these compounds the fibre is responsible for stiffness and strength of the composite and the plastic keeps the fibres in place, protects them against environmental influences and absorbs compressive loads [42].

The plastic matrix materials can be divided into thermosets, thermoplastics and elastomers [43]. Of these three the elastomers are of least importance for technical applications, due to their low stiffness. The only weakly cross-linked elastomers provide little support of the fibres under compressive loads.

In contrast, thermoset plastics are the oldest used matrix systems and used for all kind of applications. The highly spatial cross-linked polymers provide high stiffness and strength. Because of the low viscosity of the resin the fibres can be easily impregnated with it [44]. Due to the chemical cross-linking cured thermosets cannot be melted again. Different manufacturing processes were developed over the years. There are manual processes like hand layup, vacuum assisted resin infusion (VARI) or vacuum assisted process (VAP). Common for these processes is that the dry fibres are draped into the final 3D geometry, then impregnated with the resin and finally cured under temperature and pressure. A special process is the resin transfer moulding (RTM), where the resin is infused under high pressure, enabling shorter cycle times and higher fibre volume fractions (FVF). Besides that, also pre-impregnated semi-finished products, so called prepregs, were developed. Here, the fibre impregnation process is automated. Major advantage is the high and constant impregnation quality. These prepregs can be processed manually or with automated processing processes like automated tape laying (ATL) or automated fibre placement (AFP). But as the thermoset prepregs are highly reactive they have to be stored deep-freezed at -18 °C until processing.

Thermoplastic polymers consist of macromolecules that are not spatially cross-linked. The molecules are either linear or branched [44]. As the thermoplastics are not

chemically bound, they can be molten. Between the molecular chains only intermolecular forces exist, which cause cohesion and prevent slipping of the chains under external load. Under thermal load the forces are reduced and the polymer starts to soften. The thermoplastics can be divided into amorphous and semi-crystalline. Within amorphous thermoplastics the orientation of the polymer chains is completely random, causing a high impact strength and transparency. In certain areas of semi-crystalline thermoplastics, oriented polymer chains are present. Through a higher crystallinity, Young's modulus, hardness, tensile strength and melting temperature of a polymer are increased. [44]

As the viscosity of molten thermoplastics is distinctly higher than that of uncured thermoset resins, the impregnation of fibres is more difficult [45]. Also the need of high temperatures complicates the impregnation process. Hence mostly pre-impregnated semi-finished products are used. The easy storage of thermoplastics at room temperature without any special provisions and endless shelf life facilitates this. The thermoplastic pre-impregnated reinforcements (prepregs) are available as UD tapes with widths up to 500 mm and thicknesses between 0.125 mm and 0.250 mm [46]. These UD tapes can be automatically processed to flat sheets for subsequent forming using technologies like ATL or AFP. Using the AFP process, tapes can also be placed directly into a complex 3D geometry. In addition, there are impregnated weaves, so called organosheets, which can be thermoformed as well. Through the fusibility of the thermoplastic matrix other process steps such as welding or injection moulding are possible [47].

In the subsequent chapters the current state of the art regarding the thermoforming process, material characterisation and forming simulation is presented.

2.1 Thermoforming

Thermoforming describes the shaping process of an initial flat laminate into a 3D geometry under the influence of temperature. It can be applied to fibre reinforced materials with either thermoplastic of thermoset matrix system. This chapter describes the thermoforming process state of the art in research and application in the industry.

2.1.1 General process description

Thermoforming of endless FRTP is a highly automatable production process that is suitable for mass production of 3D parts because of the possible short cycle times. Pre-consolidated flat sheets are heated above the melting temperature of the respective matrix system. For that purpose, an infrared (IR), paternoster or convection oven can be used [48]. Following that the softened laminate is transferred to the forming tool. The transfer time has to be kept short to avoid extensive cooling of the material and associated reduction of the formability. For handling the laminate a support frame is used that also applies tension to the material during the forming step. The application

of tension could reduce the formation of wrinkles or other forming defects [49]. Instead of a support frame also a blankholder can be used. As forming tools either two matched metal tools or a metal tool in combination with a flexible one can be used. Two matched metal tools provide the best surface quality and the longest durability but are also expensive and have to be adapted exactly to the laminate layup. A flexible tool on the other hand is cheaper to manufacture and can match different layups and thicknesses [48, 50–52]. Directly after positioning the pre-heated laminate, the tool is closed to avoid further cooling. The tools themselves are heated to a distinct temperature depending on the polymer in order to achieve fast cooling and generate the desired crystallinity. A high pressure is applied (10–40 bar [53]) as soon as the tools are fully closed to ensure full consolidation of the plies. After some cooling time, the part can be removed of the tool. Typically, it is recommended to reach a temperature below the glass transition temperature [54, 55]. A schematic representation of the thermoforming process is shown in Fig. 2-1.
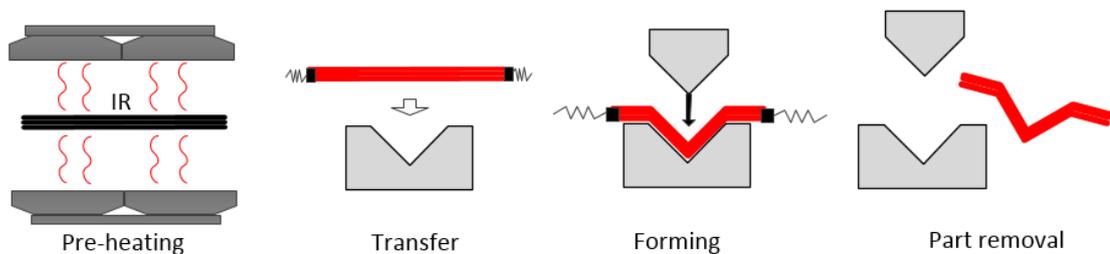
Fig. 2-1. **Thermoforming process scheme**

2.1.2 Influencing parameters

The forming process is a highly sophisticated, non-isothermal, dynamic procedure. Various parameters might have an influence on the forming results and have to be selected thoroughly to receive the optimal result. Fig. 2-2 shows a compilation of possible influencing parameters.
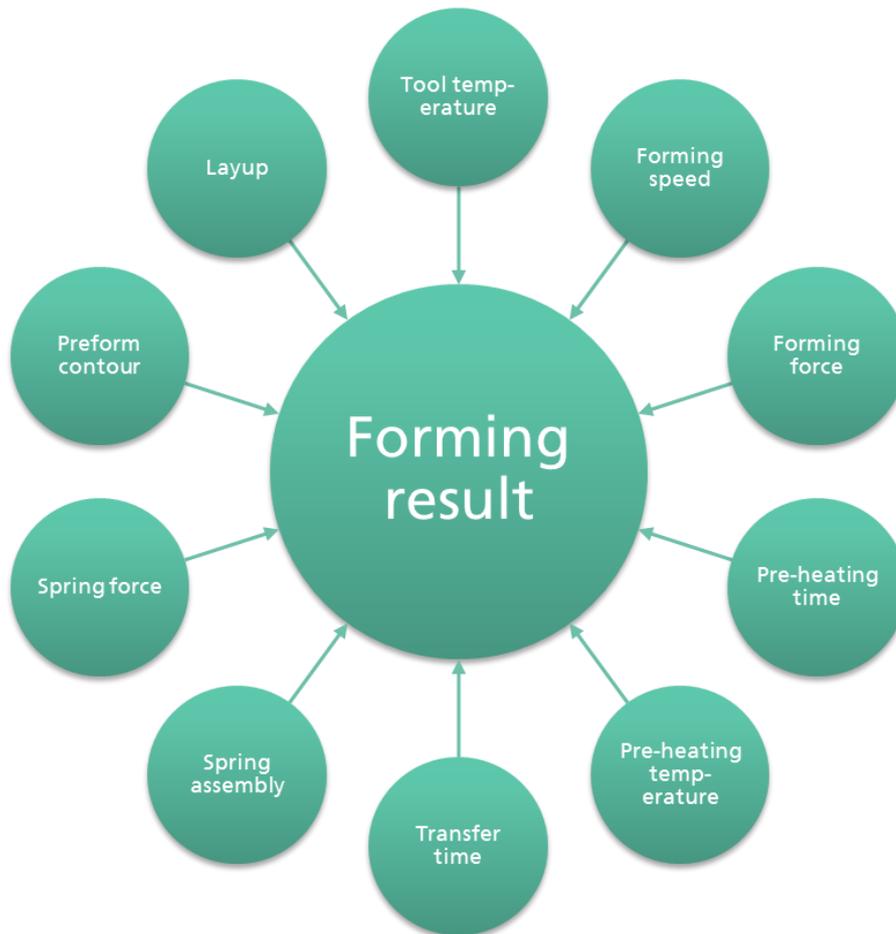
Fig. 2-2.   **Influencing parameters on the forming result**

The tool temperature especially influences the cooling time and the stiffening behaviour of the material. It should be high enough to avoid early solidifying of the matrix, enable short cycle times and generate the desired crystallinity. The forming speed, meaning the speed of mould closing, is closely related. A high forming speed could also avoid solidifying before full closure, but as some polymer melts are shear-thickening, a too high speed could reduce the formability. The forming force affects the resulting surface quality and the consolidation of the plies. A high pressure is needed for full consolidation, but too high pressure could cause matrix flow, dry spots and fibre deviations. The pre-heating time and temperature define the formability of the material. The temperature should be as high as possible to reduce the viscosity and improve the formability, whereas too high temperature could cause matrix degradation. The pre-heating time should be long enough to ensure an even temperature distribution through the thickness, but too much time above the melting temperature should be avoided. The transfer time must be kept as short as possible to avoid early cooling. When using a support frame, the spring forces and assembly affect the forming behaviour and especially the emergence of wrinkles and folds. Additionally, the number and force of the springs determine the sagging of the laminate during heating and transfer. If the sag was too large, an early contact between laminate and lower

mould could arise and the material would cool prior to forming. Hence the number, force and assembly of the springs have to be selected suitably to geometry, material and layup. The preform contour also influences the final forming results. Depending on whether a rectangular contour or one close to the tool geometry is used, differences could arise. Also cuts in the material outside of the geometry could avoid folds and improve the part quality. The best configuration has to be determined separately for each geometry and layup. The layup itself also affects the forming behaviour. As the fibre orientations depend on the desired mechanical performance, it cannot be chosen with respect to the best forming result. But with additional fibre directions the formability is worsening. Hence, further effort might be necessary for a good part quality.

2.1.3 Possible forming defects

When forming a flat UD fibre reinforced thermoplastic laminate, various forming effects could occur that reduce the optical or mechanical part quality and could therefore be classified as defects. The occurrence of forming defects is strongly dependent on the different influencing parameters that have been described before. Typical defects are described hereinafter. Regarding the mechanical performance straight fibres are always required. Fibre deflections during forming, that could occur on different scales, are often found [56]. On the smallest scale in-plane fibre waviness or undulations are possible. Larger fibre deflections could cause out-of-plane wrinkles of single plies or even larger folds of the whole laminate. The formation of wrinkles or folds could also implicate the emergence of delaminations between the plies. For visible parts an even and smooth surface should be achieved. Surface gaps or rough areas could disturb the appearance. Gaps develop trough transverse sliding of the fibres mostly caused by friction between the mould surface and the ply. Missing contact between mould and laminate at the end of the forming process could cause rough areas on the surface. This occurs primarily due to thickness changes during forming that are not reflected in the mould design. Despite the described effects also high fibre tensions could cause defects such as dry spots, radius thinning or even fibre breakage. A high fibre tension might be provoked by too high pre-tensioning forces or clamping of the fibres on the edge area of the geometry because of inaccurate cavity design. An overview of the described effects is shown in Fig. 2-3.
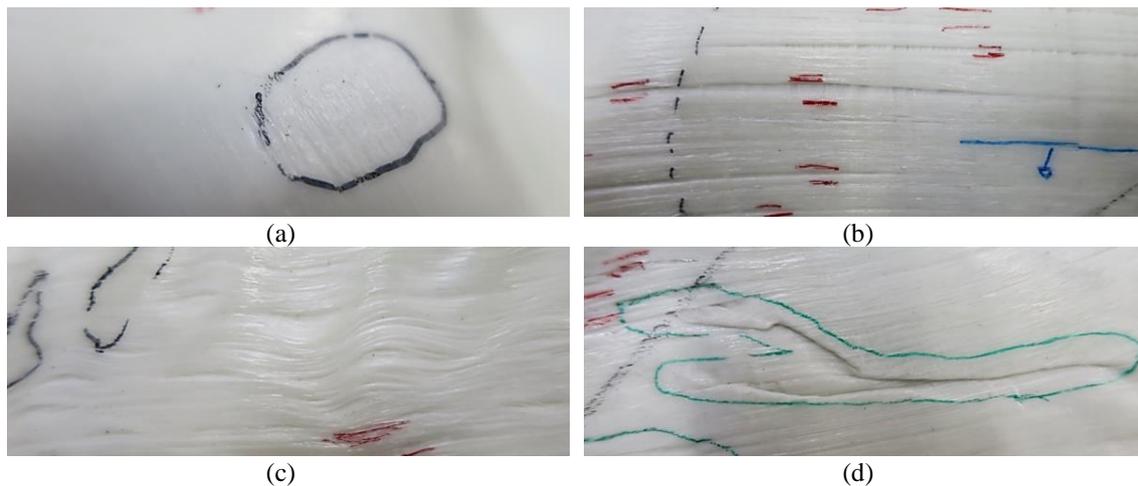
Fig. 2-3.   **Typical forming effects**
              (a) surface roughness, (b) gaps, (c) in-plane undulations, (d) wrinkles

2.1.4   Research and application

Several studies on the influence of the described forming parameters have been conducted. Selected results are described hereinafter. Hou [28] determined useful processing conditions for the forming of glass fibre (GF) reinforced polypropylene (PP). He used a hemispherical mould in combination with a hold-down arrangement for the forming studies. The focus of the study was on stamping temperature, stamping velocity and hold-down pressure. He declared that a suitable temperature range for forming is above the melting temperature. Furthermore, it was stated that the emergence of wrinkles in ±45° direction to the fibres was dependent on the initial area of the flat laminate and the hold-down pressure. Joppich et al. [57] studied the emergence of wrinkles depending on the layup and process. They used matched steel moulds with complex geometry for experimental forming experiments in an industrial environment. Different layups of UD carbon fibre (CF) reinforced polyphenylene sulphide (PPS) were formed with varying mould temperature and closing speeds. During the whole process the temperature within the laminate was recorded. They showed that at every point of the laminate the temperature during forming was above the recrystallization temperature for the studied process parameters. The wrinkle formation was measured using a laser scanner. It was revealed that the number of wrinkles depends on the layup, with a multiaxial layup producing most. Lessard et al. [58] determined the influence of process parameters on the thermoforming of CF reinforced polyether ether ketone (PEEK). Pre-heating temperature, mould temperature, transfer time and stamping force were studied. The formed parts were evaluated regarding thickness and interlaminar shear properties. It was found that there is a correlation between part thickness and shear strength. A lower thickness corresponded to a higher shear strength. The mould temperature and stamping force had the most significant influence on the part thickness. Han et al. [59] studied the

radius forming of CF/PPS weave. They evaluated the spring-in deformation depending on the mould temperature. Best results were achieved using a mould temperature of 170 °C, whereas higher temperatures caused larger spring-in deformations.

Despite the ongoing research there are already application examples for the thermoforming of CFRTP in the industry. The Premium Aerotec GmbH produces thermoplastic clips for different parts of the Airbus A350. These are formed of pre-consolidated CF/PPS and CF/PEEK organosheets. In that way, more than 3,000 clips are manufactured for every A350 [60].

2.2 Material characterisation

The material characterisation for FE forming simulations has been a core research area for the last years. It is crucial to determine the material deformation behaviour to ensure proper simulation behaviour. The characterisation test type strongly depends on the modelling approach, available material models and used material. E.g. for the characterisation of dry materials such as weaves or non-crimp fabrics (NCF) there is no temperature or deformation rate dependency expected, which reduces the complexity of the tests. A thermoset or thermoplastic matrix in contrast complicates the characterisation process as the properties become temperature and rate dependent. Especially the high melting temperatures of high-performance thermoplastics increase the characterisation complexity. In the following chapters the state of the art in material characterisation of UD FRTP is described.

2.2.1 Forming mechanisms

Different forming mechanisms enable the forming of UD laminates. They can be divided into interface mechanisms and intra-ply mechanisms, as also described in [41, 61, 62]. An overview is given in Fig. 2-4.
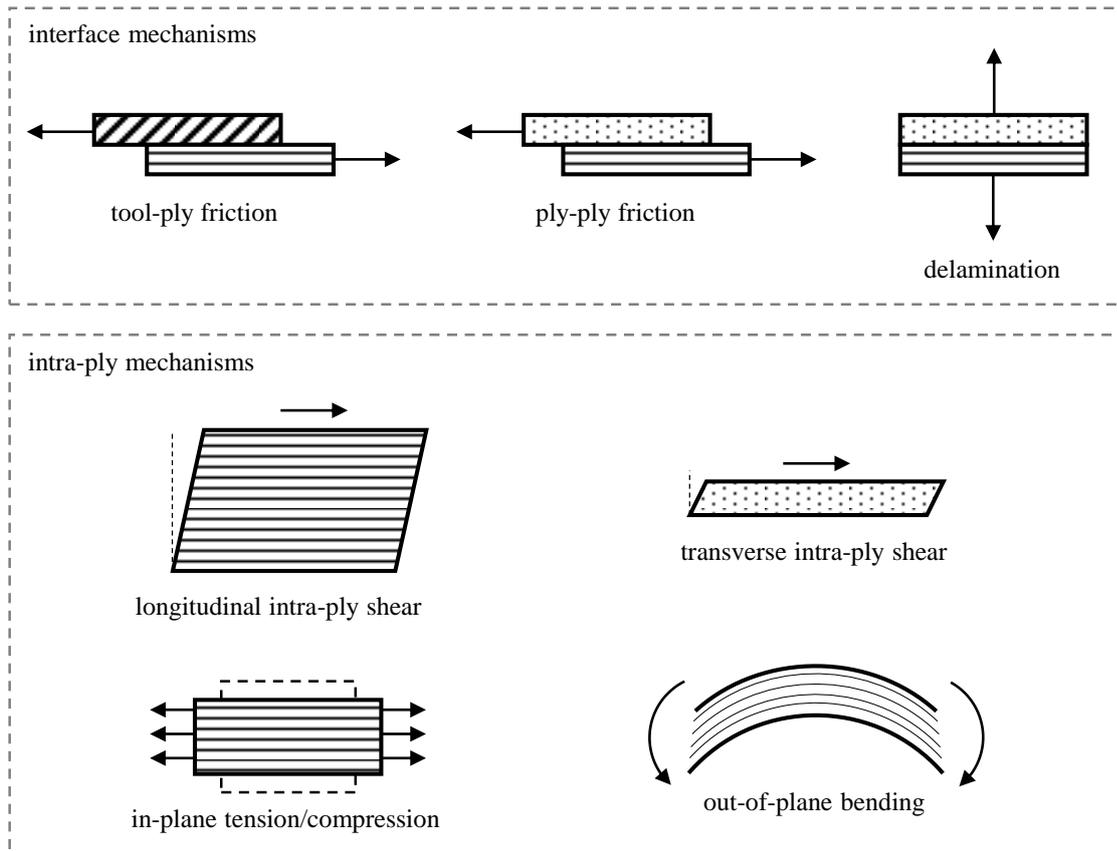
Fig. 2-4.   **Typical forming mechanisms for UD FRP (adapted from [41, 61])**

Within the interface properties there is the friction between the outer plies and the tools' surface as well as the friction between adjacent plies. These two occur when the surfaces in contact slide against each other during the forming process. The third interface mechanism is the delamination or adhesion between plies. A delamination is the result of the separation of plies due to tensions in thickness direction. The tackiness of the plies works against this effect.

The longitudinal and transverse intra-ply shears belong to the inter-ply mechanisms. They describe the parallel or transverse sliding of the fibre within one ply [41]. The intra-ply shear is supposed to be the main forming mechanisms for the forming of double curved geometries [61], whereas the longitudinal intra-ply shear is more important for the forming result [63]. The shear properties are strongly related to the viscosity of the matrix material.

The in-plane tension and compression can act along the fibre direction or perpendicular to it, referred to as longitudinal or transverse direction, respectively. Due to the high stiffness of the reinforcing fibres tensions in longitudinal direction will cause nearly no elongation. But compression in fibre direction could create fibre buckling. In transverse direction, in contrast, tension as well as compression lead to deformations of the material. Even small strains in transverse directions could cause a failure and the emergence of gaps [64].

The out-of-plane bending mechanism occurs manly during forming of complex

geometries. It enables the material to adopt to single or double curved surfaces [61]. In contrast to homogenous materials such as metals, the bending properties of FRP cannot be derived from the in-plane properties [65]. Therefore, they have to be determined in separate characterisation tests.

The state of the art in characterisation tests of the most relevant forming mechanisms is described in the following chapters.

2.2.2 Friction characterisation

The friction characterisation of FRTP has been widely studied by several authors. The presence of molten matrix material causes a mixture of dry friction and hydrodynamic friction. During the characterisation it is difficult to ensure steady boundary conditions, as the result is severely influenced by temperature, forming speed and normal pressure [66]. For that reason, different approaches were developed, which can be divided into the following categories:

- *Rotational setup*
  For this setup circular specimens are mounted between two flat steel plates within a rheometer. The device then applies a rotational movement while the occurring torque is measured. Normal pressure and temperature can be regulated accordingly. Due to different relative velocities over the radius, conclusions about the velocity dependency are difficult to obtain. Experiments with such setups were described by Groves [67] and Harrison et al. [68].

- *Horizontal pull-through/pull-out setup with normal weight*
  With the pull-through (PT) or pull-out (PO) setup a middle ply is pulled through or out of two outer plies, respectively. The difference is that for the PO setup the contact area decreases during testing, whereas pressure conditions change. Using a horizontal setup, the normal force can be adapted easily by weights. The motion can be applied either by additional actuators or by means of universal testing machine. Elevated temperatures can be achieved by heated platens or an environmental chamber. Correlating experiments were performed by Murtagh et al. [69] and Gorczyca-Cole et al. [70].

- *Vertical pull-through/pull-out setup with additional pressure application*
  The working principle of the vertical PT/PO setup is similar to the horizontal one. The difference is that the specimens are oriented vertically, which allows a direct mounting to a universal testing machine. Normal force has to be applied by actuators or other devices. Morris and Sun [71], Lebrun et al. [72] and Akkerman et al. [66] designed test stands based on the vertical PT/PO setup.

- *Sledge setup*

  In the sledge setup one specimen is mounted on the bottom of a moveable sledge and another specimen on top of a baseplate. The sledge is pulled over the baseplate and the normal weight can be adapted. The pulling is done by either a universal testing machine or other actuators. The setup is similar to the one described in the norm DIN 14882 [73]. Margossian [62] developed such a test stand and performed several friction measurements.

An extensive friction benchmark study with different setups was carried out by Sachs et al. [74] for a GF/PP fabric. The authors state that an increase of test velocity and a decrease of pressure and temperature cause an increasing friction coefficient. As the resulting friction coefficients are very sensitive to changes of pressure or fluid film thickness, it must be ensured that during experiments no misalignments occur and that test faces stay parallel with a uniform pressure distribution [66, 75].

2.2.3 Bending characterisation

Several studies on the out-of-plane bending characterisation of FRP have been performed. An overview is presented in Tab. 2-1. Numerous studies focused on the testing of dry materials such as NCF or fabrics. The standard test for these materials is the cantilever test. In this test a horizontally oriented ply is pushed over a declined inclined plane until the tip touches it. With the length of the specimen the bending stiffness can be calculated. These tests are normally performed at room temperature (RT) and the deformation rate cannot be varied. There were some variants of this test with additional weights [76], with the test setup positioned in a thermal chamber [77] or even with a vertical orientation of the specimen [78, 79]. But for a complete characterisation of FRTP, material bending experiments at elevated temperatures with varying deformation rates must be performed. Martin et al. [80] developed a Vee-bending test in a thermal chamber. But the test cannot be used for the characterisation of out-of-plane bending properties, as the main deformation mode is shear [62]. In collaboration with the ThermoPlastic composites Research Center (TPRC), the University of Twente, Enschede, developed a bending setup mounted to a rheometer [75, 81]. By using a rheometer, the temperature and deformation rate can be controlled exactly. A single ply is placed in the fixtures and deformed under pure bending. During the experiment the specimen can move unrestrictedly in the fixtures. The same setup was used by Ropers et al. [82] for characterisation tests. Margossian et al. [83] presented a different approach for the bending characterisation of UD FRTP in the molten state using a dynamic mechanical analysis (DMA) system. The goal was to be able to perform the characterisation tests with closely controlled testing parameters without the need of any custom-made setups or fixtures. In this approach the three-point bending fixtures of the DMA fixtures are used for the out-of-plane bending characterisation. The tests were performed quasistatic under isothermal conditions.

Tab. 2-1.   **Out-of-plane bending characterisation tests**

Ref.	Method	Testing temperature	Rate control
Peirce [84]	Cantilever test	RT	No
Bilbao et al. [76]	Modified cantilever test	RT	No
Soteropoulos et al. [78]	Vertical cantilever test	RT	No
Liang et al. [77]	Cantilever test + thermal chamber	RT-600 °C	No
Dangora et al. [79]	Vertical cantilever test + radiant heater	RT-120 °C	No
Lomov et al. [85]	Kawabata test	RT	Yes
Martin et al. [80]	Vee bending test + thermal chamber	RT-170 °C	Yes
Wang et al. [86]	Buckling test	RT-150 °C	Yes
Sachs [75]	Rheometer	RT-450 °C	Yes
Margossian et al. [83]	DMA	RT-600 °C	Yes
Ropers et al. [82]	Rheometer and DMA	RT-260 °C	Yes
Alshahrani and Hojjati [87, 88]	Vertical cantilever test + infrared heater	RT-600 °C	Yes

2.2.4   Intra-ply shear characterisation

An overview over the existing methods for longitudinal shear characterisation was compiled by Haanappel et al. [63] and more recently extended by Margossian [62]. For the shear characterisation of fabric, dry or impregnated, the so-called picture-frame and bias-extension tests are state of the art [89].

For the picture-frame test a cross-shaped specimen is clamped in four rigid bars that are connected by hinges. The two hinges on the side can move freely, whereas the bottom hinge is fixed, and the top hinge is moved by a universal testing machine to apply the deformation. The previous quadratic fixture deforms during the test to a rhombus. Researchers also used the picture-frame for the shear characterisation of UD materials [32, 62, 63, 90]. Due to presence of reinforcements in only one direction, the UD specimens were only clamped on two sides. During the shear experiments several problems occurred. Already small misalignments of the fibres caused high tensions, ply splitting and even fibre breakage. As the fibres were not free to rotate at the clamping, they needed to bend, which also evoked tensions. Hence, the measured force may not be the pure shear force [32]. Additionally, already at small shear angles (about 10°) out-of-plane wrinkles occurred. These experiments showed that the picture-frame test is not suitable for the shear characterisation of UD material.

The bias-extension test is an off-axis tensile test with the fibres of the rectangular specimen oriented in ±45° to the pulling direction. A shear deformation occurs as a result of the elongation. Different sheared areas then occur: non-sheared regions close

to the clamping, half sheared regions and a fully sheared region in the centre [32, 91]. Potter [92] applied the bias-extension test to UD prepregs by using cross-plied laminates. The results revealed that wrinkles occurred already at small displacements. Similar tests were performed by Larberg et al. [93]. They showed that the test method was suitable to study the deformability of different materials. But they also observed the emergence of wrinkles or material split up during testing. Haanappel and Akkerman [63] tried to apply the test method to UD FRTP, but they observed uncontrolled specimen deformations with localised strains and fibre buckling. It can be stated that the bias-extension test is not suitable for the intra-ply shear characterisation of UD FRTP materials.

Haanappel and Akkerman [63] then presented a new approach for the characterisation of longitudinal intra-ply shear behaviour of UD FRTP, the so-called torsion bar test. A cuboid shaped specimen with a close to quadratic base is mounted to a standard rheometer. The specimen has a UD layup and the fibres are orientated along the long edge. The specimen is then twisted dynamically at elevated temperatures. Fig. 2-5 shows an illustration of the torsion bar test setup.
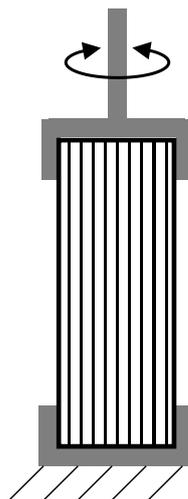
Fig. 2-5.   **Schematic illustration of the torsion bar setup**

Recently Margossian [62] successfully applied the test method. The advantages of this test method are that the testing environment can be controlled exactly, and no special fixtures or devices are needed.

2.3 Forming simulation

Forming simulations play an important role within the design and development process of thermoformed parts. The prediction of the exact geometry, shape and fibre directions is not straightforward for parts with complex geometries. Especially for the calculation of mechanical properties the knowledge of exact fibre orientations is

crucial. Time-consuming trial and error forming experiments must be avoided to keep the development costs low. [61]

As Leutz [32] stated, the forming simulation can be used for three purposes: part design, process development and optimisation and as part of the whole simulation process chain.

During the part design the forming simulation can be used to verify the applicability of the forming process for the favoured geometry. Besides that, the best laminate shape and necessary cuts can be determined to avoid possible forming defects. The final predicted fibre orientations can then be used for a structural analysis.

Within the process development the forming simulation can contribute to optimising several process parameters such as the forming speed or support frame configuration. Also, the perfect sequence of forming steps of a multi-stage forming process can be determined.

The forming simulation can also be used as part of a simulation process chain. As already mentioned above, the results can be used for a structural analysis. Despite that, the predicted fibre orientations, shear angles or thicknesses could contribute to an infiltration simulation in the case of forming dry materials.

Within the scope of this work, it shall be examined whether the forming simulation is capable of predicting occurring forming effects and fibre orientations correctly. For that purpose, simulation models corresponding to performed experimental forming studies are created and the results are compared.

The forming simulation approaches can be divided into two groups: kinematic forming simulations and FE forming simulations. These two types are further described in the following chapters.

2.3.1   Kinematic forming simulation

The earliest works regarding the formability of fabrics date back to Mack and Taylor [94]. The authors developed an approach named pin-joint method for the forming of fabrics on the tool geometries. It is also known as geometric draping, mapping method or fish-net algorithm [61]. The principle is that a mesh of quadratic elements is draped over a geometry. The adaption to the surface results only of shear deformations of the elements. Besides that the method is based on the following assumptions [32, 61, 89]:

- inextensible fibres
- no sliding between fabric and tool
- no bending
- no shear stiffness
- no thickness
- fibres are pinned together at their crossings
- warp and weft yarns are free to rotate at their crossings
- only shear deformation

In general the mapping starts with one initial point and two initial fibre directions [95]. Along these directions the next points within a certain distance are calculated. The approaches do not consider any material properties or process parameters. Thus, the result of the simulation is always the same regardless of the used material and how the forming process is performed. Influences of support frame configurations or blank holders are neglected. In addition to that, no specific defect prediction is possible.
Only by evaluating the predicted shear angles, conclusions can be drawn about critical areas. The exceeding of a previous experimentally determined locking angle, for example, could indicate the emergence of wrinkles or folds in the respective areas [62, 96]. Despite the shear angles, fibre orientations and the pre-cut geometry of the plies are results of a kinematic forming simulation. The fibre orientations are indicated by the edges of the simulation mesh. The prediction of pre-cut geometries could help to reduce material waste during the production phase.
Apart from the described limitations of kinematic forming simulations, there are also some advantages. They provide the possibility to generate simulation results quickly and accelerate the development process. Also, the available software is easy to use and no complex material characterisation experiments are necessary [49]. Finally, the approach requires only little computational effort, whereas no expensive workstations are required.

Several commercial software packages are available that are based on the kinematic forming approach: Catia CPD/CFM of Dassault Systèmes Simulia, Fibersim of Siemens, PAM-QuikForm of ESI Group or Laminate Modeler of MSC.Pastran.

Due to the mentioned properties of the kinematic forming simulations, these are most qualified for the simulation of hand layup processes of single-ply weaves over convex geometries. Also, they can be used for a fast first estimation of the forming result. For the simulation of impregnated fabrics or unidirectional materials and for the prediction of specific defects FE forming simulations are better suited. [32, 62, 89, 96]

2.3.2   Finite Element forming simulation

For a detailed analysis of the forming process of UD FRTP the simulation model must include all mechanical equations, load equilibriums and boundary conditions. A FE forming simulation can solve these equations with some approximations. Here, the tool geometry, the contact and friction behaviour between tool and ply or ply and ply and the mechanical properties of the laminate are considered. [89, 97]
During the forming of textiles high strains could occur. Thus, standard FE models that are mostly only suitable for small and moderate strains cannot be used [98]. The available FE approaches can be divided into three categories depending on the level of detail of the modelling: macroscopic approach, mesoscopic approach and microscopic approach (see Fig. 2-6). The different approaches are further described in the following chapters.

(a)   (b)   (c)
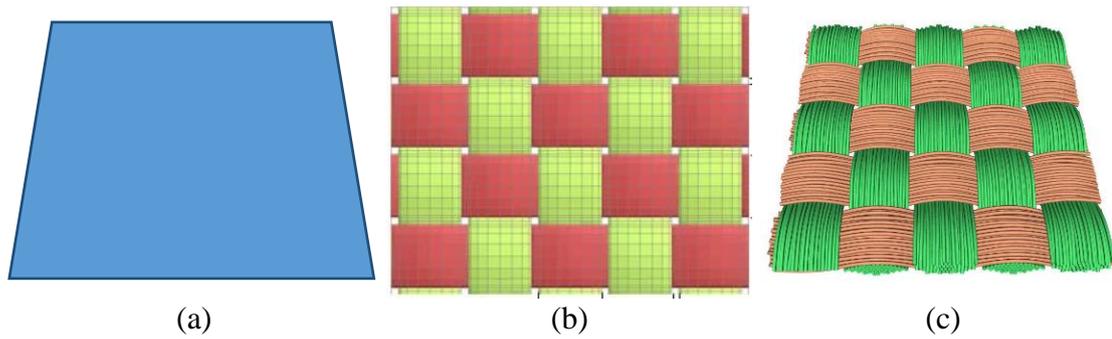
Fig. 2-6.   **Levels of FE simulation approaches**
         (a) Macroscopic approach, (b) mesoscopic approach [99], (c) microscopic approach [100]

2.3.2.1 Macroscopic FE approach

In macroscopic FE approaches the material is modelled on ply level. Yarns or single fibres are not reproduced. One single ply or several plies are modelled as a layer of shell elements. Due to the modelling approach, deformations on yarn level, e.g. yarn slippage or inter-yarn movements, cannot be predicted. Only deformations on a macroscopic level and on the interface between the plies can be modelled: intra-ply shear, ply bending, in-plane tension/compression, friction and delamination. [62]

The advantage of the macroscopic approach is that no FE codes with special elements are necessary. Standard shell or membrane elements are sufficient. For an exact description of the mechanical behaviour of the laminates mechanical models that consider all relevant aspects are necessary. As the bending stiffness of the textiles is much lower than the in-plane stiffness, the standard plate theory cannot be applied. The bending properties must be decoupled from the in-plane properties to model reasonable bending behaviour. [89]

Different material models for forming simulations on the macroscopic level have been developed in the recent years and are presented in the literature:

Boisse et al. [89, 101] proposed two different models. The first model is a hyperelastic model for textile composite forming at large strains [102]. The constitutive models are derived from the potential energy. The second model is a hypoelastic formulation for large strain analysis [103]. It was established for a single-fibre direction and extended to two-fibre directions. Both models were implemented in ABAQUS/explicit.

Further authors used the subroutines of the commercially available FE software ABAQUS, for the implementation of their material models [38, 104–107]. In doing so they could use the available elements, contact and friction models.

Dong et al. [108] developed an updated material behaviour law on the basis of changing fibre directions. The update of the fibre directions during forming should avoid the shear locking effect. This effect describes the emergence of tensile fibre stresses under pure shear loading.

Ten Thije et al. [98] published a newly developed approach which is based on an updated Lagrangian FE method. The proposed simulation model exhibited a robust and efficient behaviour during the application to materials with different degrees of anisotropy and high deformations. For further improvement they developed a multi-layer triangular membrane finite element in a subsequent study [109]. The presented element type proved to be able to predict the out-of-plane wrinkle development, but it was not possible to actually display the appearance of wrinkles due to the lack of bending stiffness of the membrane elements. To cope with that, an enhanced multi-layer element was developed by Haanappel et al. [36, 41, 110]. In addition to the membrane element a Discrete Kirchhoff Triangle (DKT) was implemented. The DKT manages the out-of-plane bending properties, whereas the membrane element deals with the in-plane properties. The DKT and membrane element share the same nodes and deform mutually. The material model was implemented in the self-made code AniForm.

AniForm Suite, which is commercially available since 2014, is an implicit FE forming simulation software. It consists of the AniForm PrePost, a graphical pre- and postprocessor, and the AniForm Core, the implicit FE solver. Several publications using AniForm can be found in research [88, 111–114].

Despite AniForm there is also other commercial FE software available, offering own material models for the forming of dry fabric or prepreg materials. PAM-FORM of the ESI Group for example is an explicit FE solver. A material model with a thermo-visco-elastic matrix model and an elastic fibre model is included [115]. Here, also the bending properties are decoupled from the in-plane properties.

With regard to the preparation of a macroscopic FE forming simulation much higher efforts must be taken than for a kinematic forming simulation. The in-plane, bending and interface properties must be determined under processing conditions for every material. Therefore, several characterisation tests are necessary that have not been standardised so far. Besides that, the complete forming process has to be modelled including all forming steps and support frame or blankholders. Also, the computational effort is much higher.

2.3.2.2 Mesoscopic FE approach

In mesoscopic FE approaches, modelling occurs on the level of yarns. Single fibres or filaments are not considered. With these approaches deformations on yarn level can be predicted: gap opening or closing, loops of the yarn, yarn slippage or inter-yarn movement. Yarns are mostly modelled by shell elements and the architecture of the fabric is reproduced. But also truss, beam or solid elements were used for mesoscopic modelling [116].

Due to the higher level of detail in mesoscopic approaches more input parameters are necessary, which are difficult to determine. Required are, for example, the inter-yarn

friction properties or the yarn mechanics [61]. In case of NCF material, also the properties of the stitching yarn must be characterised.

Nishi and Hirashima [99] presented a mesoscopic approach for dry fabric forming simulation. They used the meso-model to understand the in-plane and out-of-plane deformations of the material and implemented the results on a macro-model.

Badel et al. [117] developed an approach for modelling a woven fabric. For modelling of the yarn behaviour a specific continuum hypo-elastic constitutive model was used.

Hosseini et al. [118] developed a mesoscopic model to analyse the wrinkling behaviour of plan woven preforms under shear deformation. They investigated the deformation of the yarns to develop an analytical model to predict the onset of wrinkling. The results were validated by bias-extension tests.

Cherouat and Billoet [119] proposed a simulation model for thermoset prepreg woven fabrics at mesoscopic level. They combined two different FE families to model the matrix and fibre behaviour. For the isotropic viscoelastic behaviour of the matrix membrane elements were used. The isotropic non-linear behaviour of the fibres is modelled with UD truss elements representing the warp and weft fibre directions. The model was validated using forming experiments and bias-extension tests.

The computational effort of mesoscopic FE simulations is higher than of macroscopic approaches due to the larger quantity of elements and more complex interfaces. But in return the results provide a detailed output and more information about the deformation behaviour of yarns and their inner structure.

2.3.2.3 Microscopic FE approach

In microscopic FE approaches the material is modelled on fibre or filament level. As the modelling of single filaments is too expensive regarding computational time, usually bundles of filaments are modelled. Nevertheless, this approach can only be applied to rather small models such as unit cells or sections of parts. Thus, this approach is only rarely used and solely in science.

The first work in the field of microscopic FE forming simulations was presented by Zhou et al. [120]. The authors developed a multi-chain digital element approach and used the model to simulate textile processes.

Durville [100] presented a microscopic approach for modelling woven structures using 3D beam elements. One major challenge were contact-interactions between numerous fibres taking place within the model which have to be characterised accordingly. To cope with that the method generated contact elements automatically. By means of an implicit solver the author showed that stable results under large deformations could be achieved.

Moustaghfir et al. [121] used the approach of Durville for studying the transverse behaviour of rovings.

Green et al. [122] presented an approach for predicting the performance of 3D woven composites. In their model 61 chains of beam elements represented the yarns. The

authors were able to simulate a wider range of fabrics with different internal architectures.

The approach developed by Colin et al. [123] focused on the virtual description of a biaxial NCF. It is based on the periodicity of the textile architecture and for the modelling purpose also multi-chain digital elements were used. The model was tested under compaction and in-plane shear and was validated by using experimental data.

By utilising microscopic FE approaches most detailed information about the deformation behaviour on fibre level can be determined. Also, the influence of different weave architectures or stitching pattern on the global forming properties of fabrics can be studied. But due to the high modelling effort and computational costs, it is by now only rarely used.

2.3.3 Selected software and description

For the forming simulations within this thesis a macroscopic FE approach was used. Only this method enables simulations of large parts as experimentally studied while also considering the influence of fibre orientation or matrix material and boundary conditions such as the support frame configuration. The software package AniForm Suite of AniForm Engineering [124] was chosen. This software was developed particularly for the purpose of forming simulations of continuous fibre reinforced composites with thermoplastic or thermoset matrix material. Various material models for these kinds of materials are implemented. Besides that, the availability of software at the Fraunhofer IGCV affected the selection.

AniForm Suite comprises two software components: AniForm PrePost and AniForm Core. PrePost is a graphical user interface for the pre- and postprocessing of simulations. The meshes of tools and laminate are loaded and the respective positions and loads are defined. The layup can be assigned, and the desired material models and properties can be allocated. Until now it has not been possible to mesh CAD surfaces directly in AniForm PrePost. The meshing has to be done in another tool and then be transferred to AniForm. But when starting a simulation AniForm will automatically generate the desired mesh configurations depending on the fibre orientations of the plies so that the element edges are aligned. Also, it is possible to change the element size before starting a simulation. While a simulation is running and after it is finished the results can be analysed by means of output data such as shear angle, Green-Lagrange strains or tractions. They are sorted by ply and interface results and are displayed either by colour or vector plots. AniForm Core is an implicit FE solver for forming simulations of anisotropic materials on the basis of a fully non-linear theory. The accuracy of results is insensitive to rigid translations and rotations as it does not use geometric linearization. The Core can be installed on a separate high-performance machine and the tasks can be transferred via network. [125]

As AniForm belongs to the macroscopic FE simulations, layers of shell elements model the single plies. For the correct simulation of the mechanical behaviour, the bending properties must be decoupled from the in-plane properties. For that purpose, AniForm contains a special shell element. It consists of a three-node membrane element with linear shape functions (LTR3D) and a DKT element, which share the same nodes and deform mutually (see Fig. 2-7).
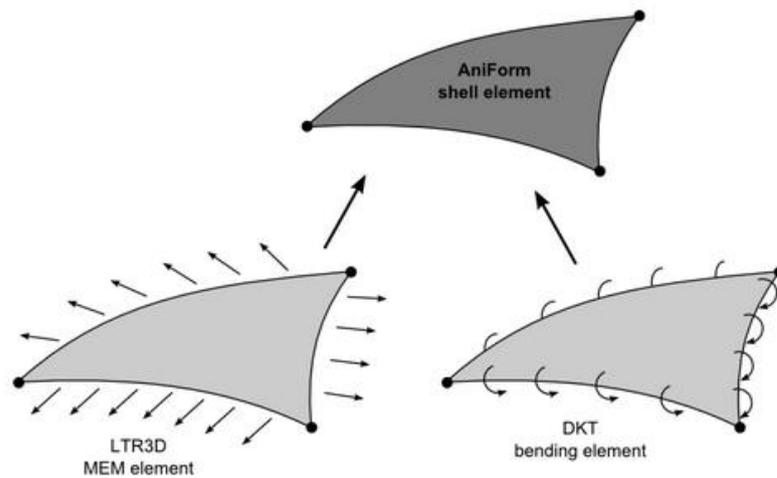
Fig. 2-7.   AniForm shell element [125]
          Combination of LTR3D membrane element and DKT element sharing the same nodes

The LTR3D element handles in-plane deformations, the DKT element the out-of-plane bending behaviour. Master and slave contact elements achieve the contact between two plies or between a ply and the tool surface. Different material models and properties can be assigned to the continuum and contact elements in order to model the material behaviour accordingly. The desired behaviour can be achieved by combining several elastic or viscous material models that are connected in parallel. Thus, the properties of fibres and matrix can be modelled independently from each other. Various material models are implemented in AniForm. An overview is given in Tab. 2-2. Despite that also own material models can be implemented utilising a user subroutine.

Tab. 2-2.   AniForm material models

Interface	In-plane	Bending
• Penalty	• Isotropic elastic	• Isotropic elastic
• Penalty with Coulomb friction	• Orthotropic elastic	• Orthotropic elastic
• Penalty with polymer friction	• Elastic fibre model	• Mooney Rivlin
• Viscous friction	• Mooney Rivlin	• Newtonian Fluid
• Damping	• Newtonian Fluid	• Cross Viscosity Fluid
• Adhesion	• Cross Viscosity Fluid	
	• Fabric Reinforced Viscous Fluid	

Within the scope of this thesis the following material models were used: For the interface modelling a combination of penalty with Coulomb friction and Viscous friction and a combination of penalty with Coulomb friction and penalty with polymer friction were applied. In some cases also an adhesion was added. For the in-plane properties the elastic fibre model and the isotropic elastic model were always combined, either with the Newtonian Fluid model or the Cross Viscosity Fluid model. In the case of bending a combination of the orthotropic elastic model with either the Newtonian Fluid model or the Cross Viscosity Fluid model was used. The applied models are further described in detail hereinafter [125]:

Penalty with Coulomb friction

This model is a combination of a penalty contact formulation and a Coulomb friction. For the penalty contact a stiffness parameter is introduced that prevents the surfaces from penetrating each other. The traction in this model is based on the Coulomb type of friction and is calculated by multiplying the normal pressure and a friction coefficient.

Penalty with polymer friction

The polymer friction is a viscous type of friction based on the shear deformation of a fluid film. A Cross viscosity model is used for the calculation of the viscosity of the polymer film. It includes also a penalty contact formulation.

Viscous friction

A viscous type of friction arises when there is a fluid between the contact surfaces. This model reproduces this effect. It is calculated based on the fluid viscosity and the film thickness and depends on the slip velocity.

Adhesion

The adhesion model is used to simulate the tackiness between the contact partners. In this model an adhesive tension is applied as soon as two surfaces approach under a certain activation trigger distance. The tension will be deactivated when the distance exceeds a deactivation trigger distance.

Elastic fibre model

The elastic fibre model is a linear elastic model for the simulation of the fibres. A Young's modulus and the fibre orientation with respect to the local coordination system are assigned.

Isotropic elastic

This model is a standard isotropic elastic model based on Hooke's law. Input parameters are the Young's modulus and the Poisson's ratio.

Orthotropic elastic

The orthotropic elastic model is also based on Hooke's law but for orthotropic materials. In addition to the two Young's moduli and the Poisson's ratio also the shear modulus is required as input parameter.

Newtonian fluid

The Newtonian fluid model only requires the viscosity as input parameter. The Cauchy stresses are then calculated with the viscosity, the rate of deformation and the Jacobian of the deformation gradient.

Cross Viscosity Fluid

The feature of this model is that the viscosity is shear rate dependent and has a viscosity plateau region at low and high shear rates. This model is suited for powerlaw type fluids.

2.3.4 Validation

Forming simulations of fibre reinforced plastics are a crucial tool for reducing time and budget during the development process. To be able to generate reliable simulation results, a validation of the forming simulations and used material parameters is necessary. The validation refers to the comparison of simulation and experimental results regarding certain characteristics. There are several characteristics available that can be used to perform a validation. The results can be compared with regard to the outer contour, the position and number of forming effects or the fibre directions. Doerr et al. [126] presented a method for validation of forming simulations based on the curvature of the formed parts. The authors measured the curvature using a conventional coordinate measuring device and compared it to the curvature predicted by the forming simulation. With the presented method a quantitative validation was possible. Another method for a quantitative comparison is based on measuring the fibre directions. A validation based on this concept has the advantage that the validated directions of the forming simulation can directly be used for a subsequent structural calculation. Several publications on the comparison between results of forming simulations and measured fibre directions in real parts exist. Eitzinger [127] and Dereims et al. [128] developed a system for optimising material data for PAM-FORM. By means of an optical sensor built-in a robot cell the authors measured the angle between warp and weft all-over the draped weave and projected the results onto a 3D-geometry of the preform. The measured angles were compared with the prediction of the forming simulation and optimised material data for the simulation generated. Leutz [32] also used an optical sensor for measuring fibre orientations of dry non-crimp fabrics and prepregs at single measuring points. Using a Matlab tool the results were compared with the simulation data. Margossian [62] applied this method to fibre reinforced thermoplastics. Bardl et al. [129] designed an algorithm that determines the fibre orientations out of an eddy current measurement. This technique also captures the

underlying plies. The applied eddy current system was developed by Heuer et al. [130]. Mallach et al. [131] also described an optical measurement system for dry non-crimp fabric preforms. They used a robot cell for the measurements as well.

3 Experimental studies

The following chapter describes the performed experimental forming studies. In total three studies were conducted, which have an ascending complexity regarding parts and process set-up. The first study (see chapter 3.1) aimed to gain knowledge about the forming process itself and to evaluate the forming of simple radius sections. Different parameters were varied to determine their influences on the part quality. For the evaluation, optical inspection, thickness measurements, microsections and mechanical testing were deployed. In the second study (see chapter 3.2) a forming tool with higher geometrical complexity was used, which was especially designed for that purpose. Lessons learned of the first study were applied to the new geometry and an extensive study regarding possible forming effects and the related process parameters was performed. A method for the quantitative comparison of the part quality based on typical forming effects was developed. As a result, the best parameter configuration could be determined. In the third study (see chapter 3.3) the forming process itself was investigated using a cone geometry. Three approaches for the forming of unconsolidated layups were compared and the emerging parts were evaluated regarding the resulting laminate quality. For the comparison of formed parts, thickness, fibre volume fraction, void content and thermography measurements were performed and microsections were made.

In addition to the variation of the geometry and the forming process, also different materials were investigated to cover the full range of FRTP. In total three different materials were used for the experimental studies: Carbon fibre reinforced polyether ether ketone (CF/PEEK) (first and second study), which is a high-performance material for aeronautic application having very high operation and processing temperatures. Glass fibre reinforced polypropylene (GF/PP) (second study), which is relatively inexpensive and has low processing temperatures. Carbon fibre reinforced polyamide 6 (CF/PA6) (third study), which is a technical material suitable for automotive applications and has intermediate processing temperatures. By varying the materials, it could be shown that all kind of FRTP are suitable for the described thermoforming process and the gathered results can be transferred to other materials.

Tab. 3-1.   **Properties of used thermoplastics (according to [21, 44, 47, 48, 132])**

	PP	PA6	PEEK
T_g [°C]	-10	57	143
T_m [°C]	173	220	343
Application	Consumer goods	Automotive industry	Aviation industry
Pros	• Inexpensive • Good mechanical properties • Low water absorption	• Good chemical resistance • High mechanical properties	• High working temperature • High chemical resistance • Hardly flammable
Cons	• Low application temperature • Brittle at low temperatures	• High water absorption	• Very expensive • High processing temperatures

3.1 Radius forming behaviour

To produce a 3D part out of the flat layups, a subsequent thermoforming step is necessary. During this forming, defects can arise, which are caused by the adaption of the material to the mould geometry and resulting forming mechanisms. Especially the corners and radius sections are prone to defects resulting from the high local forming degree [133]. Typical defects occurring in these areas are wrinkles, dry spots, delaminations or thinning of the material. Studies have been conducted regarding the forming forces [50] and temperatures [58, 134].

Most of the content of this chapter (text and figures) is based on [K1].

3.1.1 Material and experimental setup

The material used for this investigation was a CF/PEEK UD-tape (TenCate Cetex TC1200 PEEK AS4) of the Royal Ten Cate Corporate, Netherlands [53]. The tape had a fibre volume fraction of 59% and a nominal thickness of 0.14 mm. Using the ATL machine Fiberforge RELAY2000 the tapes were stacked and afterwards consolidated between two flat steel plates, which were heated by a hydraulic heating press. The test specimens consisted of the following layups: $[0]_{14}$, $[0/90]_7$, $[0]_{29}$ and a symmetrical 0/90-layup with 29 plies, which resulted in thicknesses of 2 mm and 4 mm, respectively. The consolidation temperature was 360 °C and the pressure amounted to 20 bar. The size of the consolidated plates was 750 mm x 500 mm. These were then cut into 6 samples with sizes of 310 mm x 130 mm each.

The experimental setup consisted of two matched aluminium moulds and a removable support frame. The geometry of the moulds was a 90°-angle with changeable radius inserts. This simple shape was chosen to reduce other geometrical influences [59]. The moulds were installed in a 137t hydraulic heating press. The press was used to heat the

tools to the desired temperature, apply the forming pressure and track the data during the forming. In addition to this equipment, an infrared-oven was used to heat the specimens prior to the forming step. This oven consisted of two heating fields that heat the specimens from above and below in order to achieve an even temperature distribution. The support frame was used to transfer the specimen between the infrared-oven and the heating press.

Within the support frame the specimens were tensioned on two sides by a variable number of constant-force springs. The number of springs could be varied between one and five on each side to adjust the pretension of the specimen. Each spring produced a force of 15.4 N. In that way the pretension of the specimen could be varied between 15.4 N and 77 N. On the one side the springs were fixed to the support frame and on the other side to a clamp, which was holding the specimen. The clamps were wrapped with aluminium foil to prevent the material from heating in these areas.

The lower mould was mounted to a base plate that enabled the installation in the heating press. On this base plate there were also four pillars holding the support frame in the correct position during the forming (see Fig. 3-1). The upper mould was installed in the heating press using a base plate, too. The tools were directly heated by the heating platens of the press. During the experiments the temperature of the moulds was controlled by thermocouples that were connected with the controller of the press.

(a)   (b)
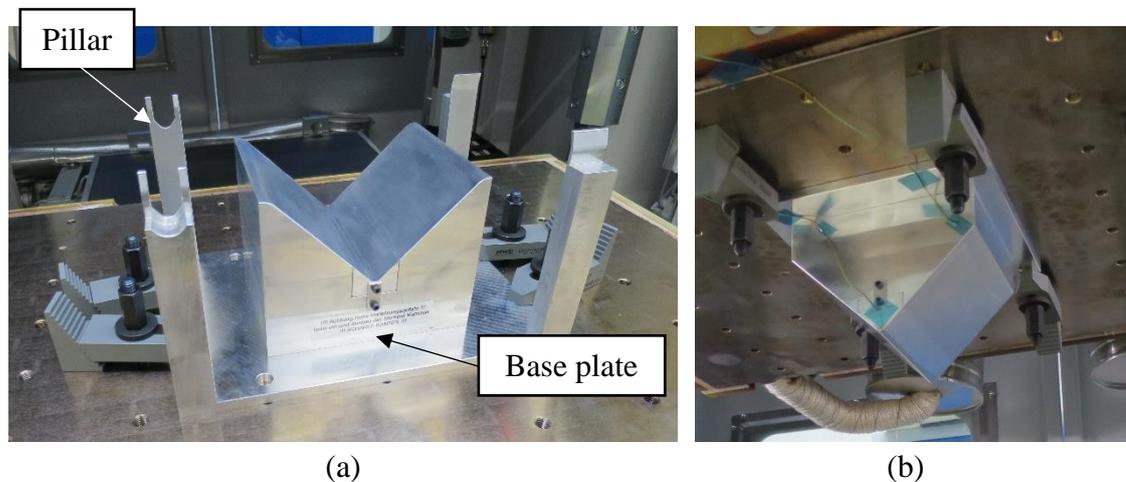
Fig. 3-1.   **Radius forming tool**
               Lower mould (a), upper mould (b)

3.1.2   Experimental procedure

For conducting the forming experiments, the specimens were tensioned in the support frame using the two clamps. The frame was then placed in the IR oven between the two heating fields and heated to the desired forming temperature, which is recommended to be between 370 °C and 400 °C [53]. To have enough time for the transfer, the temperature was set to 390 °C. During the heating process the temperature was measured by two pyrometers that pointed at the top and bottom surface and were

controlled by an integrated controller. As soon as the desired temperature was reached, the support frame was manually transferred to the press and placed between the moulds, which were held at a temperature of 200 °C. The transfer time was kept as low as possible to reduce the cooling of the specimen. Then the press was closed until the desired thickness of 2 mm or 4 mm was reached and a pressure of 18 bar was applied. The moulds were kept close for two minutes to ensure that the material was completely solidified before it was demoulded.

The varied parameters within this study are shown in the following table (see Tab. 3-2). For conducting the experiments, a full factorial parameter variation was chosen. The only exception was that for the specimens with thickness of 4 mm no tests with an inner radius of 5 mm were conducted.

Tab. 3-2.   Varied parameters

Parameter	**Unit**	**#1**	**#2**	**#3**
Thickness	[mm]	2	4	-
Layup	[-]	UD	[0/90]	-
Pretension	[N]	15.4	46.2	77.0
Inner radius	[mm]	3	5	-

The following identifier was used for the specimens: *Thickness-layup-number of springs-inner radius-repetition*, e.g. *2-UD-3-3-1* for a specimen with a thickness of 2 mm, UD-layup, pretension of three springs, inner radius of three millimetres and the first repetition.

3.1.3 Measurements

To investigate the quality of the forming experiments, different measurements were conducted. The main quality criteria in this study were the thickness and thickness distribution of the parts after forming. Besides that, the parts were also examined regarding effects such as fibre wrinkles or deflections and delaminations. First, to see, if there were differences regarding the thickness within the radius section and the flat sides, all specimens were measured using a thickness dial gauge. For that purpose, 15 measuring points were defined on the surface of the parts; six on each side and three in the radius (see Fig. 3-2). There were no measuring points near the edges in order to reduce the influences of edge-effects.
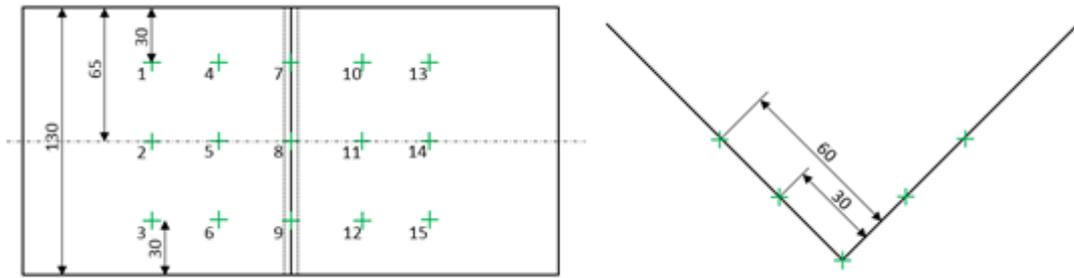
Fig. 3-2.   Positions of the measuring points

The thickness distribution served as an indicator of quality with special focus on possible thinning of the radius section caused by the pretension of the specimen or inter-laminar shear within the material. In addition, a selection of formed parts was scanned and analysed with the ATOS Core 300 3D scanner of GOM, with the aim to receive an overview of the thickness distribution and the uniformity of the surface. For that the parts were measured using the 3D scanner and data was analysed in the ATOS software subsequently. To also evaluate the inner quality of the parts, microsections of the formed specimens were made. The focus of this investigation was on the presence of defects such as delaminations, voids or fibre waviness. It should be especially compared, whether there were differences in the radius area and the flat areas regarding the laminate quality that could have developed during the forming process.

Finally, the parts were examined regarding their mechanical properties. They were tested according to ASTM D 6415 [135] to measure the curved beam strength (CBS) within the radius section. According to the testing norm the specimens were tested similar to a four-point bending test. In doing so the material is subjected to a bending, which induces interlaminar tension leading to delaminations of the material [136]. The testing setup and typical failure mode are shown in Fig. 3-3. The distance of the centre of the bottom loading bars was 100 mm and of the top loading bars 75 mm.

(a)   (b)
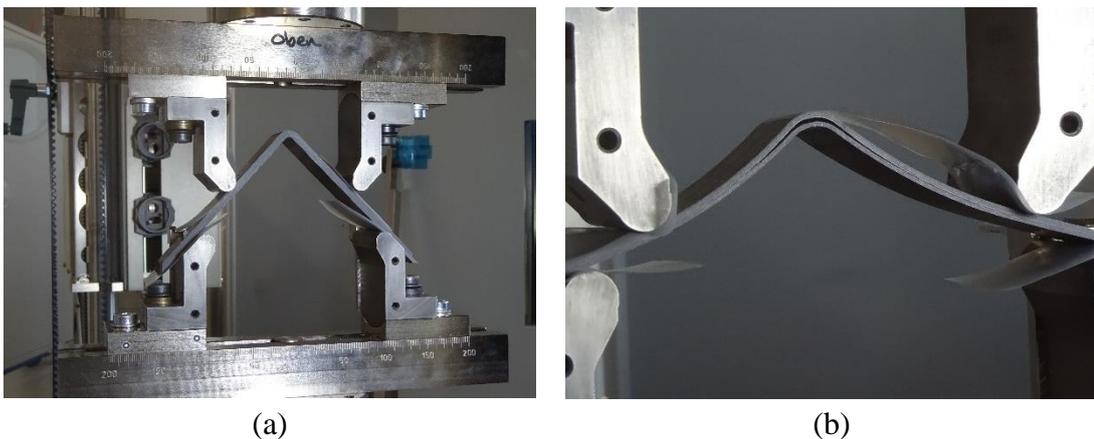
Fig. 3-3.   Curved beam strength testing
            (a) Testing setup, (b) typical delamination within the radius section

As the parts were manufactured with 3 mm and 5 mm inner radii, the demanded inner radius of 6.4 mm was not achieved. Polytetrafluoroethylene (PTFE) films were used to reduce the friction between the specimens and the four-point bending fixture, because no loading bars with roller bearings were available. The loading bars had a diameter of 10 mm. Out of every part three specimens were cut using water jet cutting. With two parts manufactured with the same process parameters, six specimens were tested for each parameter configuration. Tests were performed at a displacement rate of 10 mm/min. Force and displacement were traced by the universal testing machine. The CBS was then calculated according to equation (3-1) [135].

$$CBS = \left(\frac{P}{2w\cos\phi}\right)\left(\frac{d_x}{\cos\phi} + (D + t)\tan\phi\right) \tag{3-1}$$

Where P is the total force, w the width of the specimen, d_x horizontal distance between two adjacent top and bottom loading bars, D the diameter of the loading bars on the fixture, t the average thickness of the specimen and ϕ the angle from horizontal of the specimen's legs in degrees.

3.1.4 Results

For evaluating the thickness measurements, results of the twelve measuring points on the flat areas and the three measuring points in the radius section were averaged. Then the difference between the mean values was calculated with a negative result meaning a thinner radius section. The diagram below (see Fig. 3-4) shows the results of the thickness measurements.
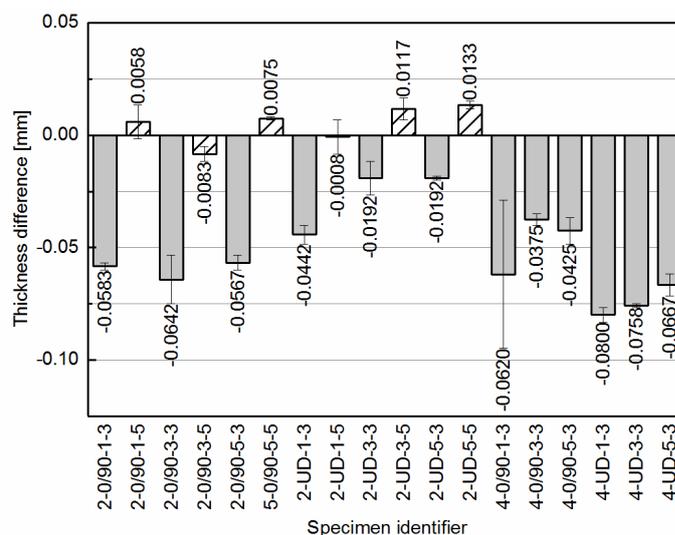
Fig. 3-4.   **Thickness differences between flat area and radius section**

It can be seen that every part formed with the 3 mm inner radius (grey columns) is thinner in the radius section, independent of other parameters. In contrast, the

thickness differences between the parts with the 5 mm inner radius (hatched columns) are clearly smaller. At some parts the radius section is even thicker than the flat areas. So it can be noted that the size of radius clearly has an influence on the thickness distribution. Therefore, the radius should be chosen as large as possible to improve the laminate quality.

Besides the influence of the radius size, the results show that dependent of the laminate thickness and layup the radius forming behaviour changes. For the laminates with a thickness of 2 mm the 0/90 layup shows more thinning than the UD layup, for the 4 mm laminates it is reversed. A reason for that could be the open cavity. As there is no barrier on the side of the moulds, the matrix is not detained of flowing and this effect seems to be lager for the 4 mm UD layups especially at the radius section. This can also be seen by the increased width of the specimen after forming. For the 2 mm laminates this effect is clearly smaller (see Fig. 3-5).

(a)   (b)
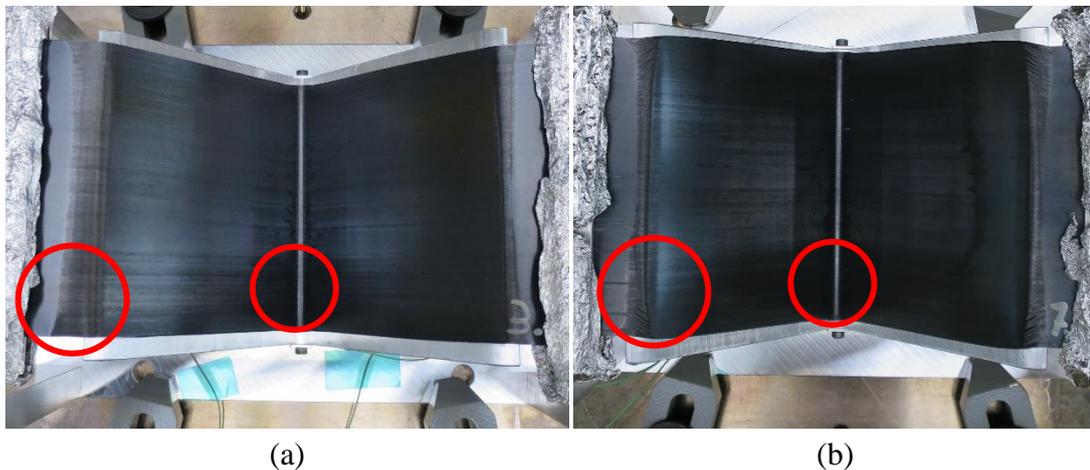
Fig. 3-5.   **Flowing of the matrix perpendicular to the fibre direction**
              UD 2 mm (a, 2-UD-5-3-1), UD 4 mm (b, 4-UD-3-3-1)

Examining the 2 mm specimens in Fig. 3-4, an influence of the pretension on the thinning in the radius can also be seen. It seems that a lower pretension causes more thinning than a higher pretension. For the 4 mm specimens this correlation is not that distinctive.

Fig. 3-6 shows the thickness distribution of five parts created with the ATOS system of GOM. Here, also the thinner radius sections can be seen.
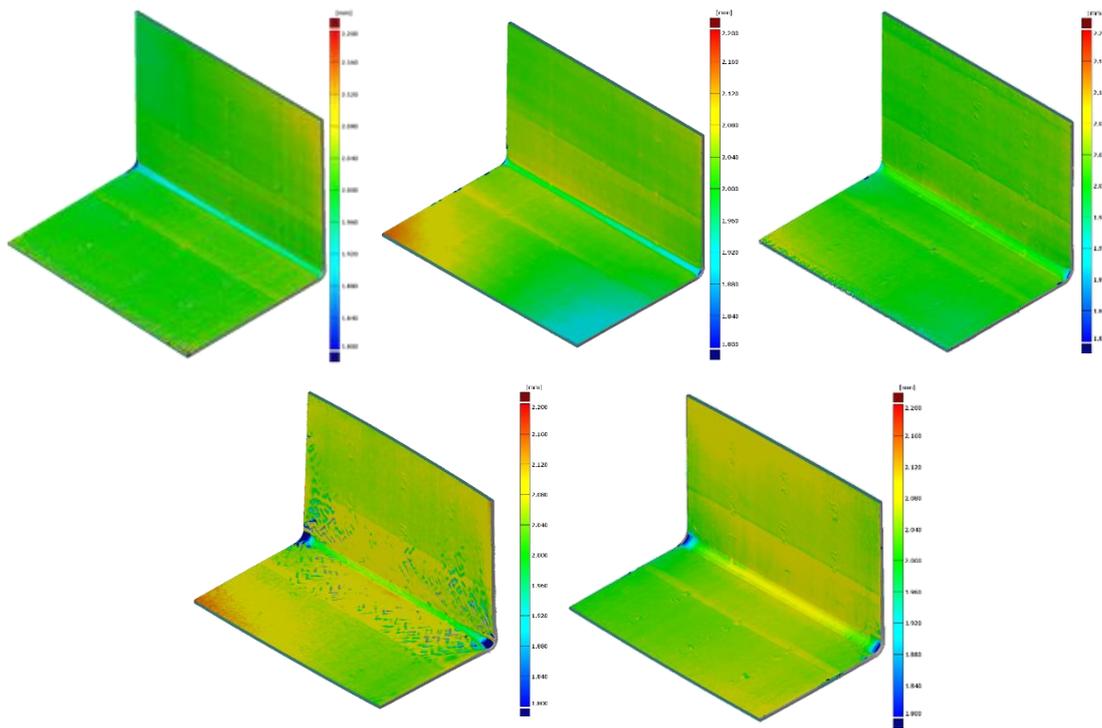
Fig. 3-6.   **Thickness measurements with the ATOS system**
            From the top left: 2-0/90-1-3-2, 2-0/90-3-3-2, 2-0/90-5-5-1, 2-UD-3-3-2, 2-UD-5-5-1

The local thinning of the laminate in the radius area leads to a locally increased fibre volume fraction in combination with a worse surface quality as there is no contact with the lower mould (Fig. 3-7).
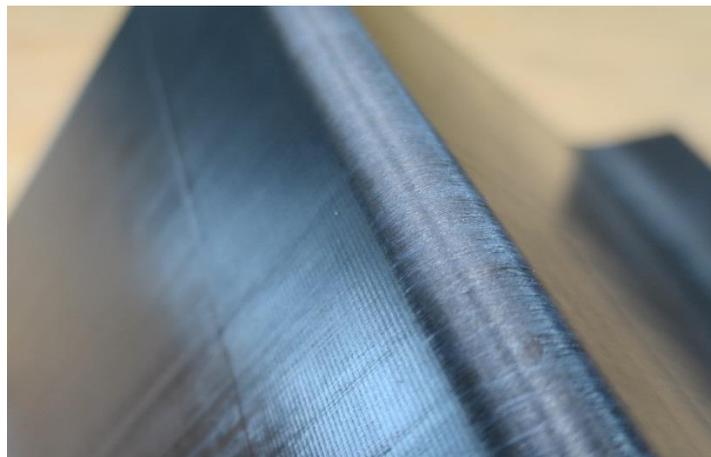
Fig. 3-7.   **Surface quality on the outside of the radius (4-0/90-5-3-2)**

Besides the thinning of the radius sections, also other effects can be noticed on the formed parts. Close to the inner radius a fibre waviness of the first ply can be seen (Fig. 3-8a), which is present on every part. In addition to that, most of the UD specimens show a severe wrinkle formation, which influences the surface quality (Fig.

3-8b). This phenomenon is less present in specimens with higher pre-tension and does not exist in the 0/90-layup.

(a)   (b)
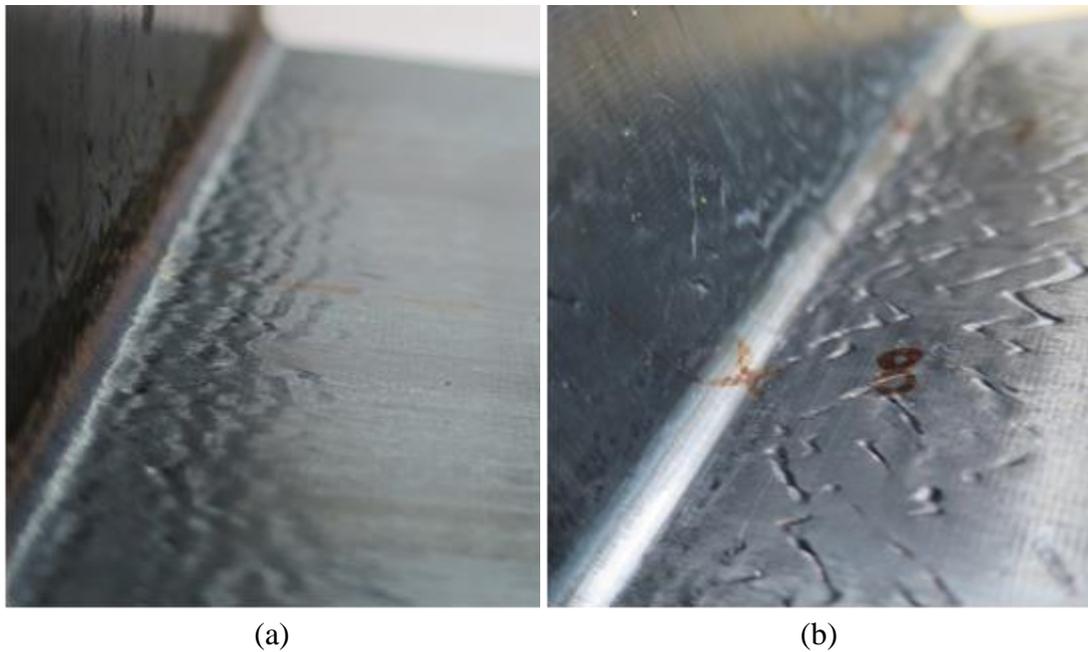
Fig. 3-8.   **Fibre distortions close to the radius area**
In-plane waviness (a, 4-UD-5-3-2), wrinkles (b, 2-UD-1-3-2)

To receive a better impression of the inner laminate quality, a microsection of the radius section was prepared (see Fig. 3-9).
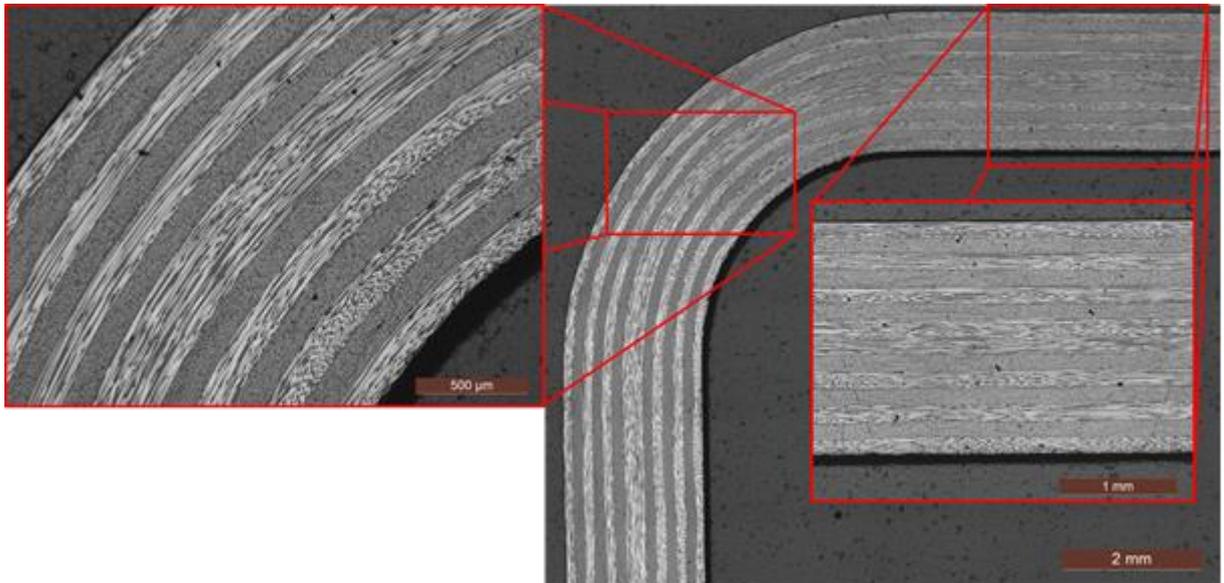
Fig. 3-9.   **Microsection of 2-0/90-3-3-2 at measuring point 8**

It can be seen that the fibres of the outer three 0°-plies are almost parallel to the picture plane, which is an indicator for stretched fibres. In contrast, the fibres of the inner three

0°-plies seem to emerge of the picture plane indicating in-plane waviness. Apart from this, the microsection reveals a good laminate quality containing very little pores and no delaminations.

Subsequently the results of the curved beam test are presented (see Fig. 3-10 and Fig. 3-11). It can be seen that the 2 mm UD specimens manufactured with a 5 mm inner radius clearly have a higher curved beam strength than the ones with the smaller radius. A similar effect was observed by Jamin et al. [136] and Avalon and Donaldson [137]. This effect is not present in the 0/90 specimens. Here, the number of springs and corresponding pre-tension of the laminates seems to have little influence. With increasing number of springs, the CBS is reduced. Also the values of the 5 mm radius are lower than the comparable configuration of the 3 mm radius. The detected radius thinning of the 3 mm radius specimens (see Fig. 3-4) does not seem to have an influence on the CBS.
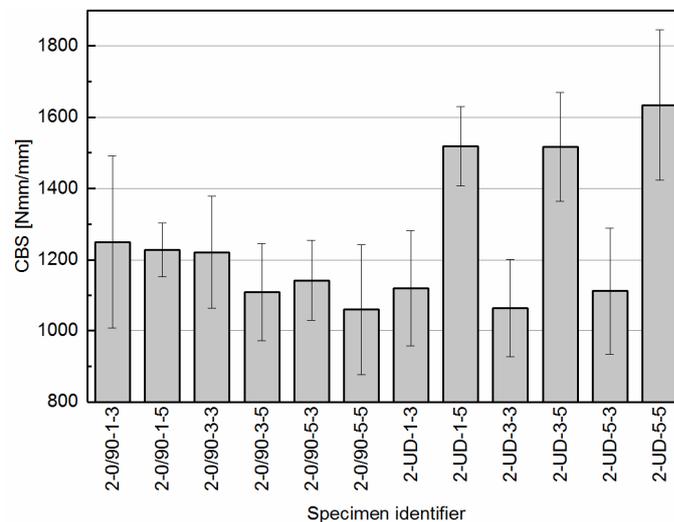
Fig. 3-10.   **Curved beam strength of the 2 mm specimens**

For the 4 mm specimens no dependency on the number of springs or the fibre orientation can be seen.
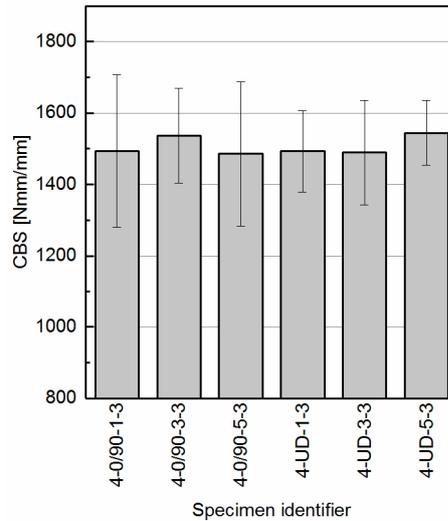
Fig. 3-11.   **Curved beam strength of the 4 mm specimens**

3.1.5 Conclusion

In this chapter, the radius forming behaviour of CF/PEEK was investigated and four parameters were evaluated regarding their influences on the laminate quality, especially on the thickness distribution. The considered parameters were the size of the radius, thickness of the specimen, fibre orientation and pretension in the support frame. The results showed that the size of the radius and the thickness of the laminate had the greatest influence on the thinning of the material in the radius area. The layup and the pretension of the specimens were of less importance. The experiments also revealed that fibre waviness of the 0°-plies can occur on the inner radius. Besides that, a good laminate quality could be achieved within the radius section and the flat areas.

3.2 Forming of a complex geometry

Based on results of the previous chapter, the lessons learned are transferred to a more complex geometry. In contrast to the described simple radius forming, the geometry should contain double curved areas and radii with different sizes, as they often exist in real parts. As a result, during the forming of such complex parts, additional effects such as wrinkles, undulations, etc. can emerge, which could have a negative impact on the part quality [36, 59, 134]. Consequently, these effects must be avoided to ensure maximum mechanical and visual properties. During the forming process, several parameters must be determined whose values may affect the result. Examples of typical parameters that depend on the choice of material include the pre-heating temperature, tool temperature and forming speed. Other parameters are independent of the material but also strongly influence the forming behaviour, e.g. the forming pressure or the tensioning unit. De Luca et al. [33] concluded that a reduced forming speed could increase the part quality. But this could also cause lower material temperatures, which must be compensated with higher pre-heating and tool

temperatures [138]. The influence of the tensioning unit, blank holder and springs has been investigated by various authors [28, 33, 41, 138, 139]. The common result was that tensioning the material is crucial to avoid folds and wrinkles. Lessard et al. [58] closely examined the influence of different process parameters on the thickness distribution and interlaminar shear strength. In contrast to their approach, this work focuses more on the development of macroscopic forming defects during the forming process and the influencing parameters.

The experiments and measurements presented hereinafter were performed in the scope of [S3]. Most of the content of this chapter, including text and figures, is based on [K2].

3.2.1 Material and experimental setup

In this study, two types of material were used. With a GF/PP UD tape of Celanese (Celstran CFR-TP PP GF70) with a nominal thickness of 0.25 mm and a fibre volume fraction of 45.3% [55] the influence of various process parameters was investigated. Subsequently, the findings were transferred to forming experiments with the CF/PEEK UD tape of TenCate, which had already been used in the first forming study (see chapter 3.1). The tapes were stacked and spot-welded using the Fiberforge RELAY2000 ATL machine. The GF/PP stacks were then consolidated by pre-heating to 190 °C in a heating table between two aluminium plates, manually transferred to the hydraulic heating press and pressed at 25 bar with 50 °C tool temperature. The CF/PEEK stacks were consolidated in a variothermal process at 360 °C and a pressure of 20 bar. After consolidation, the laminates were trimmed to the final size of 600 mm x 400 mm.

The forming tool used in this study consisted of two matched steel moulds. The geometry of the tool includes a combination of different shapes – a hemisphere with 80 mm diameter, a trapezoid with two radius sizes and a tapered front (see Fig. 3-12a). As a result, the tool combines double-curved, single-curved and flat areas. These different sections are connected via smooth junctions and generate various forming effects. As the cavity thickness is 2.4 mm, nine plies were chosen to fill it completely. Fig. 3-12b shows the lower mould.

(a)   (b)
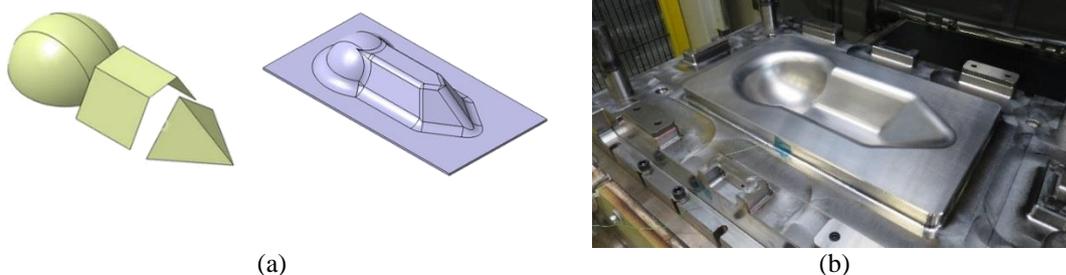
Fig. 3-12.   Forming tool with complex geometry
            (a) Tool geometry, (b) lower mould

The steel moulds were mounted in a 130 t Langzauner hydraulic heating press and directly heated. An IR oven with 12 IR heaters (KRELUS G14-25-2.5 MINI 7.5) was used to pre-heat the stacks before forming (see Fig. 3-13). The stacks were clamped into a support frame with adjustable constant-force springs to facilitate handling between the IR oven and the forming tool, and to apply local tension in order to influence the forming behaviour.
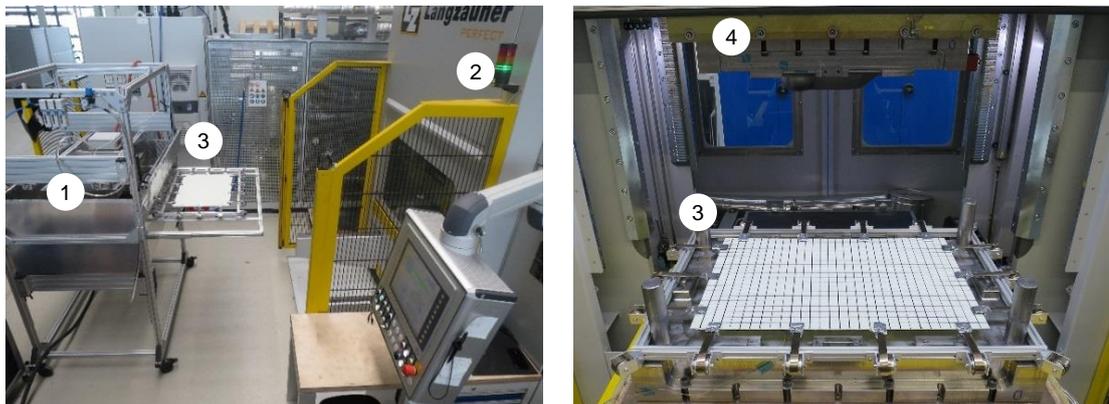
Fig. 3-13.　　**Experimental setup**
　　　　　　1: infrared oven, 2: hydraulic heating press, 3: support frame with stack, 4: upper mould

3.2.2　Forming experiments and results of GF/PP

The forming experiments were rated and compared based on the occurrence and frequency of four forming effects: wrinkles, in-plane undulations, gaps and surface roughness (see Fig. 2-3). Each of these effects was marked on the top and bottom surfaces of the formed specimen, categorized and quantified, so that the results could be compared objectively. An evaluation method was developed to quantitatively analyse the forming results. The occurring single effects (wrinkles, gaps) were counted and weighted according to their size and characteristics. The area effects (surface roughness, undulations) were measured and divided by the total area of the geometry. The factors thus obtained were then subtracted from a total score. In this way, each part was assigned a final score, which enabled objective comparison.

The forming effects mentioned above appeared in different areas of the geometry. Wrinkles were found around the hemisphere and the tapered front; their number and position depended on the orientation of the fibres, typically arising at a ±45° angle to the direction of the fibres. The same findings were reported by Hou [28], Monaghan et. al. [140] and O'Brádaigh and Pipes [141]. Rough patches were mainly present at the top of the hemisphere and the top radius at the front. The in-plane undulations, on the other hand, mostly arose on the inside of the hemisphere and in the flat area surrounding the geometry. The gaps were distributed over the whole geometry. The flat area beneath the 3D geometry was also considered by the evaluation.

In all experiments, a pre-heating temperature of 190 °C was used. After reaching this temperature, which was measured by a pyrometer on the surface of the material, the temperature was held for another 30 sec. to ensure that the temperature distribution was homogeneous throughout the material.

In the first testing phase, the tool temperature, the mould closing speed and the forming pressure were varied using a full factorial parameter variation. Each parameter was studied at two factor levels (see Tab. 3-3). The full factorial design was chosen in this case to detect possible interactions between the different parameters. Each parameter combination was repeated three times. In these experiments, the layup of the stacks was [0/90/0/90/0̄]ₛ and they were clamped to the support frame by 14 evenly distributed 11.5 N constant-force springs (see Fig. 3-14a).

Tab. 3-3.   **Varied process parameters testing phase 1**

	Tool temperature [°C]	Closing speed [mm/s]	Forming pressure [bar]
Level 1	30	20	10
Level 2	80	60	40

Statistical evaluation during testing phase one revealed the following influences: higher pressure and higher tool temperature reduced the frequency and number of in-plane undulations, with the latter exhibiting higher statistical significance. The higher level of these two parameters also improved the surface quality, but the forming pressure was more relevant for this effect. The only significant influence on the formation of wrinkles that could be detected was the tool temperature; the higher level reduced the number of wrinkles. This parameter had no significant influence on the development of gaps. The experiments with the higher forming pressure combined with the faster closing speed produced the best results. Choosing level 2 for every parameter led to parts with the least forming effects, hence these parameters were used for the following experiments.

In the second testing phase, the position and number of the constant-force springs on the support frame were varied. These springs guide the material during the forming process and apply tension to the material at discrete positions. In this testing phase, three configurations were compared (see Fig. 3-14). Option 1 was already used for test phase one, option 2 consisted of ten springs that were more clustered around the hemisphere, and option 3 had six evenly distributed springs. Three parts were formed with each configuration and then compared in terms of the number and size of the forming effects.

(a)   (b)   (c)
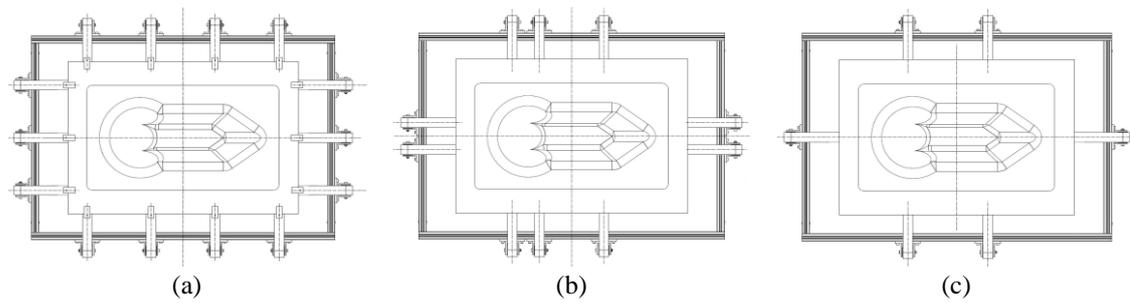
Fig. 3-14.   Support frame configurations
   (a) option 1 with 14 springs, (b) option 2 with 10 springs, (c) option 3 with 6 springs

Comparing the different configurations showed that option 1 had the fewest undulation, wrinkle and surface quality effects. Option 2 only led to better results in terms of the gaps. But the differences were not severe. Thus option 1 was chosen as the best configuration and was used in the subsequent experiments.

In the next testing phase, the influence of the spring forces was investigated. The previously used 11.5 N constant-force springs were replaced by springs with 19.2 N tensile force, while leaving the remaining process parameters unchanged. The forming experiment was repeated three times and the results were phenomenologically compared to the results obtained with the weaker springs. Evaluating these results revealed that the influence of the spring force on the surface quality, wrinkles and gaps was of little significance; however, a clear impact on the in-plane undulations was detectable. Higher pre-tension caused distinctly more and larger areas with undulated fibres. Consequently, it can be stated that the weaker springs lead to a better part quality with the support frame configuration and clamp size used in these experiments.

The resulted best process parameters for forming the orthotropic layup are summarized in Tab. 3-4.

Tab. 3-4.   Final forming parameters for GF/PP

Parameter	Unit	Value
Pre-heating temperature	[°C]	190
Tool temperature	[°C]	80
Forming pressure	[bar]	40
Closing speed	[mm/s]	60
Support frame configuration	[-]	Option 1
Spring force	[N]	11.5

Based on the results gathered from the previous experiments, the influence of the layup was investigated in the next testing phase. The orthotropic layup used in the above was

compared to a quasi-isotropic (QI) layup of $[0/+45/90/-45/0]_s$. To cope with the additional fibre directions, springs on the corners aligned in the 45°-direction were added to support frame configuration 1. This ensured that the ±45°-fibres were also under tension during the forming process. The evaluation showed that the QI layup exhibited more wrinkles and distinctly more undulations than the orthotropic layup (see Fig. 3-15). In addition to the wrinkles observed previously in the 45°-position of the hemisphere and the tapered tip, the QI layup resulted in more wrinkles around these areas, as well as other wrinkles next to the trapezoid. In contrast to these deteriorations, there was an improvement in the surface quality, with only small rough areas.

(a)   (b)
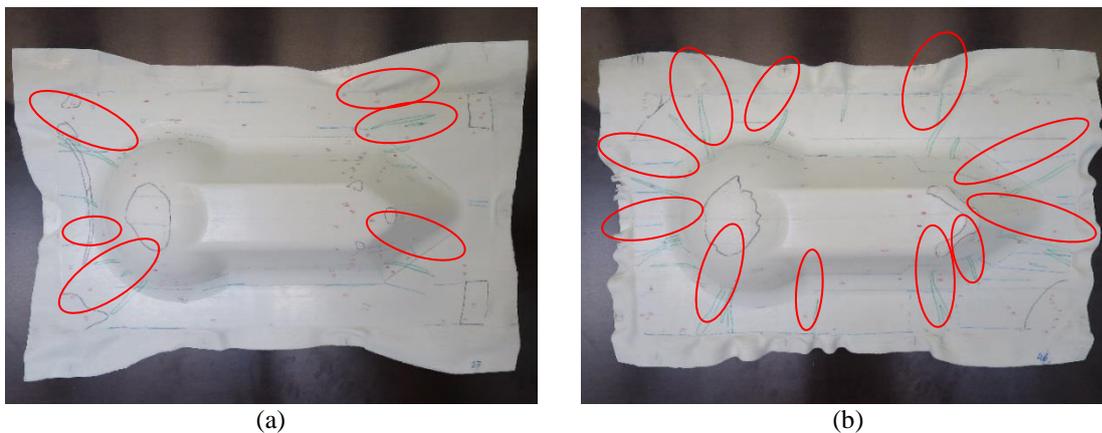
Fig. 3-15.   Top side of formed parts with marked wrinkles
(a) orthotropic layup from testing phase 1, (b) quasi-isotropic layup

To get a better impression of the development of the forming effects, four parts were partially formed with stamp travels of 20 mm, 40 mm, 60 mm and 80 mm with the latter being the mould fully closed. For these experiments an orthotropic layup with support frame option 1 was used. The parts were then scanned with the ATOS 3D scanner of GOM (see Fig. 3-16).

(a)   (b)   (c)   (d)
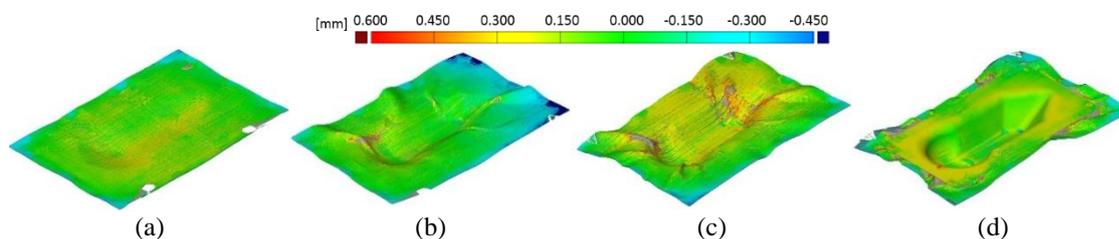
Fig. 3-16.   Thickness deviation of the nominal value (2.4 mm) of partially formed parts
3D scans of (a) 20 mm closed, (b) 40 mm closed, (c) 60 mm closed, (d) fully closed

The 3D scans clearly show the development of the wrinkles over the four forming steps. In the last step they were pressed flat by the fully closed mould. Also the

thickness deviation can be seen, which helps to draw conclusions about rough patches, because thinner areas indicate a not completely filled cavity and missing tool contact.

3.2.3   Forming experiments and results of CF/PEEK

For the forming experiments with CF/PEEK the process parameters that worked best for GF/PP were used to the greatest extent possible. Due to the lower thickness of the CF/PEEK tape the number of plies had to be raised to 17 to achieve the desired thickness of 2.4 mm. The resulting layup was $[0/90/0/90/0/90/0/90/\overline{0}]_s$. The support frame configuration, spring force, closing speed and forming pressure were directly adopted from the GF/PP forming experiments. The material-dependent pre-heating temperature and tool temperature had to be adapted. First, the settings of the radius forming experiments were used. But the initial experiments showed that a pre-heating temperature of 390 °C and a tool temperature of 200 °C were not sufficient for achieving a good part quality while forming the complex geometry. The parts exhibited numerous severe wrinkles and folds spread all over the geometry (see Fig. 3-17a, b). As known from the previous experiments these effects indicate a too low material temperature during forming.

| (a) | (b) |
| (c) | (d) |
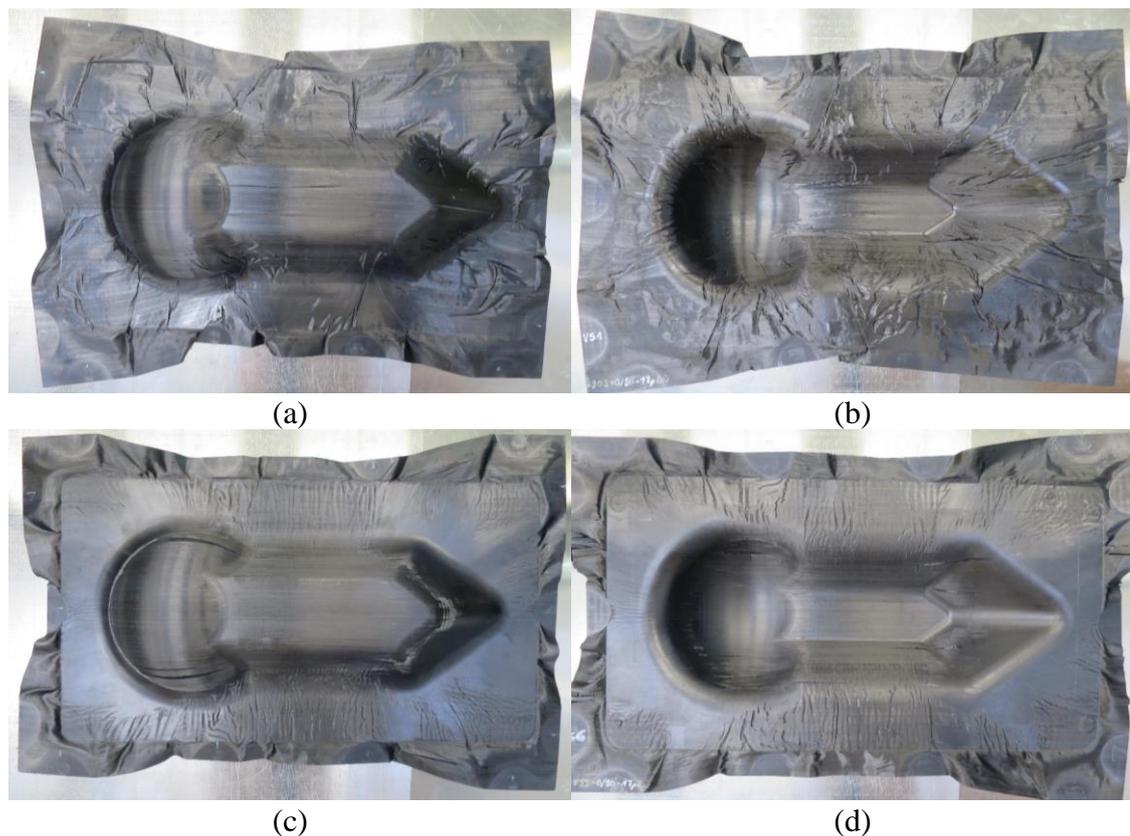
Fig. 3-17.   **Formed complex geometry with CF/PEEK**
             Lower temperatures: (a) upper side, (b) bottom side
             Improved final parameters: (c) upper side, (d) bottom side

To cope with that, the tool temperature and pre-heating temperature were raised incrementally to 300 °C and 440 °C, respectively. With these settings the part quality was improved significantly (see Fig. 3-17c, d). The size and number of folds was reduced and the surface quality was enhanced. However, the part quality was still worse compared to the best GF/PP parts. Severe fibre waviness beneath the geometry, large gaps of the surface ply on the side of the hemisphere and some rough areas could be detected.

3.2.4 Discussion

Testing phase one with GF/PP showed that higher tool temperature, higher forming speed and higher forming pressure lead to better part quality. These results may be explained by the fact that a colder tool and slower forming cause the specimen to cool down more quickly, which reduces the formability of the material. Similar observations were also made by Vanclooster [138] and Hou [28]. The forming pressure is especially relevant when attempting to achieve high surface quality, since the surface structure of the tool can only be evenly transferred to the specimen at high pressures.

The second testing phase revealed that utilising fewer springs causes more undulations, wrinkles and surface roughness. The experiments also showed that using a configuration with fewer springs causes the specimen to sag more before forming, which enables an earlier contact between the material and the lower mould. Because of this, there may be faster cooling at these areas and hence reduced formability. There may therefore exist interactions that should be investigated further, because the three spring configurations may have undergone different cooling behaviours.

Testing phase three supported the conclusion that a higher spring force leads to more undulations. This assumption deviates from the results of Hou [28], which revealed that higher pre-tension leads to better part quality. There is however a difference; Hou used a blank holder, which distributes the tension evenly throughout the material. This study on the other hand used clamps and constant-force springs, which applied the forces locally. The difference between fibres under high tension and fibres without tension side by side is suspected to cause undulations. Similar observations were also made by Harrison et al. [104].

Varying the fibre orientation in the last testing phase revealed that quasi-isotropic layups result in an increased amount of wrinkles but also in better surface quality. Wrinkles are caused by the inextensibility of the fibres combined with the resulting intra-ply shear forces, which lead to wrinkles in the ±45°-direction, as also stated by [28]. The additional fibres reduced the formability of the laminate. The surface quality, on the other hand, was improved. One possible reason for this is a reduced transverse matrix and fibre flow, which caused the thickness to be more evenly distributed and thus the cavity to be filled better. Consequently, the pressure was applied more evenly over the laminate, which reduced the occurrence of rough areas.

The determined process parameters were used for the forming of CF/PEEK laminates. Results showed that higher temperatures were necessary than for the radius forming presented in chapter 3.1. Reasons are that the handling of the large laminate between IR oven and forming tool takes more time. This causes an increased cooling of the material. Despite the shape of the geometry, more contact areas between tool and laminate already occurred at the beginning of the forming processes, which also accelerated the cooling. Additionally, the complex forming is more prone to a reduced formability of the material than the simple one-dimensional radius forming was. A further increase of temperatures might have triggered a better outcome, as also stated by Lessard et al. [58]. But a further pre-heating of the material could have caused material degradation, and higher tool temperatures were not possible either due to the used equipment.

3.2.5 Conclusion

A study of the forming of GF reinforced PP layups was conducted with the goal of investigating the influence of different parameters on the emergence of forming effects. The occurrence of the four following effects was compared in the results: wrinkles, in-plane undulations, surface roughness and gaps. After developing a method to compare the results quantitatively, the impact of each parameter on these effects was analysed and evaluated. Positive outcomes were observed for higher tool temperature, forming speed and forming pressure within the considered range. It was also shown that increasing the number of springs could reduce the number of undulations, wrinkles and rough areas; however, stronger springs led to an increase in undulations. Comparing an orthotropic and a quasi-isotropic layup revealed that better surface quality might be achieved with the QI layup, at the cost of more wrinkles and undulations.

Forming of CF/PEEK required an increase of the process temperatures to achieve satisfying results. Other determined process parameters were applied unchanged.

3.3 Forming without previous consolidation

Given the outlined state of the art forming technology, an additional consolidation step is necessary before forming, as the ATL layups are only US spot-welded and the air needs to be removed [24–26]. This not only increases the process duration, but also energy consumption and costs. Depending on the consolidation process, additional minutes (isothermal consolidation) or hours (variothermal consolidation) may be necessary. Hohmann et al. [142] stated that the consolidation process consumes 5% of the whole process energy demand. A forming process chain including tape production and ATL layup was investigated. In this scenario an isothermal consolidation process with a press running in a three-shift operation was assumed. In addition to the energy consumption, in this case also high costs for the additional press arose. The energy

demand for a variothermal consolidation would obviously be higher. Furthermore, a thermal degradation of the matrix material might occur during repeated heating above the melting temperature [143, 144].

The scope of this study was to develop alternative processes for forming spot-welded layups without prior consolidation and to evaluate the part quality that could be achieved. Little information can be found about this topic in the literature. Several studies on the direct forming of unconsolidated preforms of commingled yarns exist [145–150]. Wakeman et al. [146] primarily investigated the influence of different processing parameters on the void content and flexural properties. The authors stated that the pre-heating temperature and holding time are of greatest importance. Thereby, increased flexural strength and a lower thickness with fewer voids could be achieved. Trudel-Boucher et al. [148] identified the pressure during forming as being crucial to evade voids and porosity. Taking this into consideration, parts with mechanical properties comparable to consolidated material were achieved. Slange et al. [151] examined the influence of the pre-consolidation of UD carbon fibre reinforced polyether ether ketone on the consolidation of the final stamp formed parts. They compared the laminate quality after stamp forming of consolidated layups, AFP layups and manually US spot-welded ones, based on the void content. A correlation between pre-consolidation status and consolidation quality was ascertained, using thickness measurements for evaluation. Also it was stated that the pre-consolidation had an influence on the thermal behaviour during pre-heating in an infrared oven.

With regard to the forming of unconsolidated layups, a number of different challenges have to be overcome during the process. For short cycle times, efficient IR heating devices are typically used. The material is heated from the outside and the heat must be transferred to the centre of the laminate by heat transfer. As a result, IR heating is only suitable for consolidated layups [42]. To be able to apply it anyway, contact between the unconsolidated plies has to be ensured. In common consolidation processes, entrapped air can escape during the consolidation step and parts with low void content are possible. When bypassing this step, the air has to be removed during pre-heating and forming to achieve a comparable part quality.

This chapter contains a preliminary investigation of direct forming of unconsolidated spot-welded layups of fibre reinforced thermoplastic tapes. Three new approaches were developed and formed parts were manufactured using these approaches. The parts were evaluated regarding their final laminate quality. As reference for the evaluation flat plates and formed parts were manufactured using state of the art consolidation and forming processes, respectively. For the evaluation thickness, fibre volume fraction and void content were measured and optical analysis, thermography and microsections were performed.

The experiments and measurements presented hereinafter were performed in the scope of [S6]. The majority of this chapter's content, including text and figures, is based on [P1].

3.3.1   Material and experimental setup

The material used in this study was a UD CF reinforced PA6 tape of Celanese (Celstran CFR-TP PA6 CF60). Relevant properties of the tape material are shown in Tab. 3-5.

Tab. 3-5.   PA6/CF Material properties [54]

Tape thickness [mm]	Fibre volume fraction [%]	Melting temperature [°C]	Glass transition temperature [°C]
0.13	48.5	220	57

Prior to processing, the tape was slit from an initial width of 275 mm to 50 mm, representing the narrowest width that can be processed on the Fiberforge RELAY2000 ATL machine. Then, layups of $[(0/90)_4/0/(90/0)_4]$ were produced. This layup process was the same for all experiments.

Two different tools were used for the experimental investigation. The first experiments were performed using a flat sheet tool with an area of 350 mm x 350 mm. This consists of two flat moulds that were mounted to and heated by the press. This tool was used to gain a first impression of the different approaches while pressing flat plates. Even if the geometry required no forming in terms of changing the shape, the process sequence was still the same (see chapter 3.3.2). The second tool used for this investigation had a 3D geometry. It consists of two matched steel moulds with the geometry of a cone that has a rounded tip. The outer diameter was 186 mm, the height 70.4 mm and the radius of the tip 52.4 mm. The nominal thickness of the cavity was 2.4 mm. Both tools are shown in Fig. 3-18.

(a)   (b)
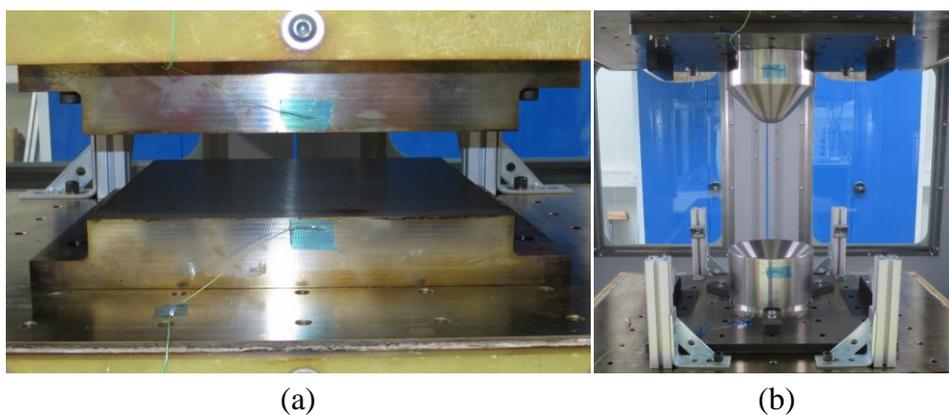
Fig. 3-18.   Used forming tools
            (a) flat sheet tool, (b) 3D cone geometry tool

For the pre-heating of the layups, the same self-developed IR oven as in the previous study consisting of 12 IR heaters was used. A support frame was utilised to fix the

layups during pre-heating, to enable handling between the IR oven and the forming tool and to apply tension during forming. The tension was applied by constant force springs (Lesjöfors KKF-C 1012), which connected the support frame and the laminate and ensured steady tension during forming. Each spring generated a constant force of 11.5 N.

3.3.2 Forming experiments

Prior to the experiments, all tools were cleaned and coated with Frekote 770-NC release agent from Henkel. The layups and PA6 films were also dried for 12 hours at 80 °C. They had sizes of 400 mm x 400 mm for the flat plates and 350 mm x 350 mm for the formed parts, respectively. An overview of the performed experiments and meaning of the designations is given in Tab. 3-6.

Tab. 3-6.   **Overview of the performed experiments**

Designation	Approach	Geometry	Film material	Film thickness [mm]	Number of parts
Ref-V	Standard	Plate	-	-	11
Ref-H	Standard	Cone	-	-	7
US-V	A	Plate	-	-	2
US-H	A	Cone	-	-	5
PI-V1	B	Plate	Polyimide	0.05	2
PI-H1	B	Cone	Polyimide	0.05	4
PI-H2	B	Cone	Polyimide	0.125	2
PA-V	C	Plate	Polyamide 6	0.2	2
PA-H1	C	Cone	Polyamide 6	0.2	4
PA-H2	C	Cone	Polyamide 6	0.05	6

General forming procedure

The forming of all parts followed the same procedure described hereinafter (see Fig. 3-19). The consolidated laminates or unconsolidated layups were clamped in the support frame by two constant force springs on each side (see Fig. 3-20a), which ensured that both the positioning and the tension applied to the material were exact. Then they were heated to a temperature of 280 °C in the IR oven and kept for 90 s to ensure an even temperature distribution over their entire thickness. After that, the layups were transferred manually to the forming tool using the support frame. Subsequently the layups were formed with a forming speed of 60 mm/s and cooled down with a tool temperature of 80 °C and a pressing force of 212 kN (40 bar), which

is also recommended by the tape manufacturer [54]. The parts were removed after a cooling time of 2 min (see Fig. 3-20b).
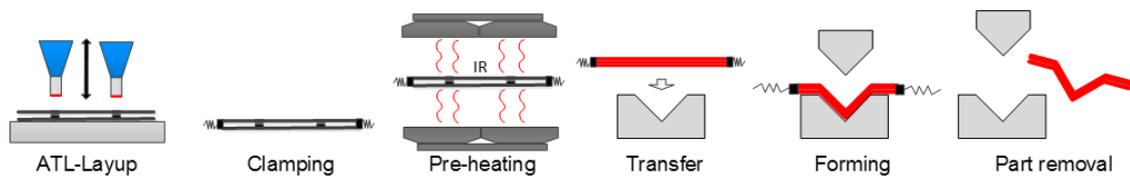
Fig. 3-19. **Schematic visualisation of the forming procedure**

Standard formed parts

Seven parts were formed of consolidated layups as basis for the comparison and evaluation of the different new approaches. The layups for these parts were consolidated prior to forming. For that purpose, they were placed between two aluminium plates and heated in a heating table (ELKOM Mikutherm Optimal Typ 2111) until a temperature of 260 °C was reached. The temperature was measured using a thermocouple, which was placed in the centre of the layup and removed after reaching the desired temperature. The staple, including the aluminium plates, was then transferred manually to the hydraulic heating press (Langzauner LZT-OK-130-L) and placed between the mounting plates without additional tools. The press was closed and the layups consolidated at 240 kN (15 bar) and 80 °C within 90 s.
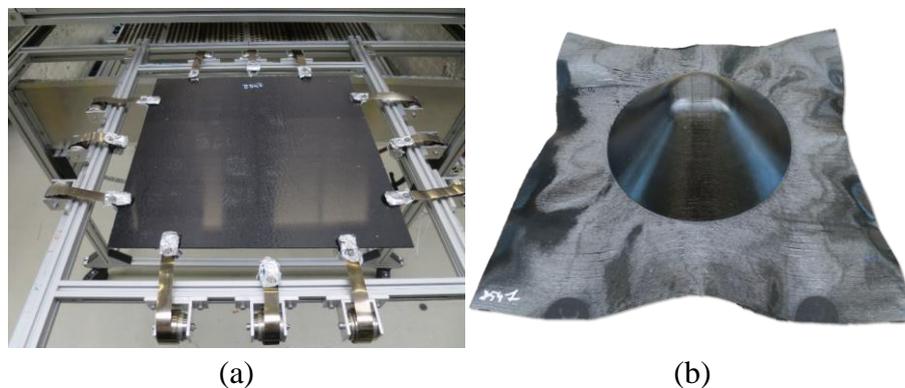
Fig. 3-20. **(a) Laminate clamped in the support frame, (b) formed reference part**

Approach A (denoted US): additional welding spots

The first approach pursues the goal of improving the heatability of the unconsolidated laminates in the IR oven by adding additional US welding spots. Pre-trials showed that the outer plies started to roll up and detach from the remaining plies when they were being heated. To cope with this, a welding spot pattern was developed which was applied automatically after the second ply, in the middle of the laminate and after the last ply (see Fig. 3-21a). This pattern was improved during several experiments using the flat moulds (see Fig. 3-21b). The black dots in the illustration are the additional welding spots, whereas the grey and white ones are generated automatically.
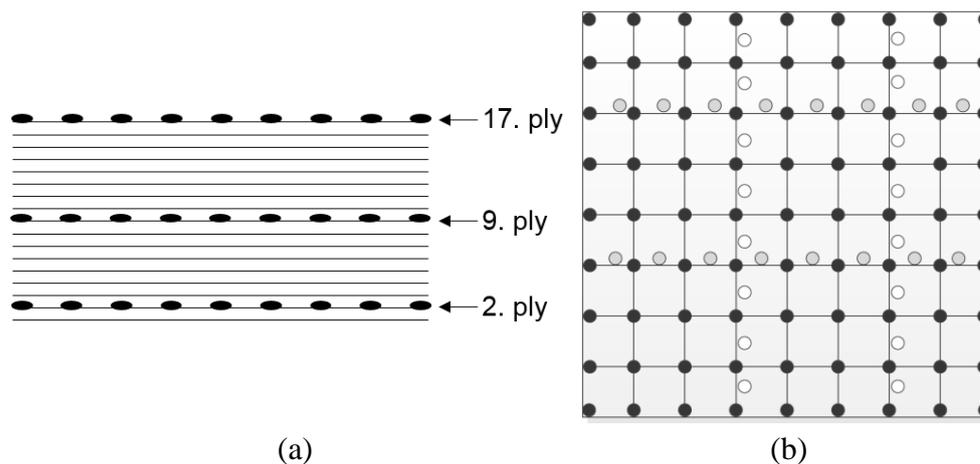
Fig. 3-21.   **Ultrasonic welding spot pattern**
(a) Positions of the additional welding spots in cross-section. Only the additional spots are illustrated as black dots, (b) Grey/white dots are automatically generated; black ones are additionally added.

The welding spots were positioned along the outer edges and on the contact line of adjacent tapes. In that way, a uniform heating of the laminate was ensured. After pressing the flat plates, five parts were formed into the 3D geometry using the optimised welding spot pattern. A thermocouple in the centre of the laminate was used during pre-heating to control the temperature. During heating, the tapes began to bulge at 230 °C and flattened again on reaching 250 °C. The process parameters were the same as for the standard formed parts.

Approach B (denoted PI): vacuum setup with polyimide films

The second approach was a vacuum setup with polyimide (PI) films. The PI was selected because of its high heat resistance of up to 400 °C. It has already been used in other publications as support or separation film during forming [58, 62]. A vacuum setup with two films and sealing tapes with the laminate in between was made (see Fig. 3-22). Using a Teflon tube and vacuum pump the air was removed to generate a vacuum, which was maintained during the whole process. In doing so, the heat conduction between the plies was improved and the tapes were prevented of bulging during heating. Slange et al. [151] also stated that an improved thermal contact reduces the heating time. This approach is similar to a double-diaphragm process. Due to the setup, the laminate could not be clamped directly, but the springs were attached to the films. The films were coated with release agent to ensure that they could be removed after forming. Films with 0.05 µm and 0.125 µm thickness were used for the experiments. The approach was first tested and optimised while pressing flat plates and subsequently four parts were formed with the thinner films and two parts with the thicker ones. In contrast to the previous experiments, three springs on each side were used to reduce the sag of the laminate during heating, as the sagging was causing wrinkling of the PI films.
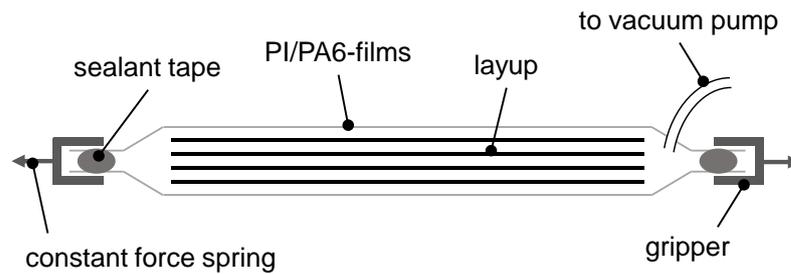
Fig. 3-22. **Schematic illustration of the vacuum setup**

Approach C (denoted PA): vacuum setup with polyamide 6 films

The third approach also involved a vacuum setup, but in contrast to approach B, PA6 films were utilised. The goal was to create the same effect as with the PI films until the melting temperature was reached and without having the problems of the PI. The PA6 films could form with the laminate and blend with the matrix of the tape material. In addition to the setup, which was already used for the PI films, aluminium foil was applied to shield the edge areas of the PA6 films during heating. Otherwise, the vacuum could collapse or the clamps would be pulled off. Two clamps and springs on each side were used, similar to the standard formed parts and the US approach. Films with a thickness of 0.2 mm were used for the pre-tests with the flat moulds. For the forming experiments, five parts were formed using the 0.2 mm film and six parts using a thinner foil of only 0.05 mm thickness. The thinner films were more difficult to handle and with two parts they ripped during forming, whereby the controlled guidance of the material could not be ensured. Despite that, both film thicknesses worked well.

3.3.3   Evaluation of the parts

After the forming experiments, the quality of the flat plates and formed parts was studied using a number of methods. The focus was on the presence of wrinkles, fibre waviness, gaps or voids within the material. Besides this, the thickness and fibre volume fraction were determined.

3.3.3.1   Optical evaluation

On the surfaces of the plates and parts of the US approach several gaps between the former tapes were visible. The plates of the PI approach revealed a very high surface quality that was even better than the one of the standard plates. The results from the formed parts showed that the PI films were prone to wrinkling because of their inextensibility. These wrinkles were pressed into the surface of the layups and caused deep cuts. The additional PA6 film could clearly be seen on the plates of the PA approach. Some inhomogeneities were present that were caused by uneven distribution of the matrix material during pressing and cooling. On the tip of the formed parts a rough area existed, which was due to the thinning of the material. Additionally, on the

bottom of the geometry matrix agglomerations were present. These effects were less distinctive with the thinner PA6 film.

3.3.3.2   Thickness, fibre volume fraction and void content

As a first indication of the consolidation quality of the parts, the thickness was measured at 13 points using an external measuring gauge. The measuring points of the flat plates were evenly distributed over the whole area. A random thickness distribution with only small standard deviations could be detected. The mean values of the measured plates are shown in Fig. 3-23.
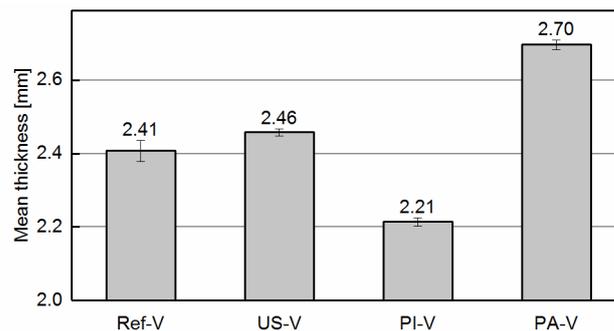
Fig. 3-23.   **Mean thicknesses of the flat plates**

The thickness value of the standard consolidated plates (Ref-V) is the mean of all eleven manufactured plates. The other values only represent one plate. It can be seen that the plate manufactured with the additional ultrasonic spots is thicker than the reference, whereas the PI approach plate is thinner. The plate pressed with additional PA6 films is obviously thicker, which could be explained by the extra 0.2 mm film on both sides. Subtracting this, the thickness is between the standard plates and the PI plate.

In addition, the thickness of the formed parts was measured at the tip and at four heights of the cone (see Fig. 3-24). The measuring points of zone 1 are still in the area of the radius of the tip. The measurements were made along the 0° and 90° directions.
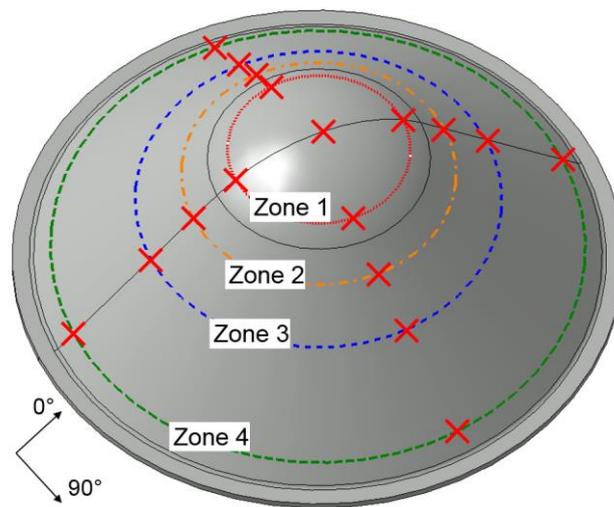
Fig. 3-24.   Thickness measuring points on the cone

A magnetic thickness measuring gauge (MagnaMike 8600 of Olympus) was used for the measurements. The mean of the thickness measurements of the different parts is shown in Fig. 3-25. PA-H1 was formed using the thicker PA6 film and PA-H2 the thinner one. PI-H1 and PI-H2 were formed with the thinner and thicker PI film, respectively. All manufactured parts were considered in the evaluation.
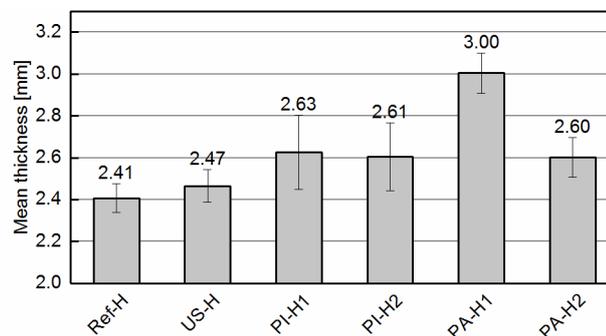
Fig. 3-25.   Mean thicknesses of formed parts

It can be seen that all parts are thicker than the standard formed parts (Ref-H), with the closest being the one with additional US welding spots. However, the thickness of the PA6 films must be subtracted again in order to make the results comparable. In Fig. 3-26, the thicknesses of the different measuring zones are shown. The thickest area of the parts is around zone 2 close to the tip radius, except for the thicker PA6 film where it is at zone 1. The thinning of the material at the tip of the cone, which was observed for all parts, could be referred to tensioning of the fibres over the geometry during forming. Thus, the outer plies were compacting the lower ones and matrix was squeezed to the area around the tip. Due to the matched metal moulds with a cavity height of 2.4 mm, different geometrical conditions resulted for the parts with the thicker PA6 films (PA-H1). As through the thicker material the moulds could not be

fully closed, the cavity at the tip was larger than on the lower areas (zone 2-4) causing the observed deviating thickness distribution.
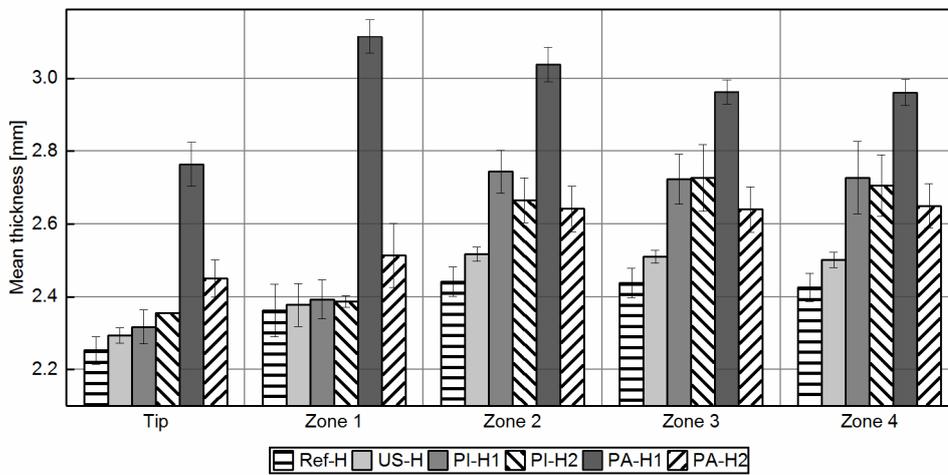
Fig. 3-26.   Thickness distribution over the cone geometry

To get a better impression of the inner laminate quality, the fibre volume fraction (FVF) and void volume content (VVC) were determined using the procedure described in DIN EN 2464 [152]. Three specimens of each plate and formed part were separated and used for the measurement.

Looking at the results of the flat plates (see Fig. 3-27), it can be seen that the highest FVF and lowest VVC were achieved for the standard consolidated plates. The values of the US and PI approach plate are almost the same with approx. two percentage points lower FVF and a VVC that was roughly one percentage point higher. The PA approach plate has the lowest FVF due to the additional matrix material, but the void content is comparable to the others.
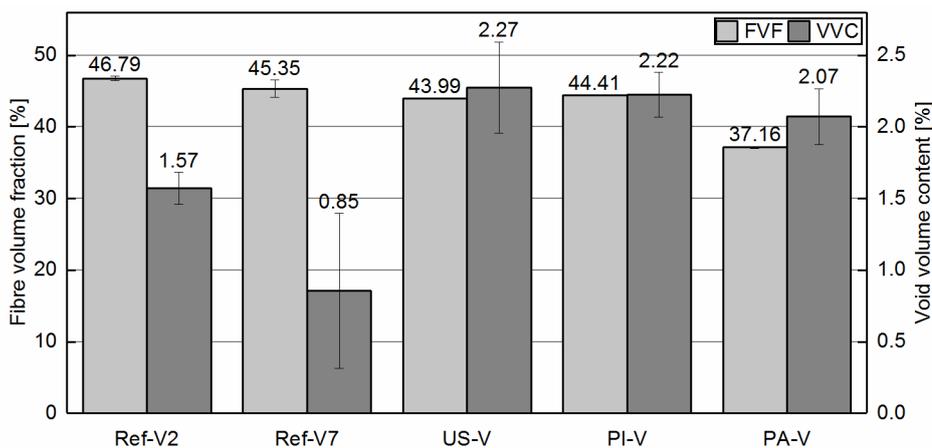
Fig. 3-27.   Fibre volume fraction and void content of the plates

The measurements of the formed parts (see Fig. 3-28) follow the trend of the flat plates. The highest FVF was achieved with the standard formed part, which is even

higher than the one of the standard plate. Besides this the VVC is lower, at only 0.25%. The US approach part shows an almost 4% lower FVF and the highest void content. The FVF of the PI approach part (PI-H1) is on the same level, again with a very low void content of 0.53%. The FVF is even higher with the thicker PI films (PI-H2). The reason could be the higher total thickness and the consequently higher compaction of the material. As regards the PA approach, two film thicknesses were also investigated. The FVF of the part manufactured with the thicker film (PA-H1) is relatively low, as had previously been expected, whereas the part with the thinner films (PA-H2) has a FVF comparable to the US and the thicker PI part.
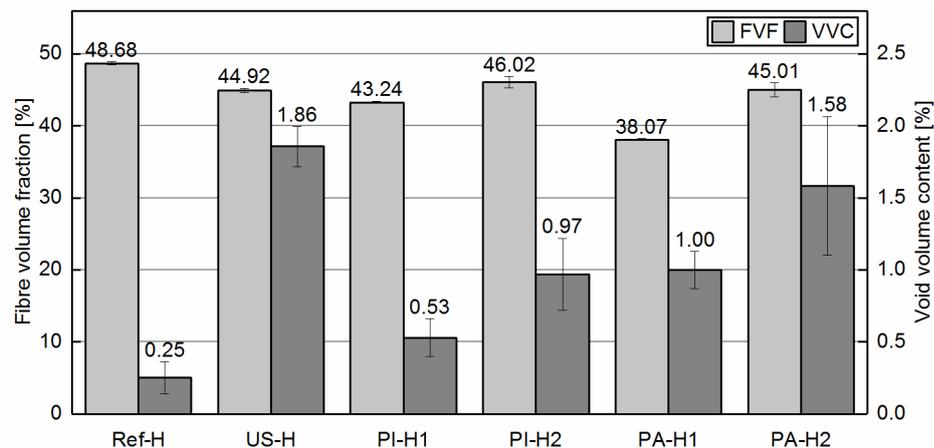
Fig. 3-28.   **Fibre volume fraction and void content of formed parts**

Local variations are possible as the FVF and VVC measurements only give information about small areas of the parts investigated.

3.3.3.3 Thermography

Another procedure for evaluating inner part quality is thermography. The lock-in thermography is based on the excitation with a sinusoidal modulated heat source. The thermal waves enter into the specimen and are reflected by defects or inclusions with a different thermal conductivity. Through the overlay of the thermal waves on the surface of the specimen a locally varying temperature emerges that can be captured by an IR camera. [153, 154] The possible measuring depth depends on the modulation frequency of the heating, which has to be adjusted according to the application. As for the evaluation the time shift between the heating and the temperature on the surface is used, influences of surface structures can be supressed. With the help of the lock-in thermography a fast non-destructive analysis of large parts is possible. [155]

Within this study lock-in thermography with halogen lamps was used to detect possible pores or delaminations in the parts. The measurements were made with the OTvis 4000 lock-in thermography module of EDEVIS in combination with the high-speed IR camera FLIR X8400sc.

Both flat plates and the formed parts were analysed. The region of interest with a size of 500 px x 500 px was positioned in the middle of the plates. Measurements were taken from both sides. The excitation frequency was varied between 0.02 Hz and 0.3 Hz, with a frequency of 0.07 Hz yielding the best results. The pictures of the front of the different plates are shown in Fig. 3-29.

(a)   (b)

(c)   (d)
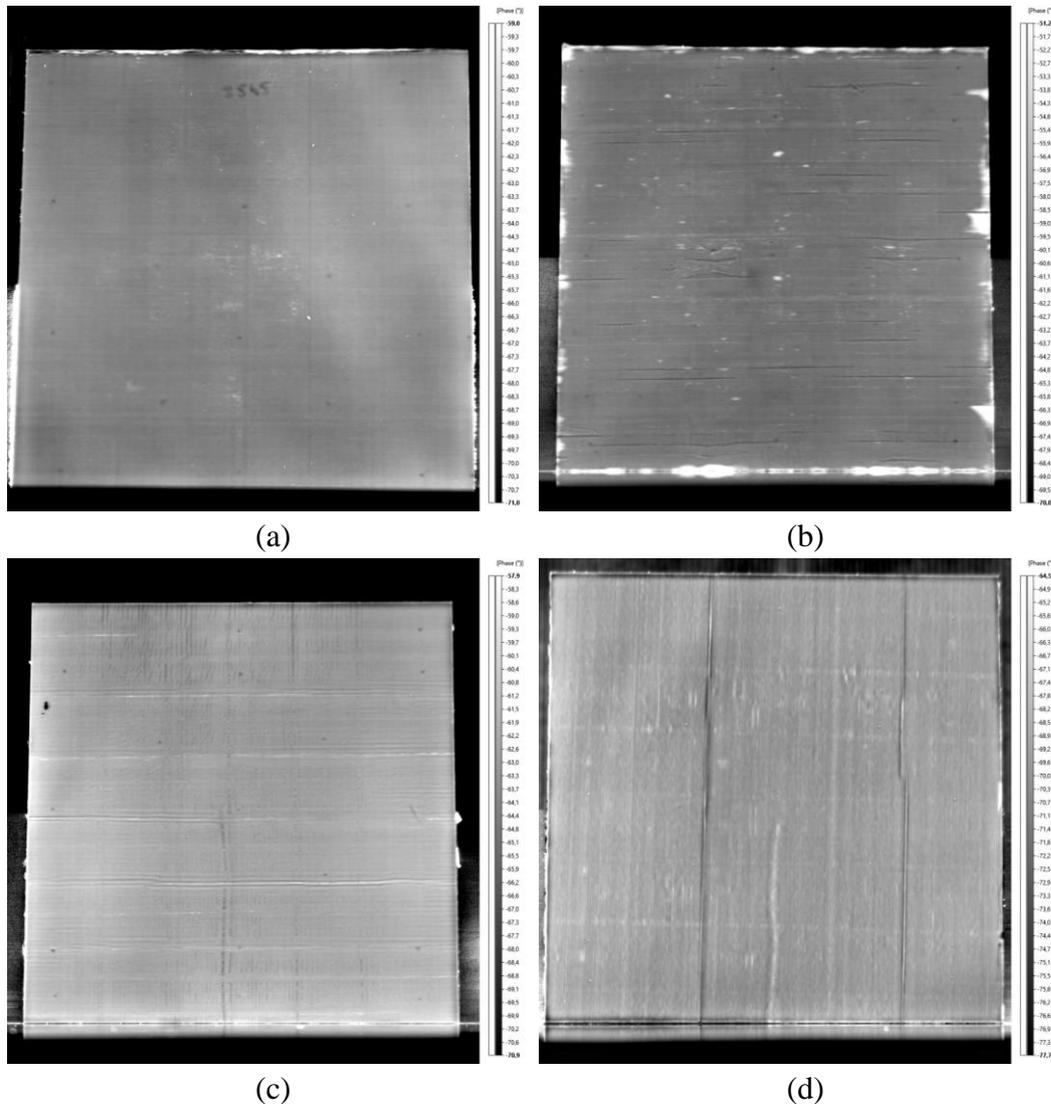
Fig. 3-29.   Thermography pictures of the flat plates at 0.07 Hz
           (a) Standard consolidated plate Ref-V, (b) US plate US-V, (c) PI film plate PI-V, (d) PA6
           film plate PA-V

Examining the pictures, some obvious differences can be determined. The standard plate (see Fig. 3-29a) reveals a high quality with almost no inhomogeneities within the material. The fibres are clearly visible and some of the tapes can still be distinguished. The brighter spots and the small amount of inhomogeneity are due to defects on the surface and reflections of the glossy surface. In contrast, the US approach plate (see Fig. 3-29b) shows obvious inhomogeneities and deviating fibre courses. In addition to

the gaps between adjacent tapes on the surface, brighter spots that might be voids or pores inside the laminate are also visible. However, the image of the PI approach plate (see Fig. 3-29c) depicts a laminate quality comparable to the standard plate. Some brighter horizontal lines are visible, resulting from folds in the PI film on the surface. The darker vertical line in the lower half is caused by the embedded thermocouple. On the thermograph picture of the PA approach plate (see Fig. 3-29d) the thermocouple and two vertical folds of the film can also be seen. In addition, some small brighter areas are present, which could indicate entrapped air or inhomogeneities on the surface. As only deviations in thermal conductivity could be detected by thermography, additional examinations, such as microsections, must be performed. Nevertheless, a good correlation with the void content measurements can be seen.

To analyse the influence of the forming on the inner laminate quality, the formed parts were also measured using the thermography system. The resulting images of the top-view are shown in Fig. 3-30. Parts with a thicker PI film and a thinner PA6 film were also included.
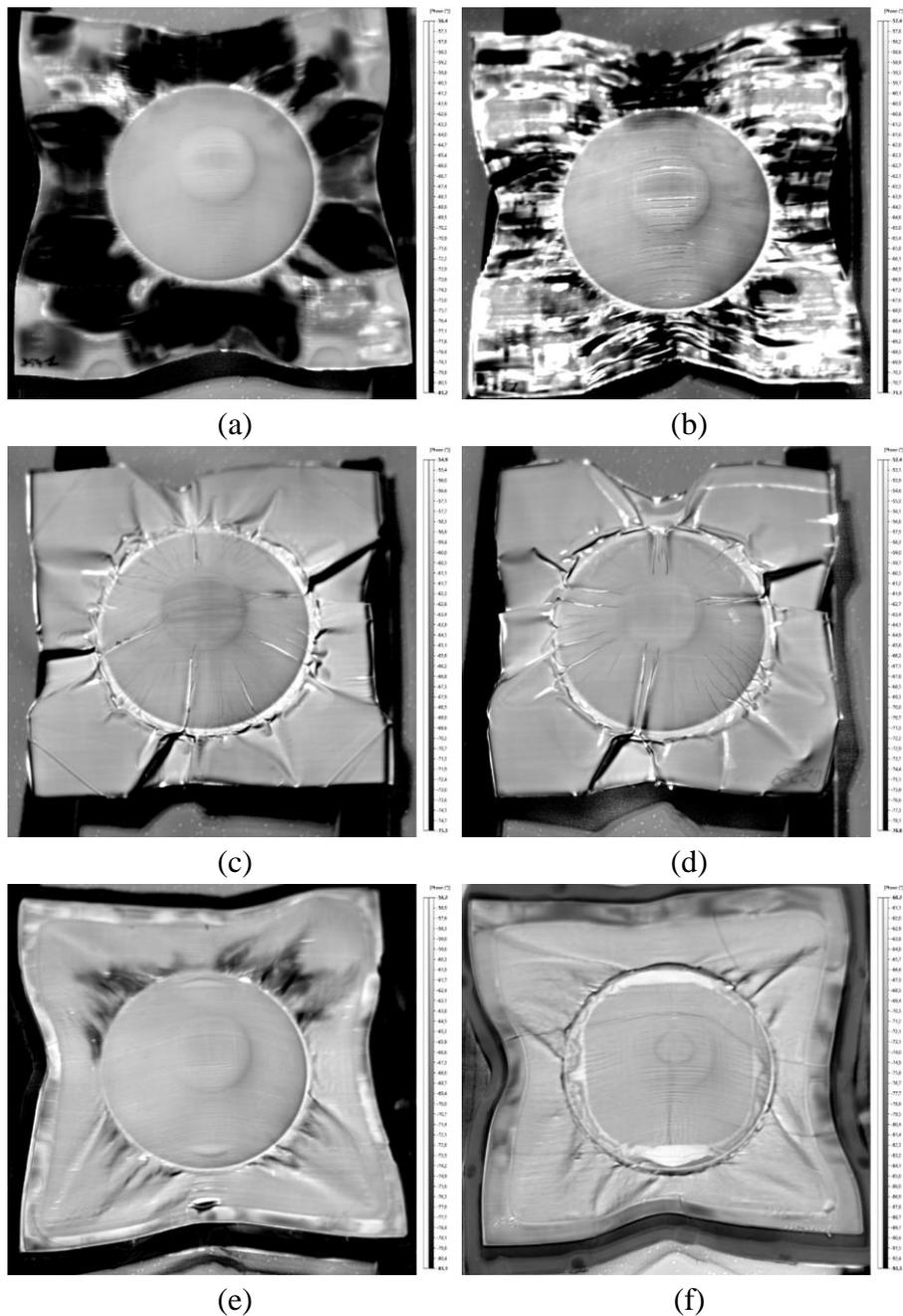
Fig. 3-30.   Top-view thermography pictures of the formed parts at 0.07 Hz
(a) Standard formed part Ref-H, (b) US approach part US-H, (c) PI approach part with
thin PI film PI-H1, (d) PI approach part with thick PI film PI-H2, (e) PA approach part
with thin PA6 film PA-H2, (f) PA approach part with thick PA6 film PA6-H1

A dark ring around the tip of all parts can be observed, only the part with the thicker
PA6 film has a ring closer to the tip. This corresponds with the thickness measurement,
which revealed a thicker laminate in the respective areas (see Fig. 3-26). The picture of
the standard formed part (see Fig. 3-30a) shows a very homogeneous laminate in the
area of the cone. Despite that, no abnormalities are present. Similar to the image of the

flat plate, the formed part based on the US approach (see Fig. 3-30b) reveals gaps between the tapes, fibre distortions and inclusions in the laminate. The thermography of both PI approach parts points out the depth of the folds in the PI films (see Fig. 3-30c and d). Despite this, both parts reveal a high laminate quality. The same can be stated for the part formed with the thin PA6 film (see Fig. 3-30e). Almost no inhomogeneities are present. In contrast, the thicker PA6 film part is very inhomogeneous around the bottom of the cone (see Fig. 3-30f). The brighter areas might be the result of accumulated matrix material.

The thermography images provide a good impression of the homogeneity of the laminates, fibre deviations and possible inclusions in the material. However, it is necessary to correlate the results with other measurements in order to validate the assumptions.

3.3.3.4 Microsections

Using thermography, an overall analysis of inner part quality was possible. To get a better impression of potential defects in the laminate and their distribution over the thickness, microsections of selected areas of the flat plates and formed parts were made. The positions of the specimens are shown in Fig. 3-31.
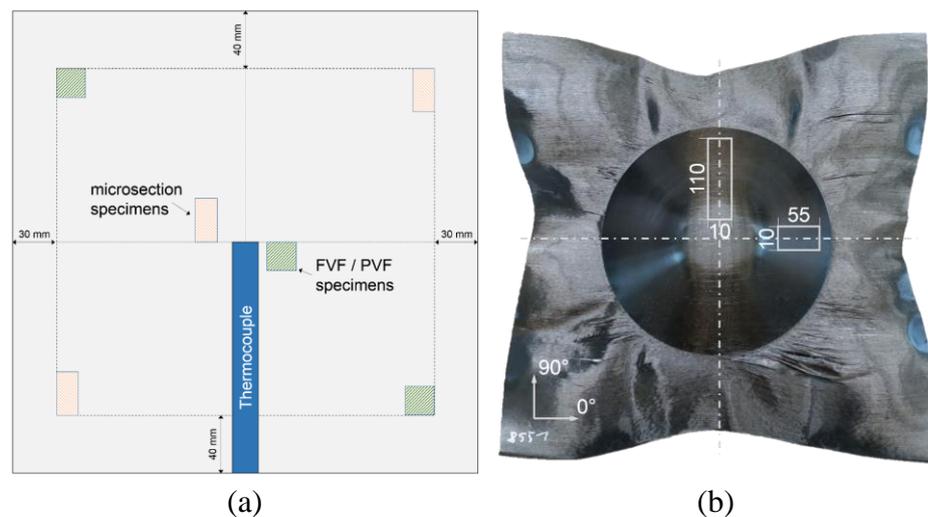
Fig. 3-31.   **Positions of the specimens**
              (a) flat plates, (b) formed cone

For a better interpretation of the laminate quality, also a micrograph of the original tape material was created (see Fig. 3-32). The image shows an even fibre distribution and certain not fully saturated fibre bundles.
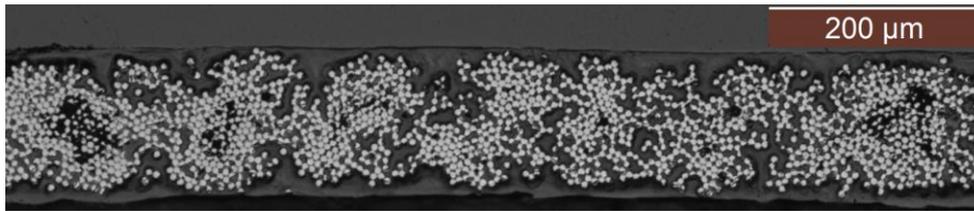
Fig. 3-32.   Microsection of original tape material

Samples of several plates and formed parts were taken and analysed for every approach. Representative images are presented hereinafter.

Flat plates

The microsections of the reference plates (see Fig. 3-33) reveal a good laminate quality with no fibre deviations in the laminate or gaps on the surface. However, single pores can be found and some fibre bundles are not fully saturated, which was also present in the original tape. The results show good correlation with the thermography measurements.

(a)   (b)

(c)
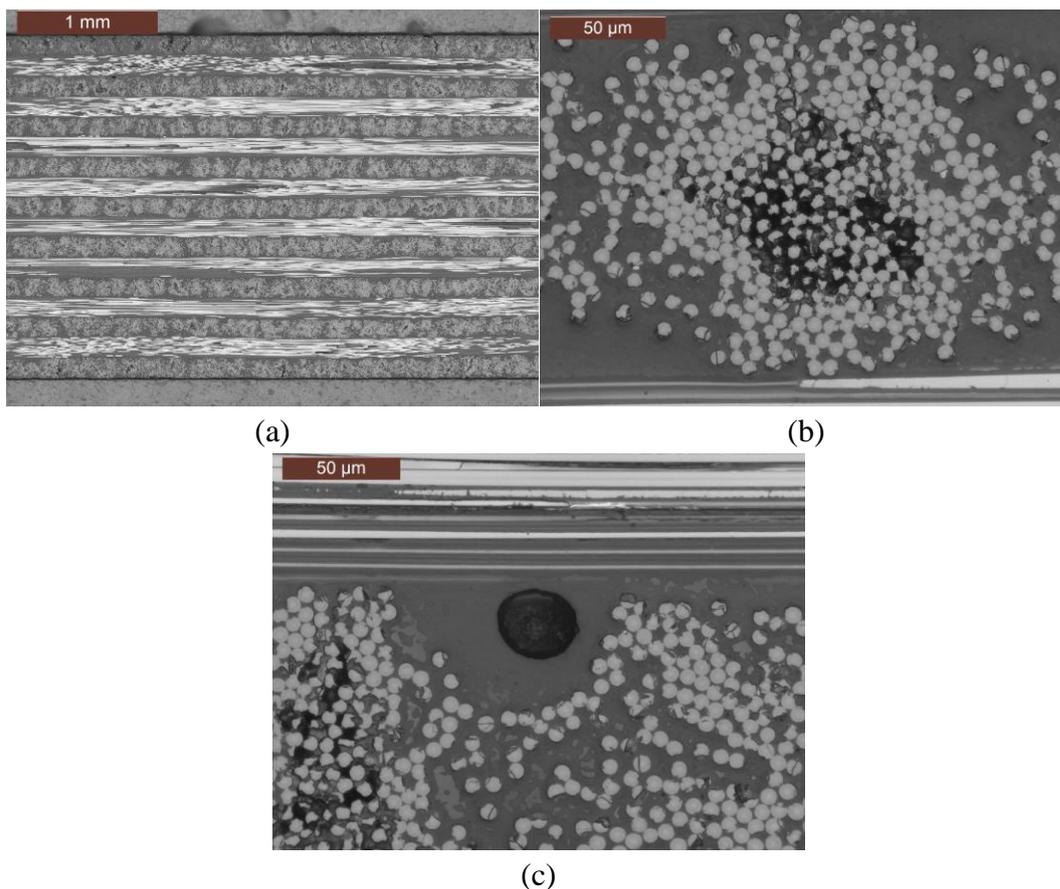
Fig. 3-33.   Microsections of standard consolidated plate Ref-V
                    (a) overview of the laminate, (b) unsaturated fibre bundle, (c) void within the laminate

The results of the US approach plates show a worse laminate quality (see Fig. 3-34). Beside some unsaturated fibre bundles, pores at the interface layers between the plies are present indicating poor consolidation. The outer plies in particular are not fully fused with the adjacent plies in the area of the tape edges, causing gaps on the surface and fibre waviness of the adjacent plies. The gaps were also visible on the thermography pictures (see Fig. 3-29b). These results agree well with the void content measurements.

(a)   (b)

(c)   (d)
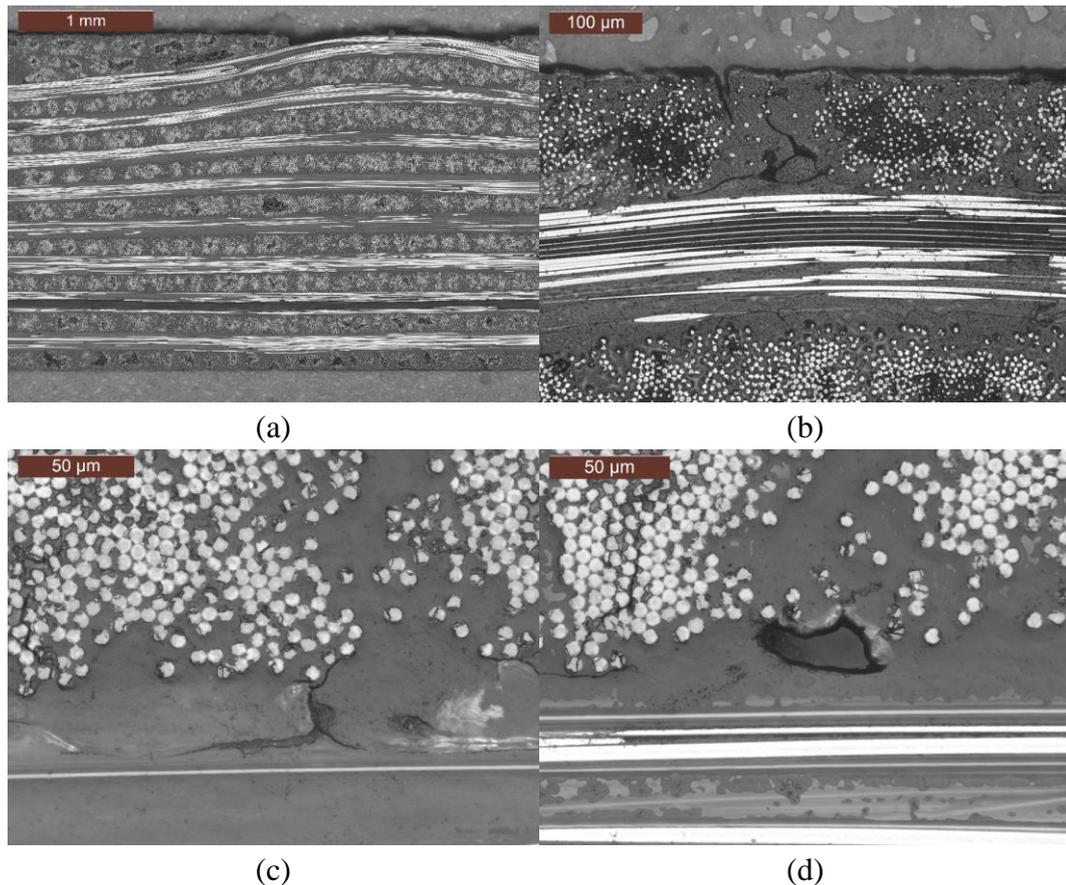
Fig. 3-34.   Microsections of plate with additional ultrasonic spot-welds US-V
(a) overview of the laminate with surface gap and bend plies, (b) tape edges that are not fused, (c) gap at the interface between plies, (d) void within the laminate

The vacuum setup with PI films produces plates with a high laminate quality (see Fig. 3-35). No pores can be found within the laminate and most fibre bundles are fully impregnated. Nevertheless, some fibre waviness can be seen, which might be caused by folds in the PI film.
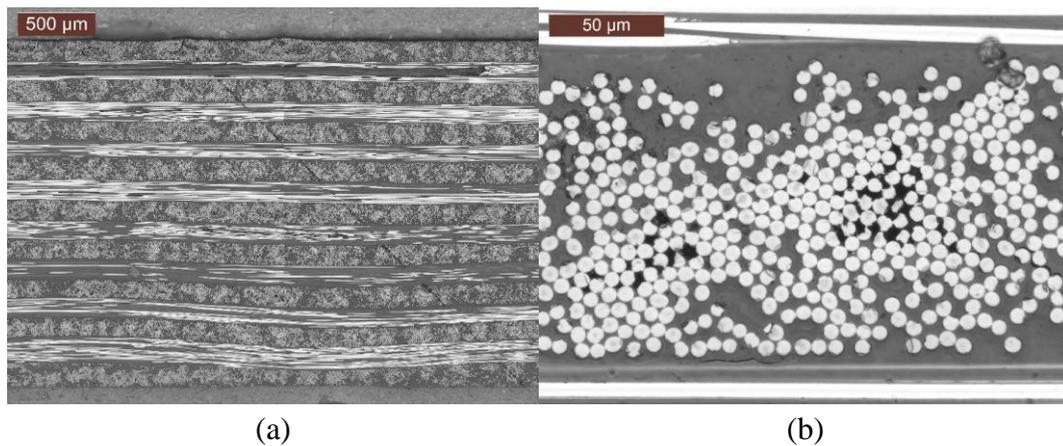
Fig. 3-35.   **Microsections of plate pressed with PI films PI-V**
                   (a) overview of the laminate with slightly bent plies, (b) well saturated fibre bundle

Looking at the microsections of the PA approach plate (see Fig. 3-36a), the pure polymer layer with an initial thickness of 0.2 mm can clearly be seen. Through pressing and matrix flow, the thickness is reduced to 0.18 mm. The additional plies are fully fused with the rest of the laminate. No fibre waviness or pores are present in the examined areas, but some fibre bundles are not completely saturated.
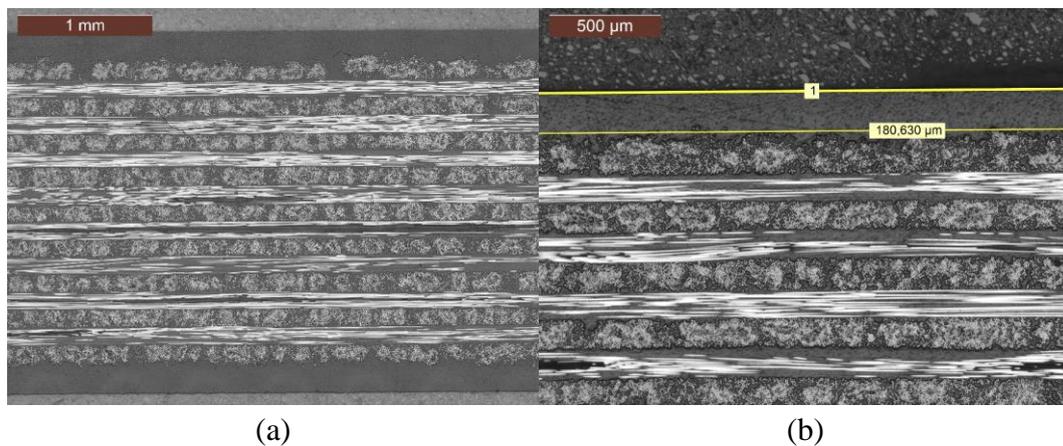
Fig. 3-36.   **Microsections of plate pressed with PA6 films PA-V**
                   (a) overview of the laminate with additional matrix, (b) close-up of the matrix layer with thickness measurement

Formed 3D parts

The standard formed parts show a good laminate quality (see Fig. 3-37). The fibre bundles are evenly saturated and no voids are present. Only a few micropores can be found and surface gaps are causing fibre waviness of the second ply at one spot.
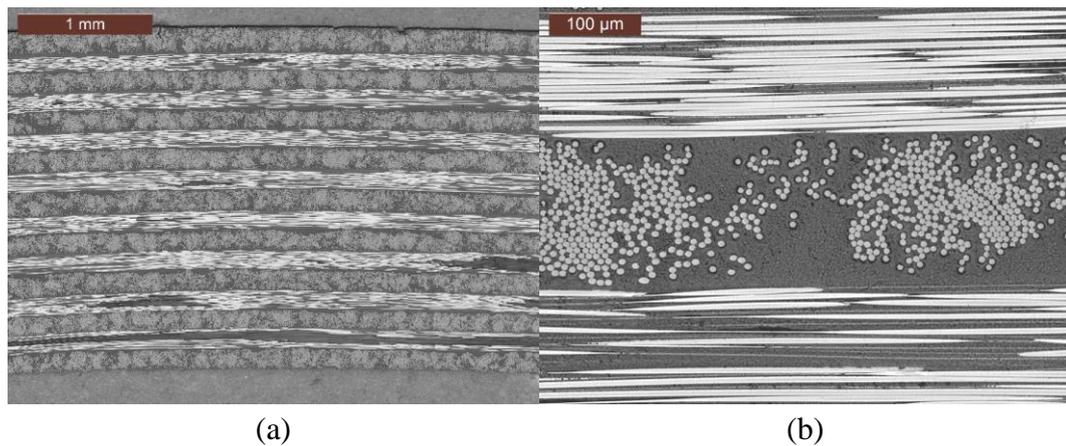
Fig. 3-37.   **Microsections of reference part Ref-H**
(a) overview of the laminate, (b) well saturated fibre bundles and micropores

As in the flat plate, a poor laminate quality can also be seen in the part formed following the US approach (see Fig. 3-38). Some of the outer plies have not fused with the laminate and delaminated areas are present (see Fig. 3-38b). Additionally, polymer aggregations without fibres are visible in the material, as well as some voids. As on the standard formed part gaps on the surface are causing fibre waviness of the lower plies.
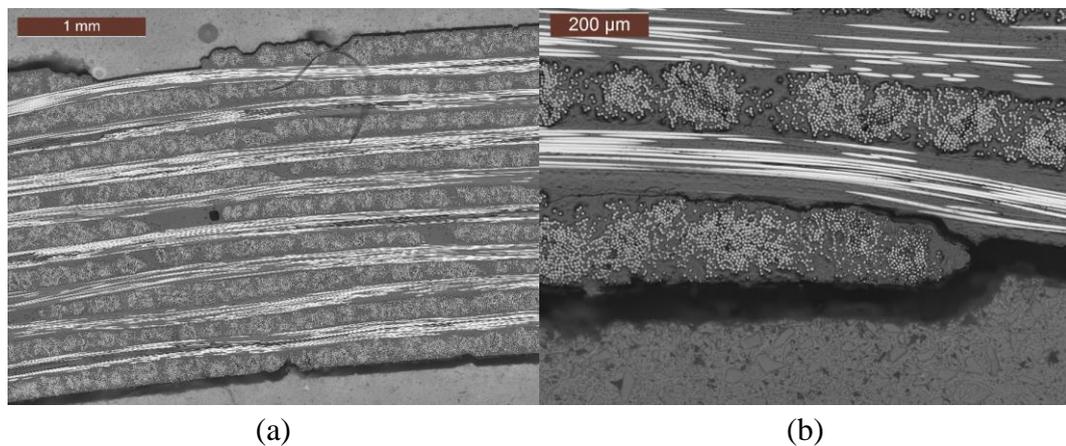
Fig. 3-38.   **Microsections of formed part US-H**
(a) overview of the laminate with surface gap, polymer aggregation and void, (b) bad consolidation of the outer ply

The high laminate quality of the flat plate pressed with the PI vacuum setup could not be reached in the formed part. Regardless of whether thin (0.05 mm) or thick (0.125 mm) PI films are used, the result is governed by the severe wrinkle formation of the PI (see Fig. 3-39 and Fig. 3-40). During forming, the wrinkles were pressed into the laminate causing fibre waviness and large gaps. In addition, polymer agglomerations and microvoids are present. Despite this, most fibre bundles are well saturated.

<center>(a)   (b)</center>
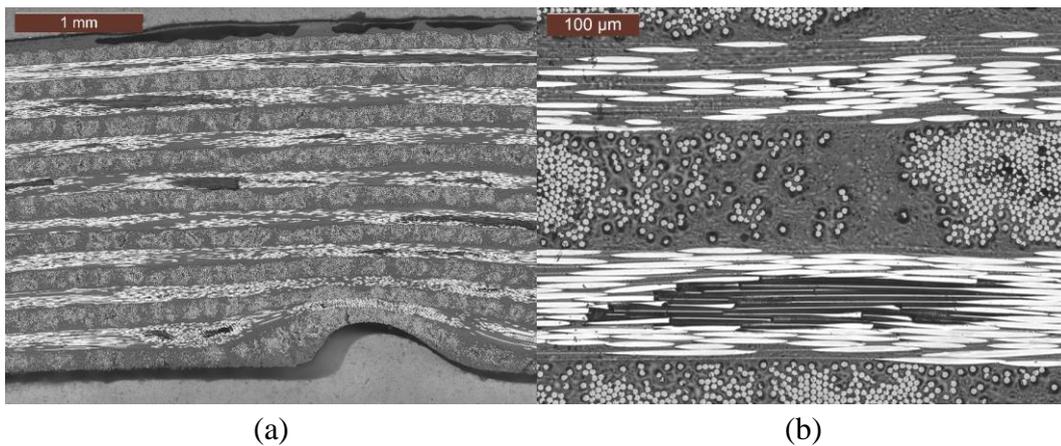
Fig. 3-39.   Microsections of formed part PI-H1
(a) overview of the laminate with polymer agglomeration on the top and fibre waviness caused by the PI film on the bottom, (b) close-up on fibre bundles and micropores in the polymer

<center>(a)   (b)</center>
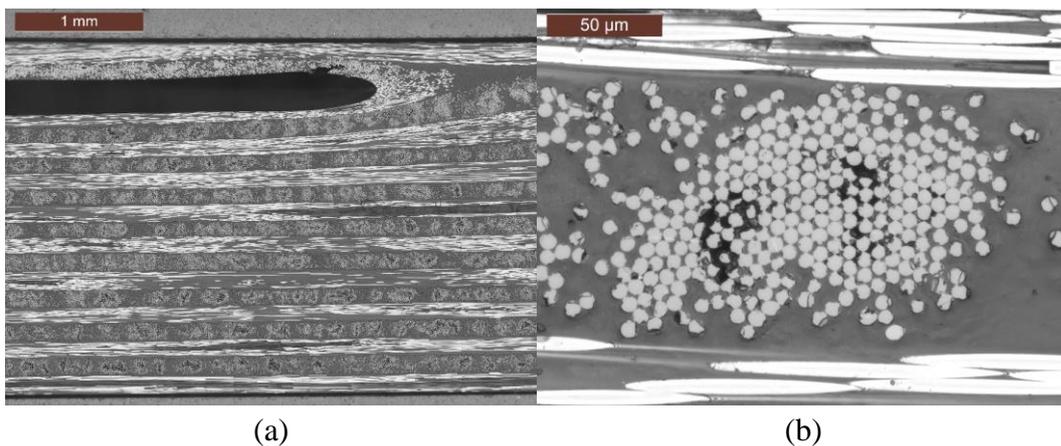
Fig. 3-40.   Microsections of formed part PI-H2
(a) overview of the laminate with large gap, (b) almost fully saturated fibre bundle

The microsection of the parts formed with the PA6 vacuum setup reveal a good laminate quality (see Fig. 3-41 and Fig. 3-42). The fibre bundles are as well saturated as with the other approaches (see Fig. 3-41b). The additional polymer layers are clearly visible when using 0.2 mm thick films. At some spots, the polymer layer and fibres of the first ply are displaced and fibre waviness occurs. Despite this, no abnormalities can be seen.
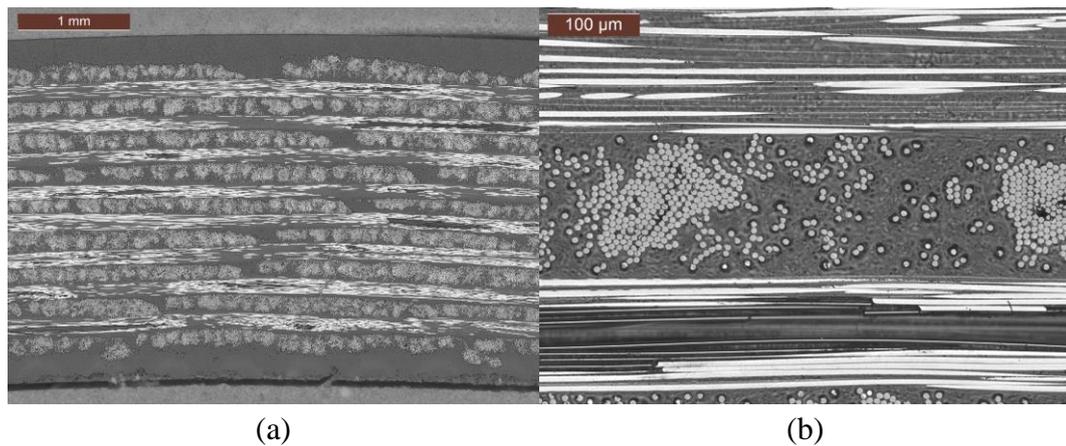
Fig. 3-41.   Microsections of formed part PA-H1 with thick PA6 films
(a) overview of the laminate with clearly visible polymer layers, (b) close-up on fibre bundles with only barely visible pores

The polymer layer of the additional 0.05 mm thick PA6 films is barely visible in the micrographs and has a thickness of about 0.035 mm (see Fig. 3-42). No larger voids can be seen.
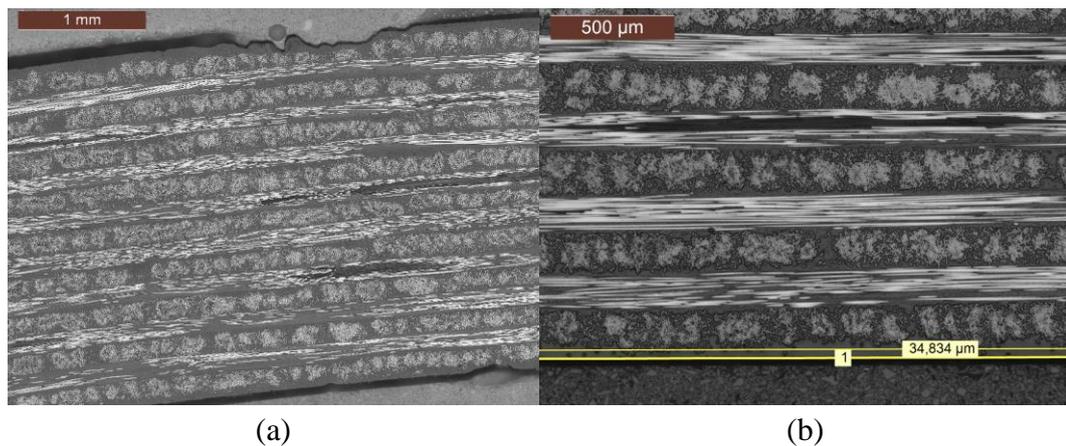
Fig. 3-42.   Microsections of formed part PA-H2 with thin PA6 films
(a) overview of the laminate revealing surface roughness, (b) thickness measurement of the polymer layer

3.3.4 Conclusion

The forming of unconsolidated US spot-welded thermoplastic CF/PA6 layups was studied. Approaches were developed and evaluated to cope with the challenges that arose within the process. Flat pressed plates and formed parts were compared in terms of inner laminate quality. Thickness, fibre volume fraction and void content were analysed and thermography measurements and microsections were conducted.

The additional welding spots of the US approach improved the heatability of the layup but the investigations into laminate quality revealed the highest void content and poor

consolidated areas. A lot of inhomogeneities were present on the thermography pictures, which could be identified as entrapped air and not fused tapes. Using the presented process chain, additional welding spots are not sufficient for producing flawless parts without previous consolidation.

The PI approach revealed a high laminate quality of the flat plates with a very even surface and fewest pores within the material. The vacuum reduced the deconsolidation of the material during heat up and the lowest thickness of the pressed plates was achieved. Nevertheless, due to the lack of elasticity of the PI films, large wrinkles occurred during forming, which caused deep folds within the material. Preparation of the laminates was also very time-consuming, the films can be used only once, and the material is rather expensive with 18-30 €/m².

The vacuum setup with PA6 films also produced flat and 3D parts with few voids and a good surface quality. Through the additional matrix material, the FVF was reduced, depending on the thickness of the PA6 films. The use of the thinner PA6 film with 0.05 mm thickness was assumed to be especially promising. In addition to a processability of unconsolidated layups, the added matrix on the surface could improve the weldability with other thermoplastic or metal parts [156]. The setup with sealing tape was rather time-consuming because of the manual cutting and preparation, but the price of the PA6 film with 0.50 €/m² is significantly lower than the PI.

As further improvement, welded vacuum bags could be used, which would also allow automated processing. Also the influence of the indirect clamping has to be investigated in further studies. The focus of this study was on the comparison of different approaches using constant process parameters. By adapting the process parameters, such as the pre-heating temperature, tool temperature or the pressing force, the part quality might be improved further. The vacuums setup with thin PA6 films produced high quality parts without the necessity of a time- and energy-intensive consolidation step.

3.4 Summary and discussion

Three experimental studies on the forming of UD fibre reinforced thermoplastics were conducted. The entire layups for the forming studies were produced using a Fiberforge RELAY2000 ATL machine. Within these studies the complexity of the forming tools as well as the used materials were varied.

Using a simple radius forming, the influence of pre-tensioning, fibre orientation and radius sizes was investigated with CF/PEEK. The results showed that depending on the configuration radius thinning and fibre waviness close to the radius section occurred. The thinning emerged especially with a smaller inner radius. Hubert and Poursartip [133] also observed a thinning behaviour for thermoset prepreg and a convex radius tool. The wrinkling of thermoset prepreg was also investigated by Potter [64]. The author stated a correlation between forming speed, temperature and wrinkle formation. In the described study the wrinkling was dependant on the applied pre-tension of the

support frame. Within the investigated range a higher pre-tension reduced the wrinkling tendency.

The second study focused on the forming of a complex geometry. The influence of the process parameters tool temperature, forming speed, forming pressure, support frame configuration and spring force on the part quality of UD GF/PP parts was examined. The quality was evaluated based on four forming effects: out-of-plane wrinkles, in-plane undulations, surface quality and surface gaps. In this study also an influence of the pre-tensioning on the emergence of undulations and wrinkles was detected. A higher number of springs reduced the quantity of these defects. Additionally, higher levels of tool temperature, forming speed and forming pressure improved the part quality. The reason is that especially higher tool temperatures and forming speeds prevent an excessive cooling of the laminate before the forming is completed. The higher forming pressure generates a flat and even surface. Obviously, there are limits to the observed behaviour. Further rising the tool temperature would extend the cooling time and cause increasing matrix flow. With higher forming speeds the formability might be reduced due to possible shear thickening of the matrix. A too high forming pressure could also induce matrix flow or even cause fibre breakage.

After the experiments with GF/PP also laminates of CF/PEEK were formed with the complex geometry. It was shown that the process temperatures of the radius forming study could not directly be transferred. Significant pre-heating and tool temperature rises were necessary to achieve satisfying results. The reason could be the longer handling time of the larger laminate and the higher complexity of the geometry causing more material deformation.

The third experimental study was dedicated to improving the thermoforming process of spot-welded ATL layups. The aim was to exclude the time and energy consuming consolidation step and to directly form spot-welded layups. The consolidation should then be achieved during the forming step. The study was performed with CF/PA6 UD tape. Three different approaches were developed to facilitate the forming without previous consolidation: application of additional welding spots to improve the cohesion and heat transfer of the layup, a vacuum setup with PI films to remove the air prior to forming and achieve a good consolidation during forming and a vacuum setup with PA6 films. The third approach showed promising results. Part qualities comparable to consolidated laminates could be achieved. The part quality was ascertained via optical inspection, microsections, thermography, FVF and VVC measurements. The approach revealed to be a valuable alternative to the common consolidation process. As drawbacks the additional steps for the preparation of the vacuum setup and the remaining PA6 films on the surface of the final parts must be mentioned.

4 Numerical studies

Besides the described experimental studies regarding the forming behaviour of fibre reinforced thermoplastics the second focus of this thesis was on the forming simulation of the respective materials. As consistent material data are significantly important for reliable simulation results, the first part of this chapter is dedicated to the development and application of material characterisation methods (chapter 4.1). Based on the measured material data, forming simulations accompanying the experimental studies were performed (chapter 4.3) and were validated using the experimental results (chapter 4.4).

4.1 Material characterisation

The aim of the material characterisation is to determine the material behaviour regarding the most relevant forming mechanisms and the input parameters for the FE forming simulation. The characterisation must be performed under environmental conditions and should be as similar as possible to those carried out in real-world forming processes.

As there are no standardised characterisation tests available, new tests have to be developed or test methods proposed by other researchers applied. In doing so, it is necessary that the test methods provide reproducible results for measurements above the melting temperature of FRTP.

4.1.1 Friction

The literature review showed (see chapter 2.2.2) that several test setups for the characterisation of ply/ply and tool/ply interface properties have been developed. All test stands have in common that a custom-made device is necessary. Hence it was concluded that designing a test setup for characterisation under varying testing conditions is vital.

4.1.1.1 Development of a friction test stand

Based on the literature review it was decided to design a friction test stand using the pull-out (PO) as well as the pull-through (PT) principle. In either case one specimen is situated in between two other specimens. In that way it is possible to compare the results of both test methods and to also combine the advantages. In addition to the test principles the following requirements were specified:

1. Test stand should be mounted in the universal testing machine

2. Temperature-resistant up to 400 °C to be able to measure high temperature thermoplastics
3. Different fibre orientations possible
4. Testing speed as high as possible (stamp closing speed ~3600 mm/min)
5. Easy preparation of the samples
6. Simple handling
7. Variation of the normal force

The development of the friction test stand was mostly conducted as part of the scope of [S1].

The test stand should be mounted in the thermal chamber of a universal testing machine to be heated to the desired temperature. As a result, there was only limited installation space for the test stand. Taking this into account as well as the advantage of using weights to adjust the normal force, a horizontal testing plane was chosen. Hence it was necessary to redirect the pulling force to the vertical working direction of the testing machine. The following figure shows the first draft of the test stand.
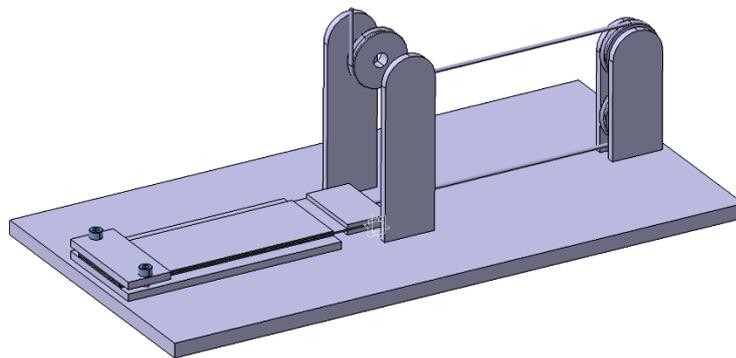
Fig. 4-1.   Draft of the friction test stand
        Illustration of the concept of a horizontal testing plane and vertical pulling direction

Based on this draft the concept was developed further. As illustrated, the redirection of the rope was realised by pulleys. But in contrast to the first draft only two pulleys were used with one being oriented horizontally. The advantages of this assembly are a lower height of the test stand and fewer parts. To reduce the friction of the redirection the pulleys were mounted on ball bearings. Because of the potential high testing temperatures ceramic bearings (type 6001 of Sturm Präzision GmbH [157]) were used. Hence the universal testing machine could only perform testing speeds up to 600 mm/min, which is much lower than actual forming speeds, a transmission was included in the testing stand. With a gear transmission ratio of two a doubling of the testing speed could be achieved. For that purpose, a pulley with two diameters was designed (see Fig. 4-2). To use the transmission, one rope is mounted between the testing machine and the smaller diameter and another rope between the larger diameter and the pulling clamp.
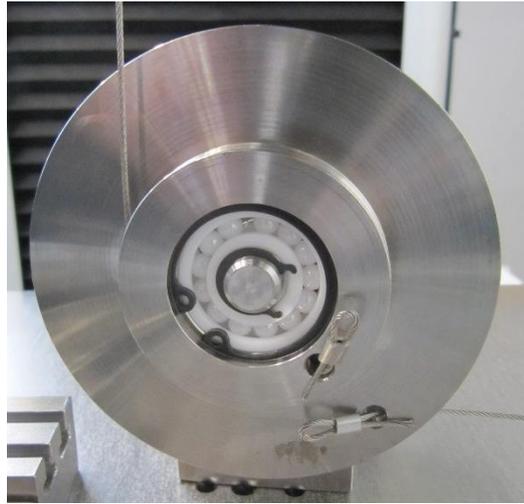
Fig. 4-2.   **Transmission pulley with two diameters**

For an optimal connection between the testing machine and the pulling clamp different materials and rope sizes were tested. Steel wire cables were initially favoured, but they were not ideal because of their stiffness and problems clamping them. Instead, an aramid rope showed an easy handling with good temperature stability and was thus selected for the experiments.

As already mentioned, different fibre orientations should be measured, which required different clamping positions. The middle specimens always need 0°-fibres in pulling direction, which is why the outer specimens have to be oriented accordingly and be clamped on the side in the respective position. As far as possible the specimens must be clamped in fibre direction to avoid warpage and displacement of the material. The clamping of the outer plies was conducted by quick release clamps, the inner ply by contrast was clamped using bolts. Depending on the investigated fibre orientations and used testing principle, different setups of the test stand have to be implemented. The following figure shows the clamping position and specimen geometry for all possible configurations.
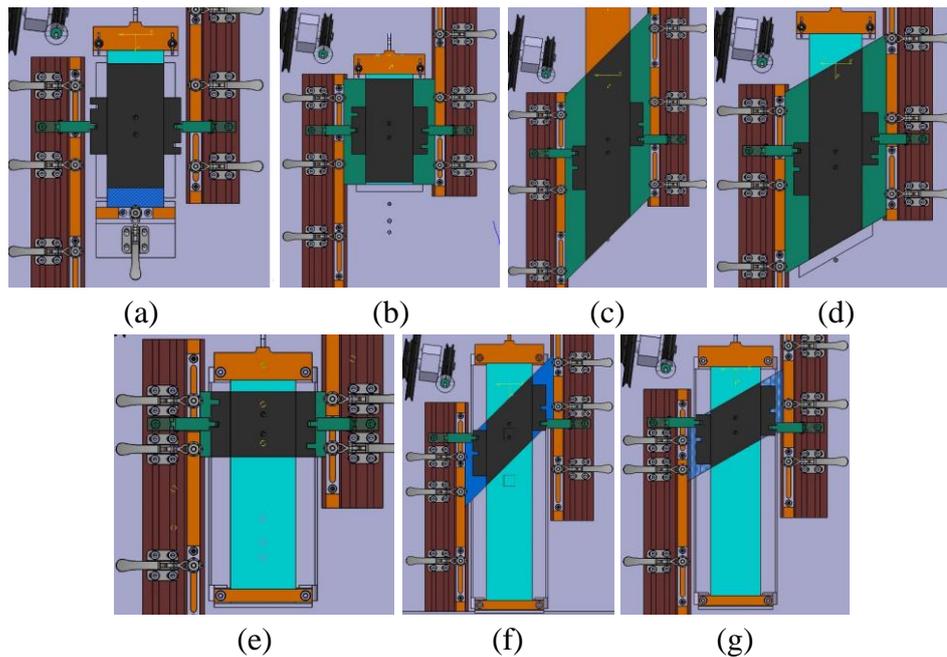
Fig. 4-3.   **Setup for different fibre orientations**
(a) PO0/0, (b) PO0/90, (c) PO0/45, (d) PO0/60, (e) PT0/90, (f) PT0/45, (g) PT0/60

As seen in Fig. 4-3 the different setups lead to different sizes of the testing area. The reason is that a test length of at least 100 mm should always be achieved, which leads to various sizes given the combination with different fibre orientations. To account for that and ensure a clearly defined force application for every setup a fitted basis below the plies and pressure plate were designed. On top of the pressure plate different weights could be positioned to vary the normal force. The weights were centred on the pressure plate using two dowel pins to ensure an even pressure distribution. On the sides of the pressure plate handles were mounted to enable an easier positioning of the plate and to also prevent it from moving during testing. In addition to that the lateral quick release clamps, three on both sides, are relocatable to apply the clamping force on the desired position. Fig. 4-4 shows the final version of the friction test stand in the PT0/90 configuration. All parts were manufactured out of stainless steel.
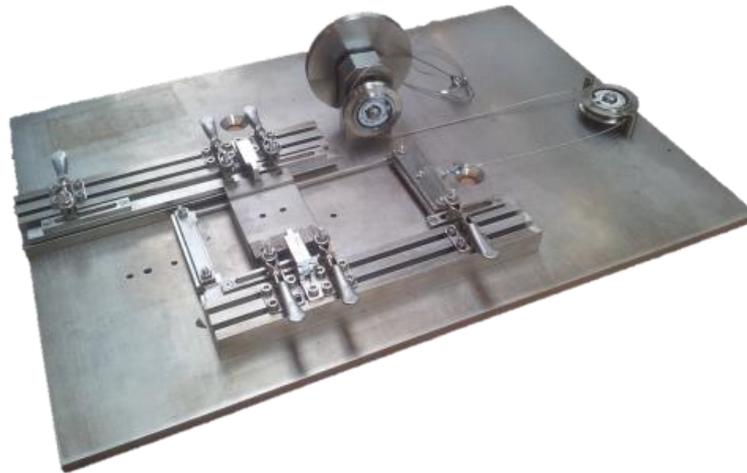
Fig. 4-4.   **Final version of the friction test stand**
            PT0/90 configuration with support frame

During the development and the initial experiments some challenges occurred, which will be described hereinafter:

Tilting of the normal weight during the pull-out tests:

During the PO test the normal weight might tilt at some point causing uneven pressure distribution in the contact plane (see Fig. 4-5a). To avoid this problem two solutions are possible: On the one hand a vertical guidance of the normal weight could avoid the tilting but would also require a complex construction with bearings. On the other hand, a compensation ply that remains at the end of the specimens achieves the same effect with less effort (see Fig. 4-5b), which is why this solution was selected.

(a)   (b)
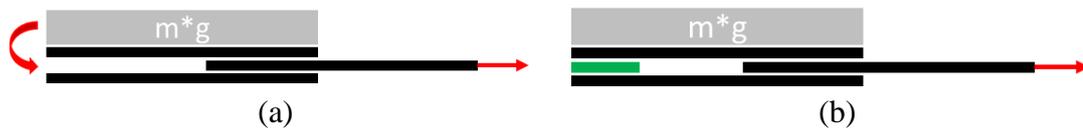
Fig. 4-5.   **Illustration of possible tilting of the normal weight during PO tests**
            (a) Tilting problem when the middle ply gets pulled out, (b) selected solution with
            compensation ply (green)

Since the normal weight during the test is also placed on the compensation ply the actual normal force for the evaluation of the friction test has to be calculated. Based on the torque equilibrium (see Fig. 4-6) the following equation for the actual normal fore F_N results:

$$F_N(u) = mg \frac{l_m - l_1}{l_1 + 2d + l_2 + u}$$

(4-1)

where m is the mass, l_m is the length of the pressure plate, l_1 is the length of the compensation ply, d is the initial gap between the compensation ply and the inner

specimen, l_2 is the length of the inner specimen under the pressure plate and u is the displacement.
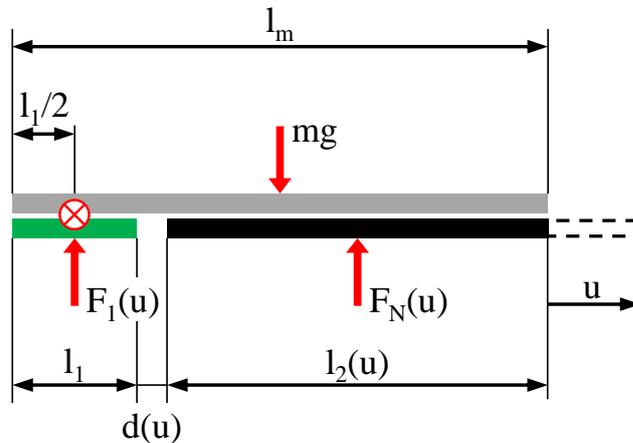
Fig. 4-6.   **Torque equilibrium scheme of the PO setup**
For the calculation of the actual normal force, the force application points are assumed to be in the centres of gravitation

For the calculation of the correct PO friction coefficient the length of the compensation ply under the weight l_1 and the gap between the plies d have to be measured accurately before testing.

Clamping of the material:

Securely fastening the material during testing is important to avoid slippage and deviations of the fibre orientation but is very challenging for fibre reinforced thermoplastics. The material is clamped in the solid state; however, as soon as the material is heated above the melting temperature, the matrix is squeezed out and the clamping forces are reduced. As a result, either the fibres of the outer plies were moved in the pulling direction (see Fig. 4-7a) or the inner ply slips partly or completely out of the pulling clamp. Therefore, it is necessary to clamp the material very tightly and possibly retighten the clamps after reaching the testing temperature. As during the initial tests the inner ply mostly slipped out of the clamp (see Fig. 4-7c), it was decided to wrap the material around the clamp to also have a form fit (see Fig. 4-7d).
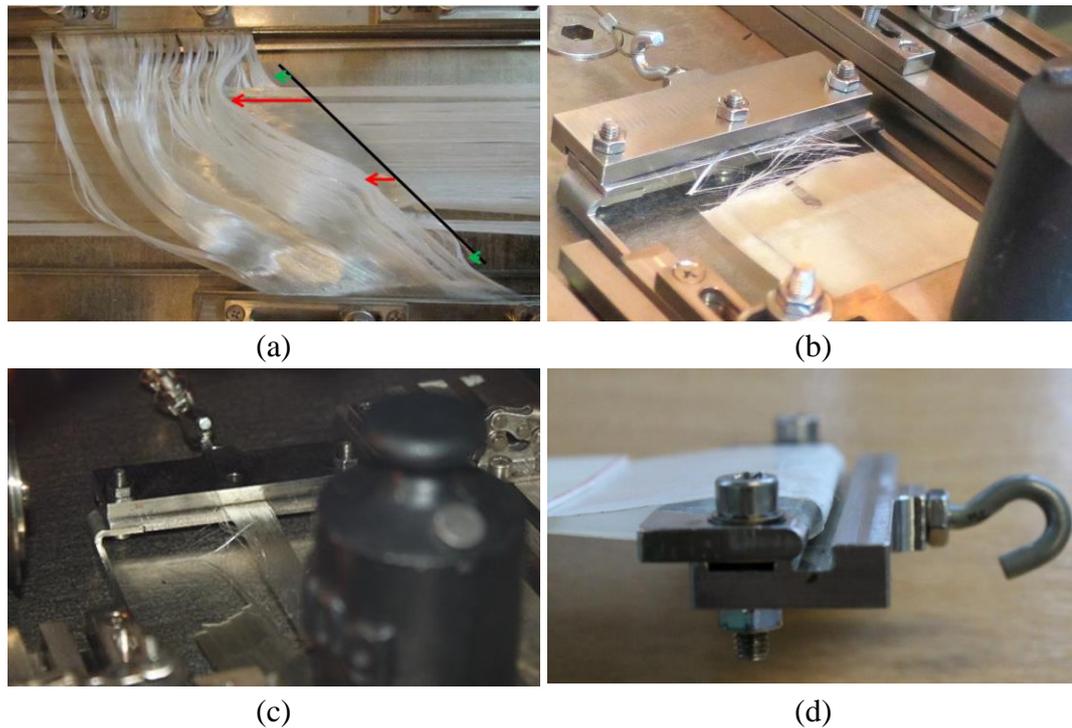
Fig. 4-7. **Occurring clamping problems**
(a) fibre deviation PT 0/45, (b, c) slipped out material at the pulling clamp, (d) material wrapped around the clamp to avoid slipping

To generally improve the clamping of the material, notches were milled into the steel contact area. In that way the clamping force was concentrated on a small area and a higher pressure could be achieved.

Sag of the inner specimen during the PT tests:

Attributable to the construction and the horizontal orientation of the testing plane during the PT test the inner ply is only supported in the contact area and at the end with the pulling clamp. The other end of the specimen is free and could bend down during the test causing additional friction between the ply and the base plate (see Fig. 4-8). This uncontrollable interaction has to be avoided to achieve constant testing conditions.

Fig. 4-8. **Sagging of the free end during PT test**

To solve this problem a support frame was designed that consisted of two clamps connected with two straight elements. It allows to clamp both ends of the ply and keeps the material straight. As disadvantage the frame generates additional friction,

because it slides over the base plate. To evaluate whether it has a relevant influence on the results, calculations of the friction force and measurement with the support frame alone were conducted. Both revealed friction forces of about 0.3 N, which could be neglected for the friction measurements.

4.1.1.2 Friction measurements

After manufacturing and validation of the test stand the friction measurements were executed. The goal was to determine the influence of normal force, test velocity and fibre orientation on the friction behaviour of fibre reinforced thermoplastics above melting temperature. Measurements were conducted with both test principles to see whether results are comparable. The focus of the measurements was on the 0°/0° and 0°/90° orientations as these are most often used. The friction parameters for the materials used in the forming experiments of chapter 3 should be determined as basis for the forming simulation. As the thermal chamber of the testing machine was limited to 250 °C, friction measurements with CF/PEEK were not possible. Hence the focus of the study was on the GF/PP tape of Celanese [55]. For the test 50 mm wide UD tapes were used. The desired specimen lengths were cut from the roll and stacked to the desired orientations.

In the case of the PO test setup the area of friction shrinks during testing, causing a change of pressure between the specimens. As a result, the graph of the measurements differs from the PT measurements (see Fig. 4-9). Because of that it was not possible to also evaluate the steady state dynamic friction, besides the static friction. Also it was stated that the relative slippage during forming happens within the range of a few millimetres, whereas the peak friction coefficient is more relevant for that application [75]. Hence subsequently only the static coefficient of friction is evaluated.

(a)   (b)
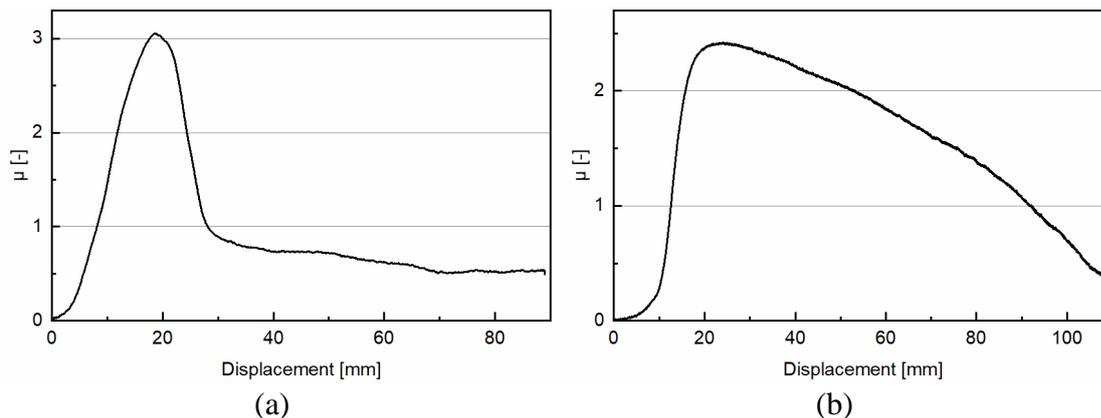
Fig. 4-9.   **Typical friction behaviour**
              (a) PT test, (b) PO test

The majority of the below presented experimental measurements were conducted in the scope of [S5].

The measurements were conducted with 50 mm/min to 1200 mm/min and additional normal weights of 0.5 kg, 1 kg and 1.5 kg resulting in different normal forces and pressures depending on the test setup. For every configuration at least three tests were performed and only valid results were evaluated. The peak coefficient of friction (CoF) can be calculated using equation (4-2):

$$\mu_{peak} = \frac{F_{peak}}{2 \times F_N(0)} \tag{4-2}$$

where F_{peak} is the peak force during the measurement and F_N is the normal force. The following figure shows the calculated peak CoFs of the PO0/0 measurements.
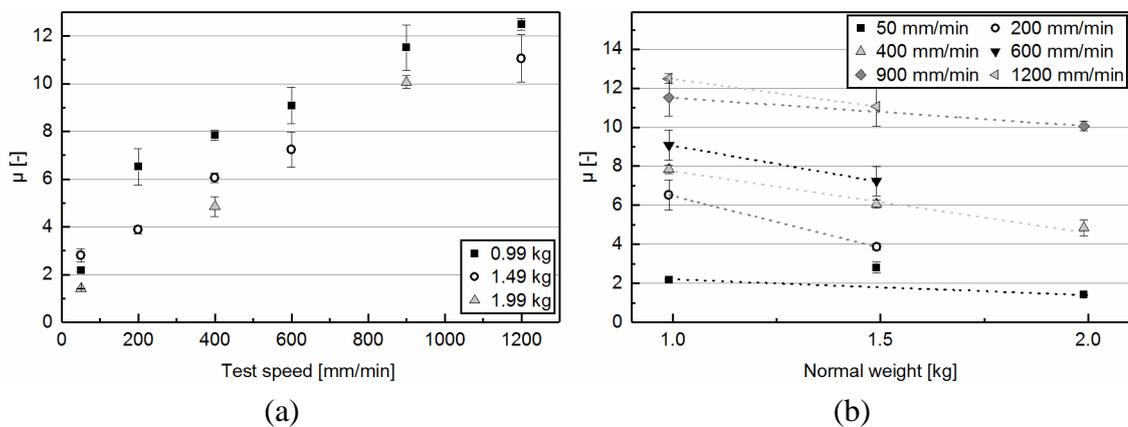
Fig. 4-10. **Peak coefficients of friction PO0/0 of GF/PP**
(a) Velocitiy dependency, (b) normal force dependency

The results reveal that a higher test speed causes an increase of the coefficient of friction. Also it can be seen that a higher normal force reduces the CoF, meaning that the friction force does not increase as much as the normal force.

For the PO0/90 tests a similar behaviour can be seen (see Fig. 4-11), but in contrast to the PO0/0 measurements the CoFs are apparently lower.
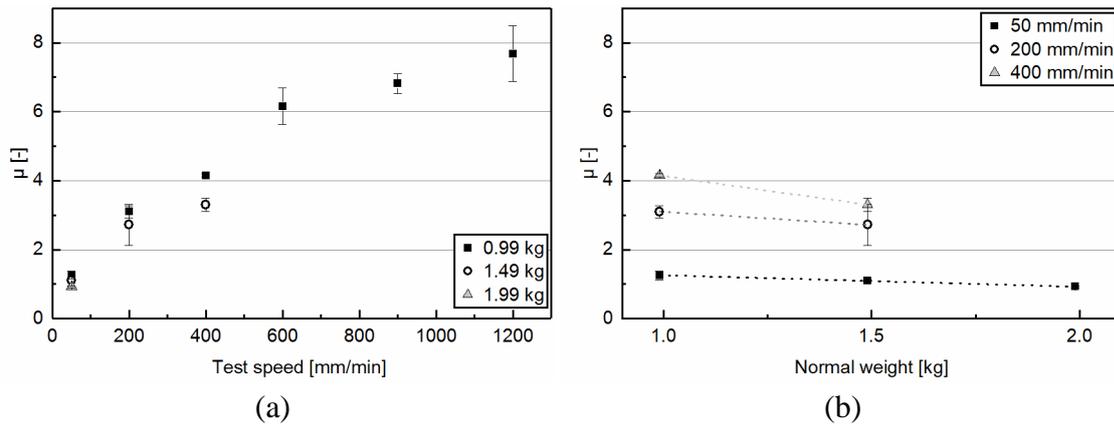
Fig. 4-11. **Peak coefficients of friction PO0/90 of GF/PP**
(a) Velocitiy dependency, (b) normal force dependency

With the pull-through set up an extensive study could have been conducted only with the 0/90 configuration. The reason is that with the 0/0 configuration no secure clamping of the outer plies was possible as the fibres could not have been clamped directly. In contrast to the PO measurements the graphs of most PT test showed a plateau representing the steady state dynamic friction. However, for a better comparison the peak CoFs were evaluated. The following figure depicts the results.
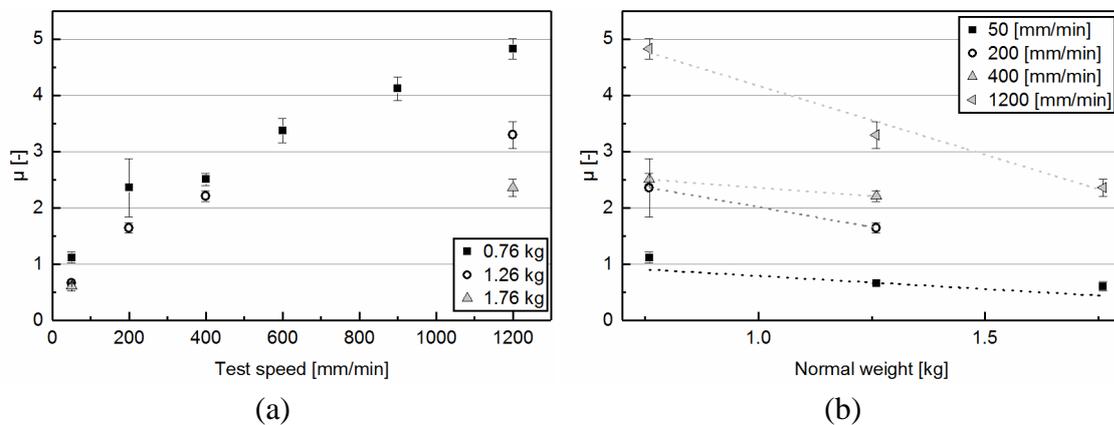
Fig. 4-12. **Peak coefficients of friction PT0/90 of GF/PP**
(a) Velocitiy dependency, (b) normal force dependency

Tendencies are similar and the CoFs are within the same order of magnitude as the ones of PO0/90. But they are not directly comparable as the pressures were different. To verify whether PO and PT tests produce comparable results, measurements with identical pressures of 50 mm/min were executed. Tab. 4-1 shows the obtained CoFs.

Tab. 4-1.   **Comparison between PO0/90 and PT0/90 at the same normal pressure**

	Units	PO 0/90	PT 0/90
Normal pressure	[kPa]	2.955	2.989
Peak CoF	[-]	1.092	1.117

Here it can be seen that both friction setups yield comparable results for the peak CoF when performed with similar test parameters and contact pressures.

4.1.1.3   Summary of the friction measurements

All measurements showed a clear relation between testing speed and friction response. Higher testing speeds led to higher friction coefficients. Similar findings were stated by several authors [50, 62, 75, 138, 158]. It could also be seen that the fibre directions have an influence. The friction coefficients between 0°/90° plies were smaller than between 0°/0° plies. This is in good correlation with the observations by Margossian [62]. The reason could be that during the 0°/0° measurements the fibres interlock and hence the friction is increased. To corroborate this assumption a microsection of a PO0/0 specimen was made after testing (see Fig. 4-13). It can be seen that the plies merged and only some matrix-rich areas are present.
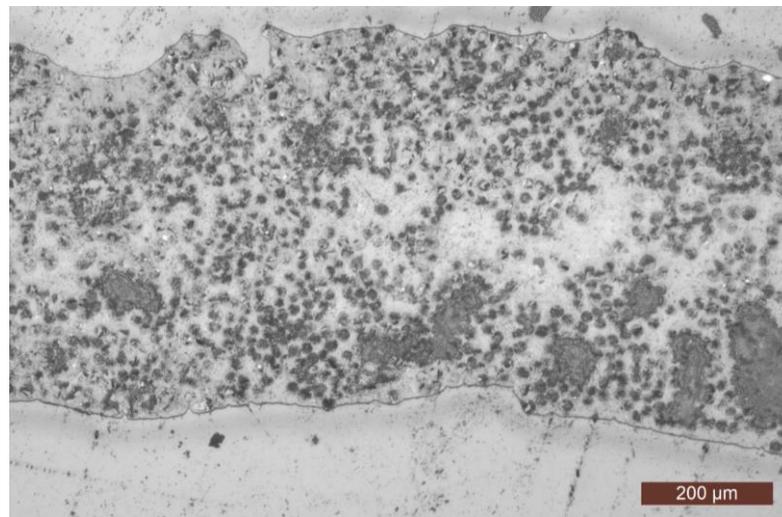
Fig. 4-13.   **Microsection after friction testing of PO0/0**

The measurement series also revealed that a higher normal force reduces the friction coefficient. A similar behaviour was also detected in the benchmark friction study presented by Sachs [75]. The influence of the normal pressure was also investigated by Vanclooster [138] for fabric reinforced thermoplastics. He observed a decrease of the in-plane traction with increased normal pressure due to a reduced matrix interlayer. But as the in-plane traction did not decrease as much as the normal pressure was increased, a lower friction coefficient was the result.

4.1.2 Bending

The bending characterisation was conducted based on the method developed by Margossian et al. [83] (see also chapter 2.2.3). The authors describe a testing method for the out-of-plane bending stiffness of CFRTP using a DMA system. The well controllable environmental conditions within the testing chamber and the resolution of small forces were used for a quasistatic three-point bending test. The three-point bending device of the used DMA provides span widths L of 20 mm and 50 mm, whereas only the smaller span width was utilized. With the help of this method, the GF/PP tape of Celanese [55] was characterised.

The experiments were performed at the Chair of Carbon Composites (LCC) at the Technical University of Munich (TUM) with a Q800 DMA system of TA Instruments. For the characterisation a full factorial experimental design was used. The parameters temperature and testing speed were investigated on three levels with a displacement of 1500 µm. Each configuration was repeated three times. The test plan is shown in Tab. 4-2.

Tab. 4-2.   **Test plan for bending characterisation**

Parameter	Units	#1	#2	#3
Temperature	[°C]	170	180	190
Speed	[µm/min]	2500	5000	7500

The specimens for the tests were produced with the Fiberforge RELAY2000. Layups of four UD plies were created with a size of 350 mm x 350 mm and afterwards consolidated in the static press. Then the plates were cut to the desired sizes of 30 mm x 15 mm (l x w). Prior to testing each specimen was measured exactly (thickness t, width w, length l) and placed into an oven at 120 °C for preheating. A single specimen was then removed from the oven and positioned in the three-point bending device of the DMA (see Fig. 4-14). After a temperature equilibrium was achieved in the test chamber, the measurement was initiated.
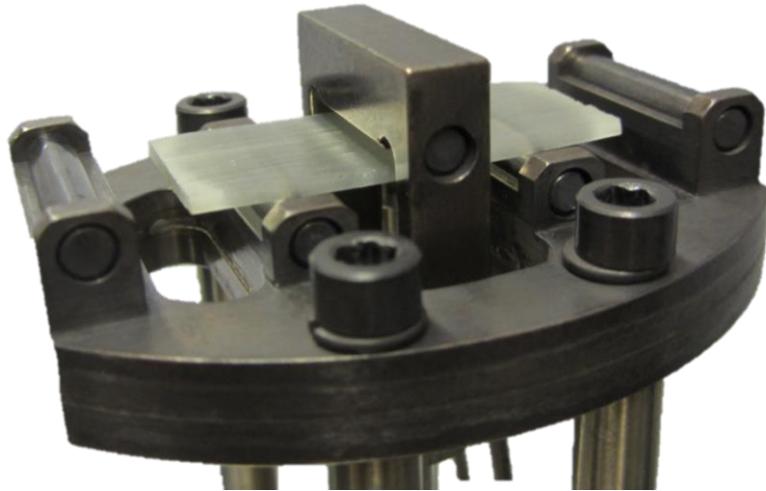
Fig. 4-14. **Bending characterisation setup**
Three-point bending device of the DMA at LCC

During the test several measurement data were recorded: temperature T, displacement D_m and static force F. Based on the data the resulting strain ε in the outer fibre at mid span can be calculated using equation (4-3) [83, 159]:

$$\varepsilon = \frac{6 D_m t}{L^2} \tag{4-3}$$

where t is the thickness of the specimen and L the free span length. For the specimens with a rectangular cross-section the stress σ in the outer fibre is calculated using equation (4-4) [83, 159]:

$$\sigma = \frac{3FL}{2wt^2} \tag{4-4}$$

where w is the specimen width. The resulting stress strain curves of the measurements are shown in Fig. 4-15.
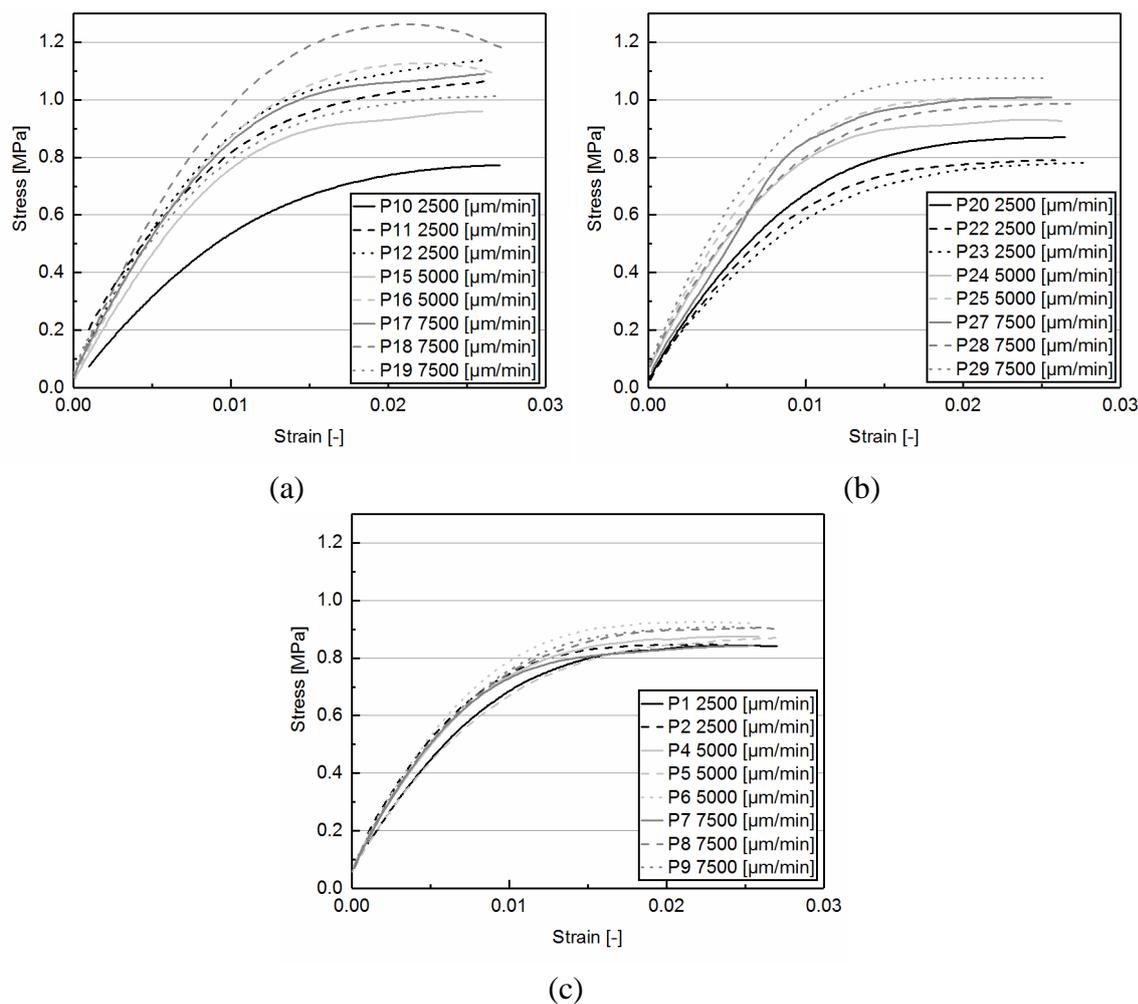
Fig. 4-15.   Stress strain curves of the bending characterisation
(a) Results at 170 °C, (b) results at 180 °C, (c) results at 190 °C

Two measurements at 5000 µm/min were invalid and could not be evaluated. Due to this there are only two results for this testing speed at 170 °C and 180 °C.

Summary of the bending measurements

Examining the results, especially for the measurements at 170 °C and 180 °C, a strain rate dependency can be determined. A higher testing speed causes a higher stress. This effect is less distinctive for the 190 °C results. Despite that also deviations of the repetitions of one parameter configuration can be seen.

Higher testing speeds were not possible because the DMA system experienced problems with controlling the movement at higher displacement rates, as also described by Margossian et al. [83].

4.1.3   In-plane shear stiffness

For the in-plane shear characterisation the method developed by Haanappel and Akkerman [63] was used. The described procedure is based on the usage of a torsion bar specimen tested in a rheometer. A detailed description of the method can be found in chapter 2.2.4. For this test specimens with a thickness of ~10 mm are necessary. The characterisation was conducted for the GF/PP UD tape of Celanese [55]. For the measurements a rheometer MCR 302 of Anton Paar was used (see Fig. 4-16a). As for the bending characterisation, a UD layup was created using the Fiberforge RELAY2000 and afterwards consolidated. To create a plate with the desired thickness, a layup with 40 plies was necessary. As severe material flow during consolidation could occur with this thickness, the layup was pressed within a closed mould. After consolidation the specimens were cut to the desired measures: 47 mm x 11 mm x 10 mm (l x w x t). Prior to testing each specimen was measured exactly. The specimen was then mounted to a special fixture in the rheometer (see Fig. 4-16b), where it was clamped at both ends. It was important to leave a small gap between the specimen and the upper clamp to compensate thermal expansion. Then the testing chamber was closed and heated to the testing temperature.

<div align="center">(a)   (b)</div>
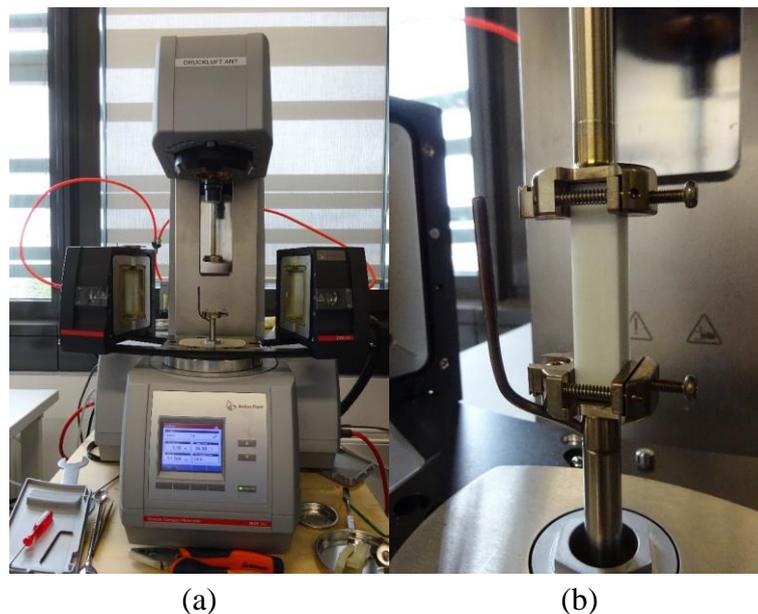
Fig. 4-16.   **Setup for the shear stiffness characterisation**
            (a) Rheometer MCR302 of Anton Paar, (b) specimen in the testing fixture

As also described by Margossian [62], the measurements were started with an amplitude sweep to detect the linear viscoelastic (LVE) region of the material. Within this LVE region subsequently frequency sweeps were performed.

The results of the amplitude sweeps are shown in Fig. 4-17. The measurements were performed at three frequencies (1 rad/s, 10 rad/s and 100 rad/s) within a strain range from 10^{-4}% to 10%. Each frequency measurement was repeated three times.
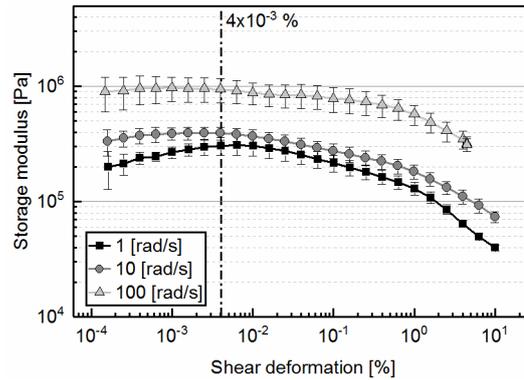
Fig. 4-17.   Amplitude sweep results
          GF/PP specimens tested at 1 rad/s, 10 rad/s and 100 rad/s

Based on the results of the amplitude sweep the LVE range can be determined. According to [160] the LVE region ends when the storage modulus varies more than 10% from a plateau. According to that the maximum shear strain γ_{max} can be calculated for all frequencies. For further testing the lowest value of γ_{max} was chosen, to ensure that all measurements were within the LVE.

With the determined maximum shear strain the frequency sweeps can be performed. They were conducted from 0.1 rad/s to 600 rad/s. The results are shown in Fig. 4-18.
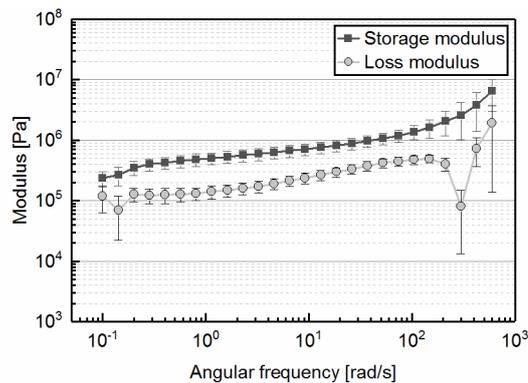
Fig. 4-18.   Frequency sweep results
          GF/PP specimens tested at 4×10^{-3}% shear strain

Based on the method described by Haanappel and Akkerman [63] and also repeated by Margossian [62] the shear relaxation modulus G_r was determined using the frequency sweep results (see Fig. 4-19).
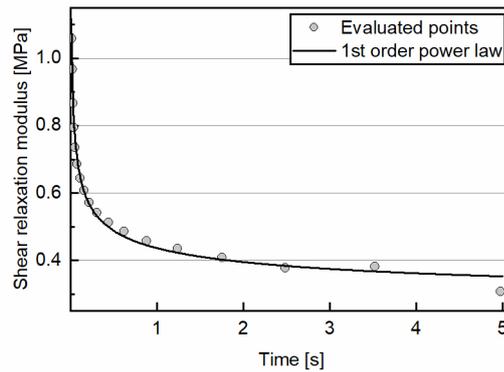
Fig. 4-19. **Approximated shear relaxation modulus of GF/PP at 190 °C**

The stress strain relation (see Fig. 4-20) was then calculated using the following equation [62]:

$$\tau(t) = \dot{\gamma}\left(G_\infty t - \frac{a}{b-1} t^{1-b}\right) \tag{4-5}$$

where $\dot{\gamma}$ is the shear strain rate, t is the time and G_∞, a and b are constant coefficients determined by curve fitting of the shear relaxation modulus. The results reveal a slight rate dependent but mostly elastic behaviour. Similar was also observed by Margossian [62].
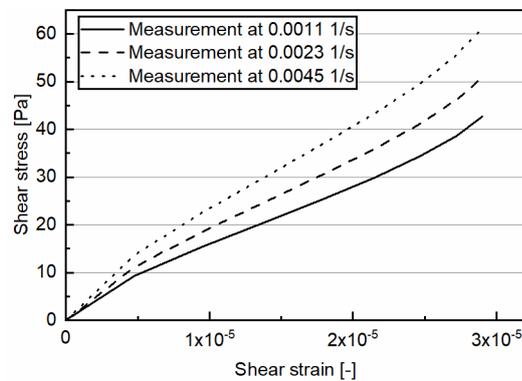
Fig. 4-20. **Stress strain response of GF/PP at 190 °C**

4.2 Material data fitting

Based on the material characterisations described in the previous chapter, routines were used to adapt the input parameters of the simulation material models to the measured material behaviour. The goal of the material data fitting is to ensure that the material behaviour of the simulation reproduces the real-life setting. In the used AniForm simulation software the material behaviour is modelled with constitutive models, which require several input parameters. As the parameters cannot be directly measured with the characterisation tests, an automated fitting routine is necessary. For the fitting of the interface properties a self-developed fitting routine was used. For the

in-plane and bending properties a tool of AniForm was applied. After determining the input parameters, the material data have to be validated. Therefore, the characterisation tests were modelled, the measurements under comparable boundary conditions simulated and the resulting material behaviour compared to the experimental results.

4.2.1   Fitting of interface properties

The basis for the fitting of the interface properties were the results of the friction measurements described in chapter 4.1.1. The fitting was conducted for the PO0/0 and PT0/90 measurements. The fitting routine was programmed in Matlab.

After loading the experimental data, the material models for fitting are chosen. All relevant AniForm interface models (see chapter 2.3.3) are implemented. Different configurations were tested in order to achieve the best result. The friction testing setup was also modelled in AniForm (see Fig. 4-21) to verify the fitted material parameters. It consists of one fixed tool at the bottom and one tool applying the pressure and a ply in between representing the laminate. The size of the friction area is 50 mm x 50 mm. It corresponds with the PT setup, but was also used for verification of the PO experiments. The normal pressure was adapted to the start value of the real experiments. The middle ply was pulled by a line gripper at the corresponding displacement speed.
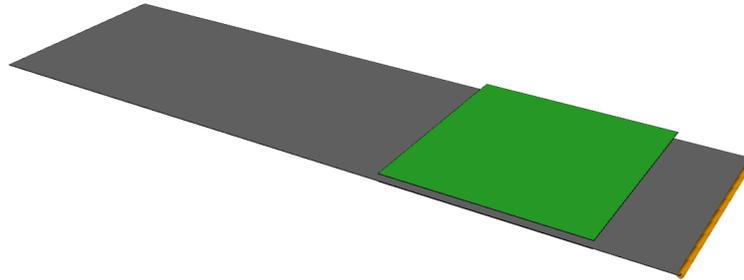
Fig. 4-21.   **Friction model in AniForm**
                 Pressure plate (green), line gripper (orange) and ply (grey)

The highest value of the pulling force was evaluated for the calculation of the CoF, which can be compared to the peak CoF of the friction measurements. The following figure (see Fig. 4-22) shows the comparison of experimental and simulation results for the PO0/0 configuration.
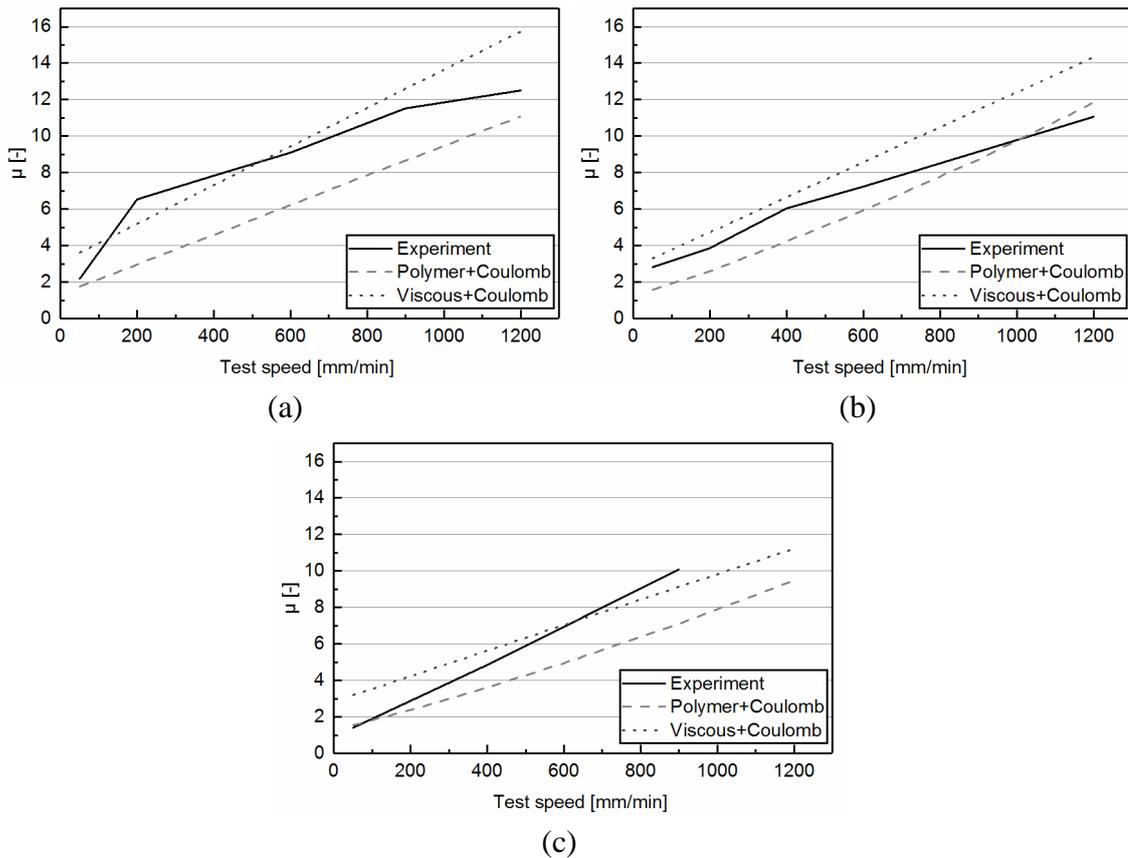
Fig. 4-22.   Comparison of friction experiments and simulation of PO0/0
(a) 0.99 kg normal weight, (b) 1.49 kg normal weight, (c) 1.99 kg normal weight

Combinations of Polymer & Coulomb friction and Viscous & Coulomb friction were compared. Both models reproduce the friction behaviour well, but the congruence of the Polymer & Coulomb model is better, especially at higher test speeds, which is more relevant for the forming process. Therefore, the Polymer & Coulomb friction model was chosen for the PO0/0 configuration.

The same procedure was executed for the PT0/90 measurements. Also Polymer & Coulomb friction and Viscous & Coulomb friction models were considered. But only the Viscous & Coulomb friction model provided plausible results (see Fig. 4-23). All simulations of the Polymer & Coulomb friction showed a high force peak at the beginning, which would obstruct the sliding of the plies during forming simulations (see Fig. A-1). For that reason, the Polymer & Coulomb friction model was not taken into consideration for the PT0/90 setup.
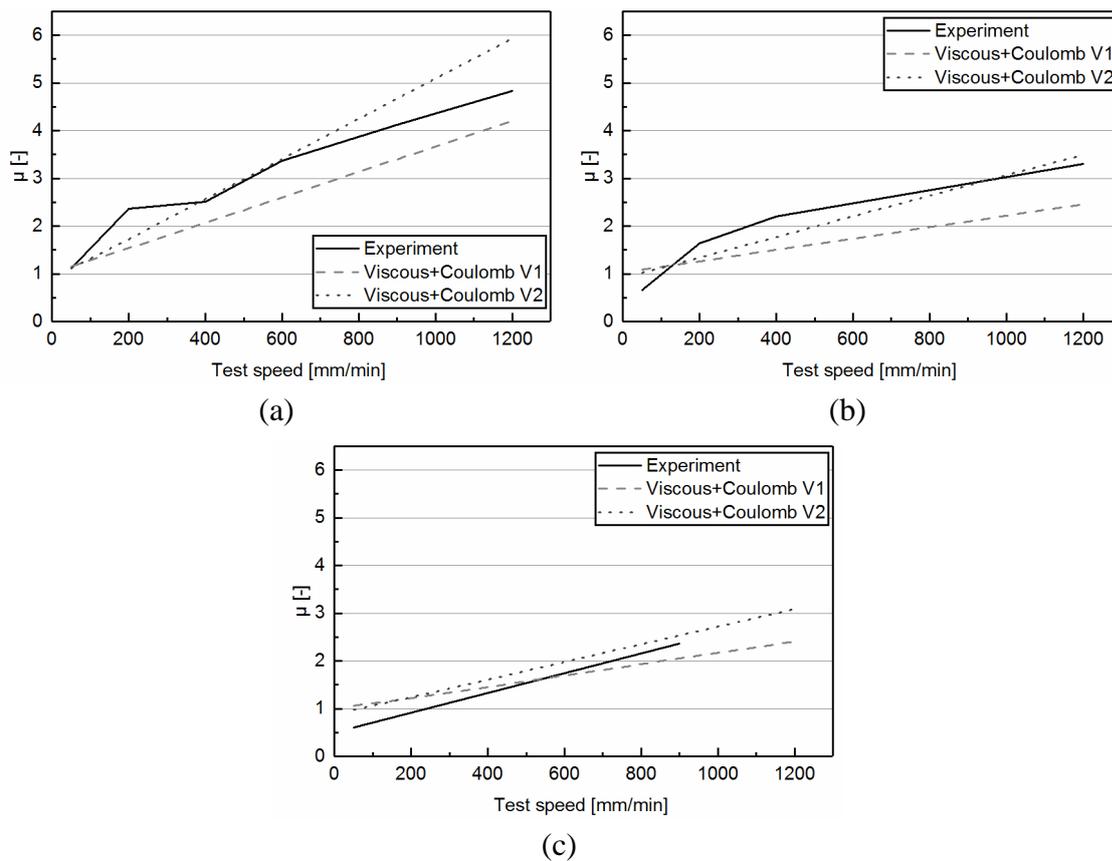
Fig. 4-23.   **Comparison of friction experiments and simulation of PT0/90**
(a) 0.76 kg normal weight, (b) 1.26 kg normal weight, (c) 1.76 kg normal weight

Comparing the two versions of Viscous & Coulomb friction models in the diagrams, it can be seen that the behaviour is similar, and both models fit the experimental data well. The slope of the first version fits the curves of the lower normal weights better, whereas version two is closer at the higher load. But for version two an over-estimation of the friction coefficient at higher test speeds could be expected. For that reason, the first version was selected for the PT0/90 friction configuration.

All studied friction parameters are listed in Tab. A-1 and Tab. A-2 within the Appendix.

4.2.2   Fitting of bending properties

For the fitting of the bending properties a Matlab tool supplied by AniForm was used. The tool was originally developed for a one-ply characterisation test in a rheometer described by Sachs and Akkerman [161]. The input parameters are additional to the specimen dimensions, time, curvature and torque. As in this study a three-point bending characterisation test with a four-ply specimen was used, the curvature κ_{mid} and torque M_{mid} had to be calculated in advance. The calculation was performed based on the Euler-Bernoulli beam theory with the following equations:

$$M_{mid} = \frac{FL}{4} \tag{4-6}$$

$$\kappa_{mid} = 12\frac{D_m}{L^2} \tag{4-7}$$

where F is the bending force, D_m the displacement at mid span and L the free span length. Material data fitting has to be carried out for a single ply, because the material data input of the simulation accounts for one ply. As the deformation during the characterisation test was very low, the friction between the plies was neglected and assumed that the laminate behaves like four single plies. For the calculation of the torque M_{mid} for the fitting routine one quarter of force F was used.

The three-point bending test was modelled in AniForm to verify the fitted bending parameters. The tools were modelled as rigid half cylinders with diameters of 4 mm as in the experimental setup. The distance of the supports was 20 mm. Each ply was modelled with 0.4 mm shell elements. The fitted friction parameters (see chapter 4.2.1) were applied to the interfaces. The bending test was simulated with speeds of 2500 µm/min, 5000 µm/min and 7500 µm/min with a maximum deformation of 1.5 mm in accordance with the experimental tests.
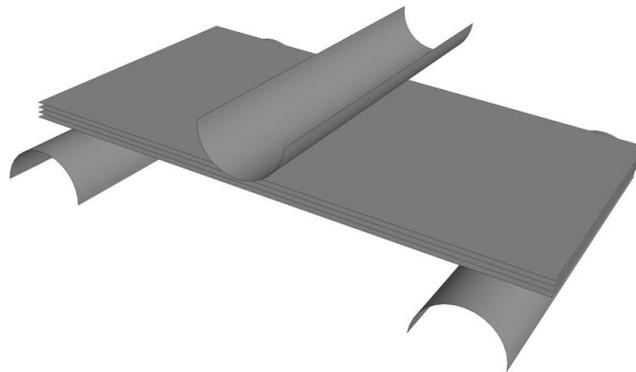
Fig. 4-24. **3-point-bending model in AniForm**

Only the combination of an elastic model with the Cross Viscosity Fluid model resulted in comparable material behaviour. Different parameter configurations were tested to achieve the best result. Force-displacement diagrams were used to evaluate the simulations (see Fig. 4-25).
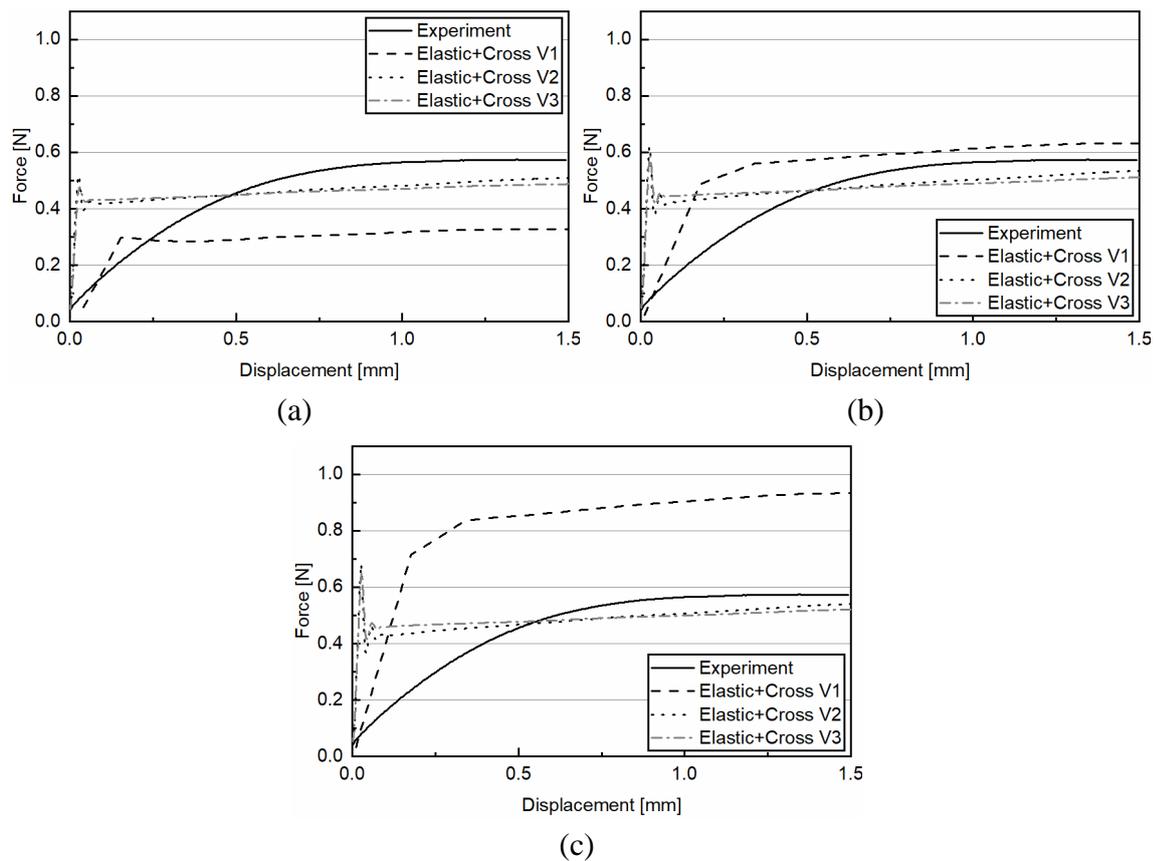
Fig. 4-25.   **Force displacement diagrams of 3-P-bending simulations and experiments at 190 °C**
                   (a) 2500 µm/min, (b) 5000 µm/min, (c) 7500 µm/min

Results show that the force response of the forming simulation is within the same order of magnitude as the experimental data. Also the trend of the curves at higher displacements was fitted well, especially by the V2 and V3 parameter configurations. But at the start of the measurement there seem to be higher deviations. The simulation curves, except for V1, show a force peak at the beginning, which is growing with increasing displacement speed. This might be caused by numerical issues. Neglecting that, the best fit was achieved by parameter configuration V3, which is also showing lower force peaks. This parameter set was used for the subsequent forming simulations. The exact parameters can be found in the Appendix (see Tab. A-3).

4.2.3   Fitting of in-plane properties

As for the bending fitting, the AniForm fitting tool in Matlab was also used for the in-plane properties. The input parameters for the fitting routine are the specimens' dimensions and the correlation of time, rotational angle and torque for different deformation rates. Data were obtained by the described amplitude sweeps. The specimen of the shear experiment was modelled using four node tetrahedron 3D elements. The sizes of the cuboid shaped model were 10 mm x 11 mm x 33 mm in accordance with the experimental setup. The nodes of the shorter edges of both ends

were fixed, representing the clamping of the specimen. On one end the rotation was applied. These nodes could also move freely in z-direction.
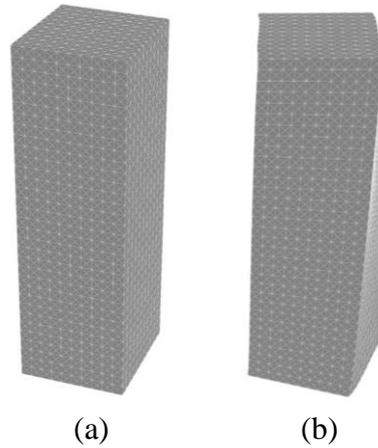
Fig. 4-26.   Torsion bar model in AniForm
         (a) Undeformed, (b) deformed

The required torque was tracked and used for the comparison with the results of the frequency sweep (see Fig. 4-27). One combination of elastic & Cross Viscosity Fluid model and one variation of an elastic & Newtonian Fluid model were compared.
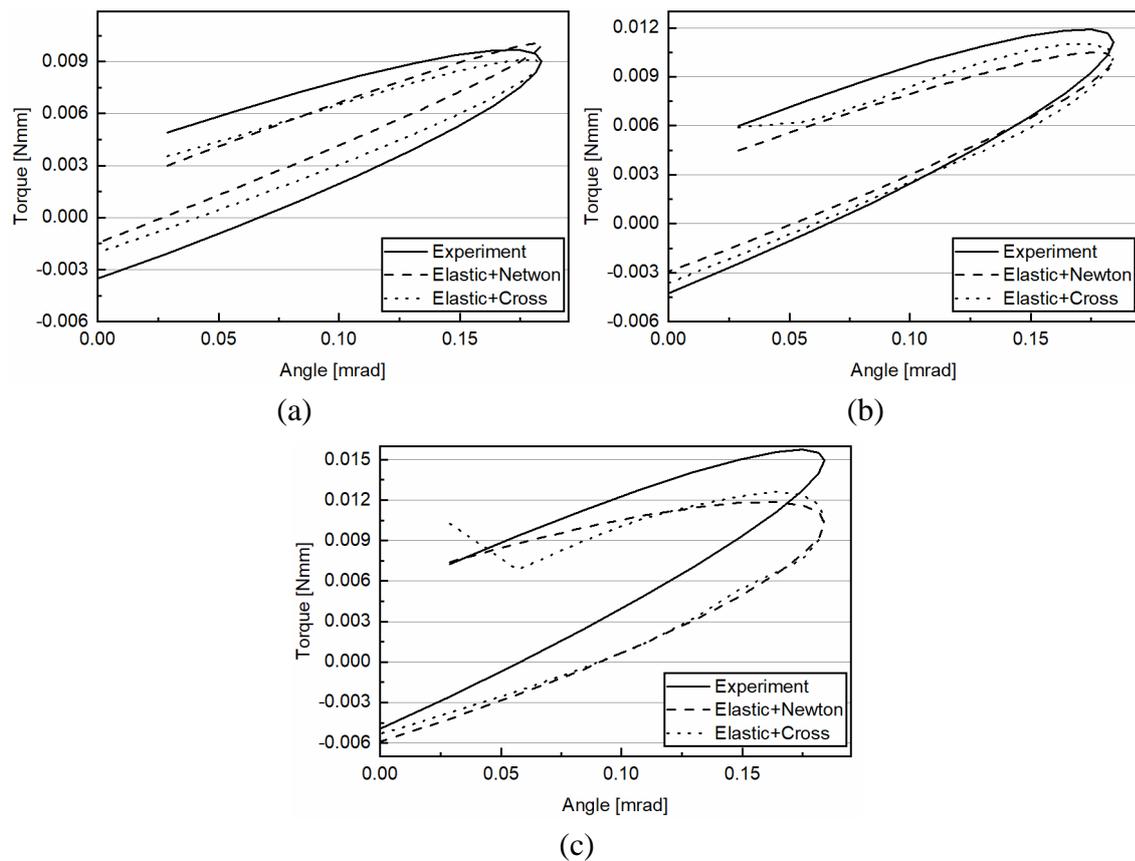
Fig. 4-27. **Torque angle diagrams of shear simulations and experiment at 190 °C**
                a) 37.1 rad/s, (b) 74.4 rad/s, (c) 149 rad/s

The diagrams show that the simulation can sufficiently reproduce the material behaviour of all considered deformation rates. Both material models depict a very similar behaviour. The reproduction of the lowest deformation rate and especially of the medium rate is very good. Only for the 149 rad/s deformation rate there are larger deviations. For all angles the torque of the simulation and the slope of the curve is too low. As both models seem to be comparable the elastic & Newtonian fluid model will be used for the simulations of GF/PP described in the next chapters. The detailed input parameters for the material models can be found in Tab. A-4.

4.3 Forming simulations

All forming simulations in this thesis were performed with AniForm (see also chapter 2.3.3). Within the following chapters the forming simulations associated with the performed experimental studies (chapter 3) are described. As input parameters either the fitted parameters of the previous chapters or parameters provided by AniForm were applied, depending on the respective material. For all simulations a macroscopic approach with shell elements was used. The tools (stamp and matrix) and the support frame (if one is used) were modelled as rigid bodies. This is acceptable as the tools are

much stiffer than the laminate and are not expected to deform during the forming process.

The goal was to figure out whether the simulation is capable of predicting the observed forming effects. These studies should help to define the limits of the macroscopic forming simulation and improve the usage during the manufacturing development process.

4.3.1 Radius forming

The forming simulations of the radius forming experiments described in chapter 3.1 are presented in the following chapter. The model was generated in accordance with the experimental setup. It consists of a rigid stamp and matrix with the respective radius sizes and the laminate in between (see Fig. 4-28). Each ply was modelled of separate shell elements. The number of plies was set to 14 and 29 to obtain 2 mm and 4 mm of total thickness, respectively. The element sizes were 1.9 mm for thinner laminates and 2.8 mm for thicker ones due to computational reasons. Two line grippers at the end of the laminate simulated the clamps. A constant force was applied to the line grippers in horizontal direction for pretension and guidance of the laminate during forming. The force was set according to the number of constant force springs in the experiment. The line grippers could rotate freely around their longitudinal axis. Every combination of inner radius, laminate thickness, layup and pre-tension as described for the experiments was simulated.
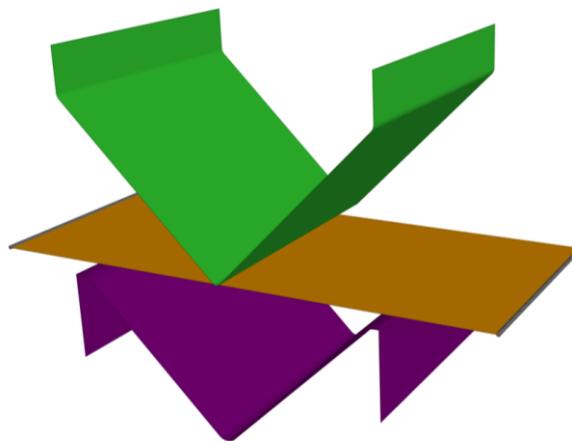
Fig. 4-28.   **Simulation model of the radius forming setup**
            Stamp (green), matrix (purple), laminate (orange), line grippers (grey)

For the used material (TenCate Cetex TC1200 PEEK AS4) fitted material input parameters were provided by AniForm for three different temperatures: 365 °C, 385 °C and 405 °C. During the experiments the material was heated to 390 °C and then transferred to the forming tool. The material started to cool down during the transfer and upon contact with the tools. To cope with that, a temperature parameter of 365 °C

was chosen for the forming simulations. The used material models are shown in Tab. 4-3.

Tab. 4-3.   **Material models for CF/PEEK at 365 °C**

In-plane	Bending	Interface tool	Interface plies
Elastic fibre	Orthotropic elastic	Penalty with	Penalty with
Isotropic elastic	Cross Viscosity Fluid	polymer friction	polymer friction
Cross Viscosity Fluid			Adhesion

The layup and forming speed corresponded to the experimental settings. The stamp was closed until the target cavity thickness was reached. The results of the simulation are shown in the following figure. The used identifiers correspond to the ones described in chapter 3.1.2.

(a)   (b)

(c)   (d)
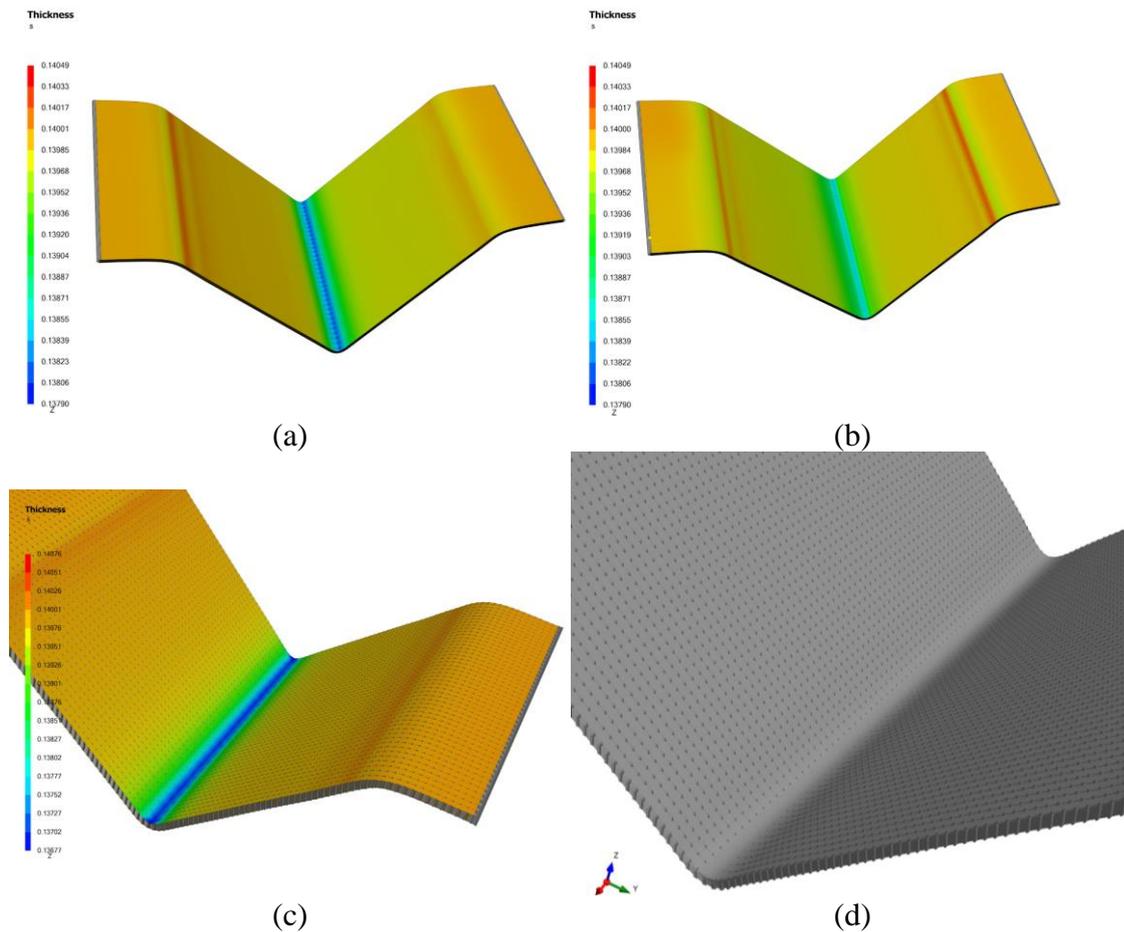
Fig. 4-29.   **CF/PEEK radius forming simulation results**
      Ply thickness of (a) 2-UD-3-5, (b) 2-UD-5-5, (c) 4-UD-3-1
      Fibre directions of (d) 2-UD-3-1

In Fig. 4-29 the ply thickness of three simulations (a-c) and the resulting fibre direction of one simulation (d) are shown. As determined during the experimental forming experiments, thinning of the radius sections and fibre waviness close to the inner radius could occur during radius forming. In the simulation results also a thinning of the plies in the area of the simulation is present. The thinning is not equally distinct for every configuration and for some it was not existent at all. Unlike in the experimental studies, no coherences could be recognised. The thickness in the simulation is calculated based on a constant volume. If the surface area of an element is changed due to in-plane deformations, the thickness change is calculated accordingly. It is not coupled to the contact logic operations but will be determined during post-processing. In contrast, the thickness change observed in the experimental studies is not due to in-plane deformations but results from matrix squeeze flow due to compression of the plies.

Fibre waviness as observed in some formed parts was not detectable in any simulation. The reason might be that the element sizes are too large to simulate this effect. Summing up it can be stated that the macroscopic simulation approach is not capable of reproducing both effects, which emerge on a microscopic scale.

4.3.2   Cone geometry

Subsequently the forming simulations for the cone geometry experiments described in chapter 3.3 are presented. Only the forming of the reference parts of CF/PA6 was modelled. Forming without previous consolidation was not conducted. The model setup consisting of stamp, matrix, support frame, laminate and tensioners with line grippers connecting support frame and laminate is shown in Fig. 4-30. The tensioners applied a constant force of 11 N to the laminate during forming. The position of the tensioners was identical to the experimental setup.
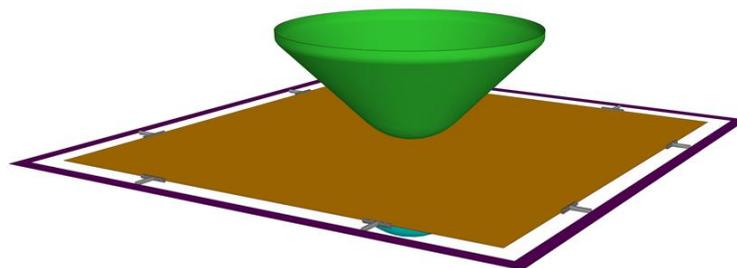
Fig. 4-30.   **Simulation model of the cone geometry**
              Stamp (green), matrix (cyan), support frame (purple), laminate (orange), line gripper and
              tensioner (light grey)

AniForm also provided input parameters for the used Celanese (Celstran CFR-TP PA6 CF60) material. The same material models as for the CF/PEEK were utilised but with different input parameters. Here, parameter sets for 240 °C, 260 °C and 280 °C were available. Again, parameters for the lowest temperature were chosen to take the

cooling during forming into account. The stamp was lowered with a speed of 60 mm/s until the final cavity thickness of 2.4 mm was reached. The element size was set to 3.7 mm due to computational reasons. The results of the simulation in comparison with the real formed part are shown in Fig. 4-31.

(a)   (b)

(c)   (d)
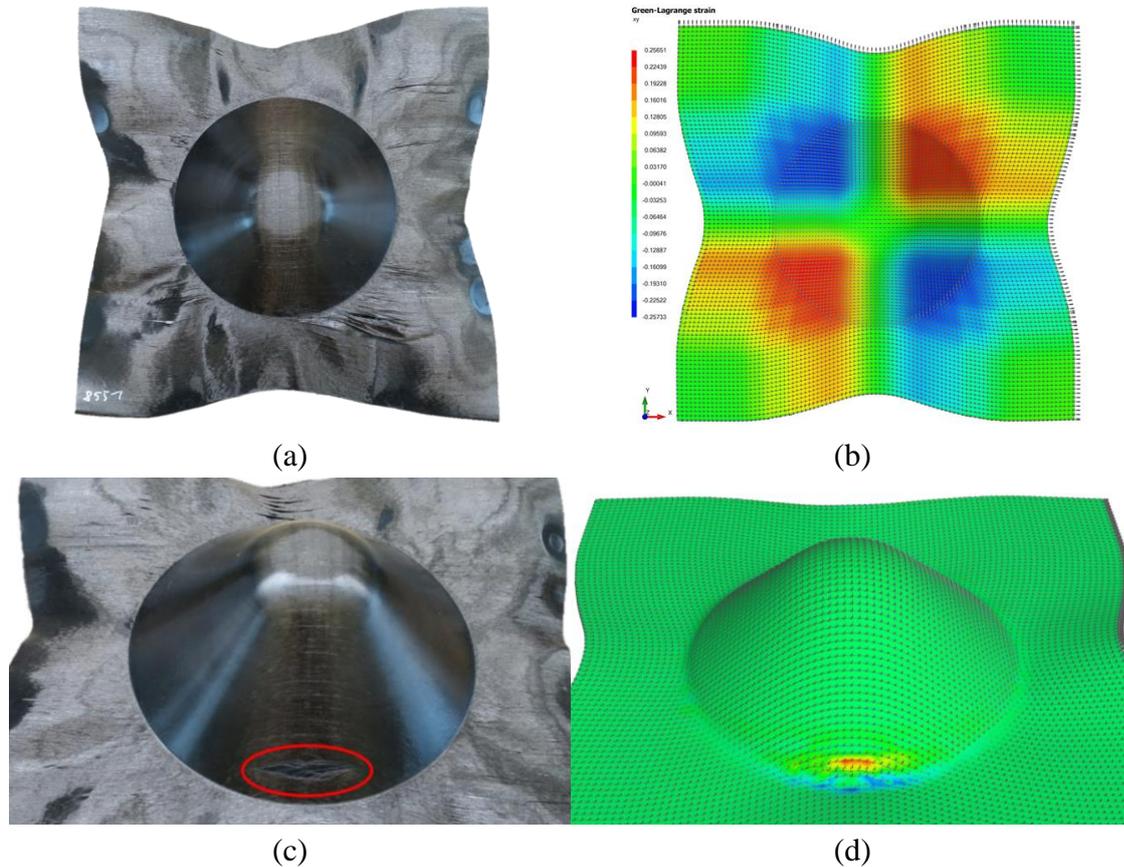
Fig. 4-31.   PA6/CF cone geometry experimental and simulation results
            (a) Top view of formed part, (b) top view of simulation with shear strain, (c) gap on the
            surface of the part, (d) transverse strain of the simulation indicating a gap

Considering these figures, it can be seen that the outer part contour of the simulation is rather similar to the one of the real parts (see Fig. 4-31a and b). Within the cone geometry no lager wrinkles are present, which is also predicted by the simulation. The shape outside the cone geometry differs. The real part shows a wavy surface with some wrinkles and in addition to that the laminate is delaminated in the corners. In contrast, the surface in the simulation is smooth and even with no existing delaminations. Fig. 4-31c shows a large gap of the top ply caused by transverse sliding of the fibres. At the same spot in the simulation a high strain transverse to the fibre direction is shown (see Fig. 4-31d).

To sum this up it can be stated that in the case of the cone geometry the forming simulation of CF/PA6 can predict the overall behaviour of the material in the area of the cavity correctly. Also, possible critical areas regarding the emergence of gaps are

highlighted. Outside of the cavity the modelling is less accurate. Overall waviness and delaminations of the plies are not represented by the simulation. The reason could be that the element size of 3.7 mm is too large to model these effects. Another reason might be that the bending stiffness of the plies is too high and prevents them from wrinkling.

4.3.3 Complex geometry

For the complex geometry that was used for the forming experiments described in chapter 3.2 forming simulations were performed as well. The studies of GF/PP and of CF/PEEK were modelled. The model setup was the same for both materials, only the material input data varied. It consisted of stamp, matrix and support frame as rigid tools (see Fig. 4-32). The constant force springs for pre-tensioning the laminate were modelled as line grippers and tensioners connecting the support frame and laminate. These apply the respective force during the forming process. The line grippers ensure that the tension is spread over several nodes of the laminate comparable to the real setup. The position and number of springs varied according to the experimental setup.
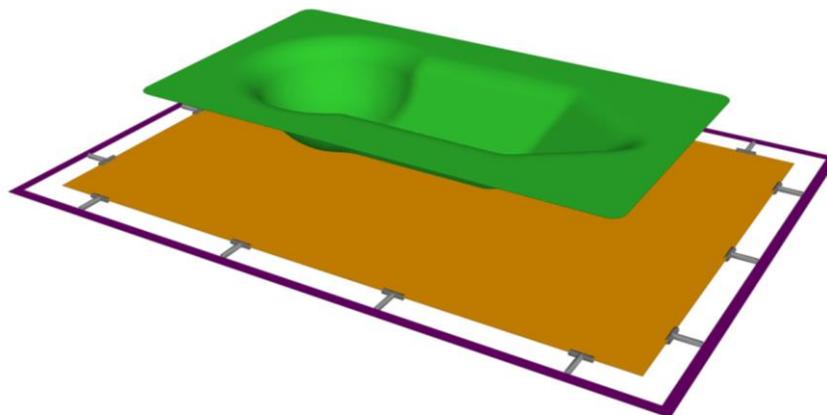
Fig. 4-32. **Simulation model of the complex geometry**
Stamp (green), support frame (purple), laminate (orange), line gripper and tensioner (light grey)

For simulating the GF/PP forming experiments, the material parameters as described in chapter 4.1 were used. Only for the bending properties the isotropic elastic model was replaced by an orthotropic elastic model and the Young's modulus in transverse direction degraded by factor 100. These parameters were determined at a temperature of 190 °C as this was also the pre-heating temperature during the forming experiments. After the characterisations the available material models in AniForm were fitted to the recorded material behaviour. Finally, the characterisation tests were modelled virtually, and the material models were validated. The resulted material input parameters are shown in Tab. A-1 – Tab. A-4.

The same process parameters as in the experiments were used (see chapter 3.2.2). The basis was the parameter configuration producing the best results: Support frame option with 14 springs of 11.5 N constant force and a closing speed of 60 mm/s. Other process parameters (tool temperature, forming pressure) were not relevant for the simulations.

Subsequently the results of the simulation with an orthotropic layup $[0/90/0/90/0]_s$ are presented. The chosen element size was 3.5 mm, as a smaller size was not possible due to computational reasons. A comparison with the experimental results is shown in Fig. 4-33. It can be noted that the formed simulation model almost shows the same outer contour as the real formed part (see Fig. 4-33a, b). As described in chapter 3.2.2 several forming effects were present on the formed parts. One effect were wrinkles of the fibres close to the hemisphere in a 45° direction (see Fig. 4-33c). Examining the same area of the forming simulation result, no wrinkles can be observed (see Fig. 4-33d). The colour in the image represents the occurring shear strain of the top 0° ply. A high shear strain in the 45° direction is displayed (blue area). Despite the localization of the shear strain, also an uneven distribution is revealed. This can be interpreted as an indication for the occurrence of wrinkles. In addition to the shear strain, also the fibre directions are shown as little arrows. Within the course of the fibre directions discontinuities are present, also pointing to the emergence of wrinkles.

(a) (b)

(c) (d)
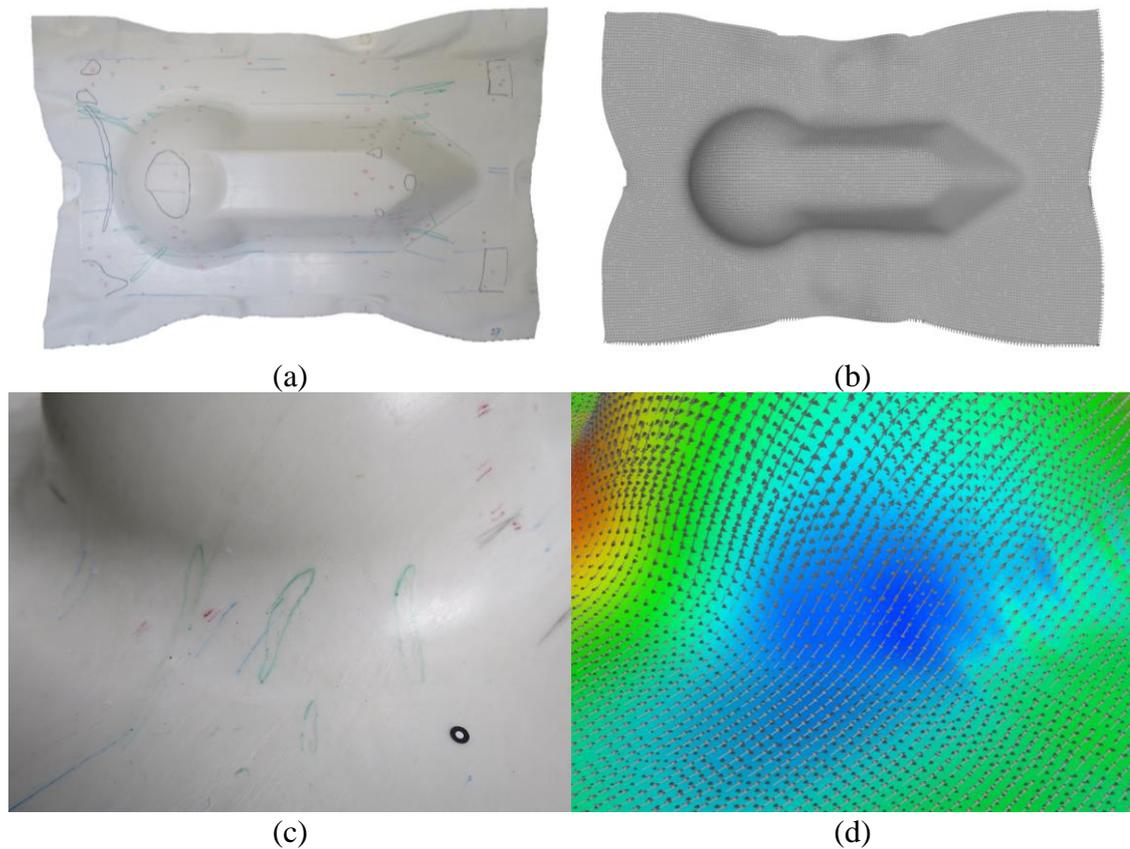
Fig. 4-33. **Orthotropic GF/PP complex geometry experimental and simulation results**
(a) Top view of formed 0/90 part, (b) top view of the forming simulation, (c) wrinkles
(green lines) close to the hemisphere, (d) predicted shear strain close to the hemisphere

In addition to the simulations of the orthotropic layup, simulations with QI layup were performed. The layup was identical to the one used in the experimental studies (see chapter 3.2.2). For the simulation the same material models and parameters were used as for the 0/90 layup. As no friction measurements for 0°/45° were performed, the 0°/90° parameters were also used for the interface. To cope with the additional fibre directions and ensure an even pre-tension of the plies, tensioners at the corners were added. These applied a constant force of 19 N during the forming process in 45° direction. For these simulations the element size was 5.9 mm. The results of the forming simulations in relation to the experimental results are shown in Fig. 4-34.

(a)   (b)

(c)   (d)

(e)   (f)

(g)   (h)
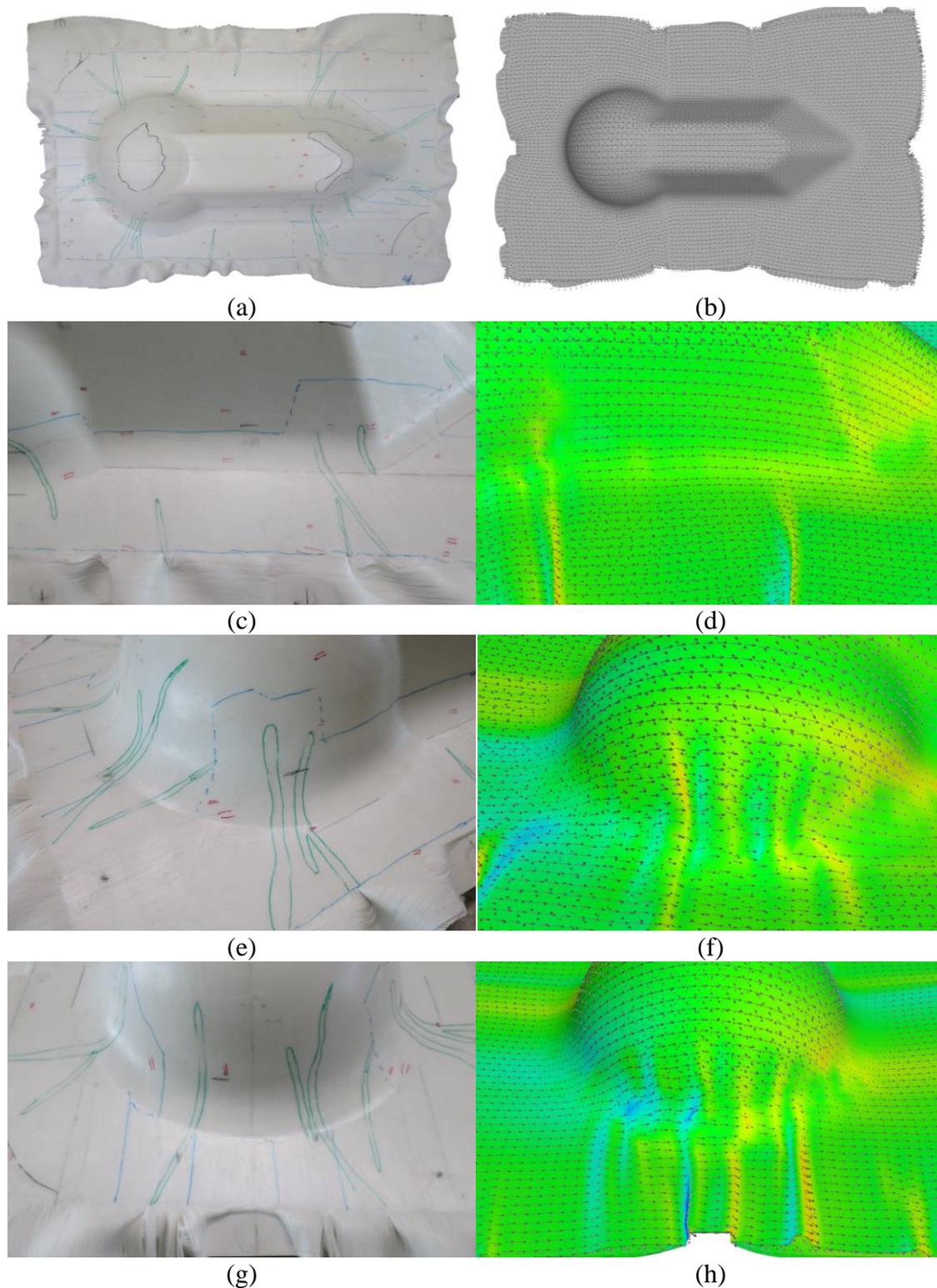
Fig. 4-34.   Quasi-isotropic GF/PP complex geometry experimental and simulation results
(a) Top view of formed quasi-isotropic part, (b) top view of the simulation result, (c) wrinkles (green) on the side, (d) localized high shear strain of 0° ply, (e) wrinkles (green) in 45° direction on the hemisphere, (f) localized high shear strain of 45° ply on hemisphere, (g) wrinkles (green) in 0° direction on the hemisphere, (h) localized high shear strain of 90° ply on hemisphere

The accordance between experiment and simulation regarding the outer contour is worse for the QI layup (see Fig. 4-34a, b) than for the orthotropic layup. In the simulation the deformation of the plies around the geometry is completely flat and no wrinkles or folds occur. On the real part, in contrast, several wrinkles spread over the whole geometry emerged during forming (see Fig. 4-34c, e, g) because of the added fibre directions. This might be the reason for the differences regarding the outer contour. By analysing the shear strain of the simulation model, also critical areas can be identified. Local high shear strains (red and blue areas) are indications for the emergence of wrinkles or folds. In addition to that, the course of the fibre directions can be analysed. Around possible wrinkles, discontinuities of the fibre directions occur. Depending on the position of the wrinkles, different plies have to be analysed. The direction of the wrinkles is oriented perpendicular to the fibre direction of the respective ply. Examples are shown in Fig. 4-34d, f and h. Comparing them to the images of the formed part, it can be noted that all critical areas prone to wrinkling can be identified.

Using the complex geometry also forming simulations for the CF/PEEK material were performed. The material parameters provided by AniForm for the radius forming simulations (see chapter 4.3.1) were used again. The experiments described in chapter 3.2.3 showed that for forming complex geometry higher pre-heating and tool temperatures are necessary as for the radius forming. The rapid cooling during the transfer and upon contact with the tools reduced the formability distinctly and caused wrinkles and folds. Nevertheless, the material parameters for a temperature of 365 °C provided by AniForm were used to cope with the reduced formability. A comparison between existing forming defects of the formed part and the simulation results is presented in Fig. 4-35. Here an element size of 4.6 mm was used.

(a)

(b)

(c)

(d)

(e)

(f)
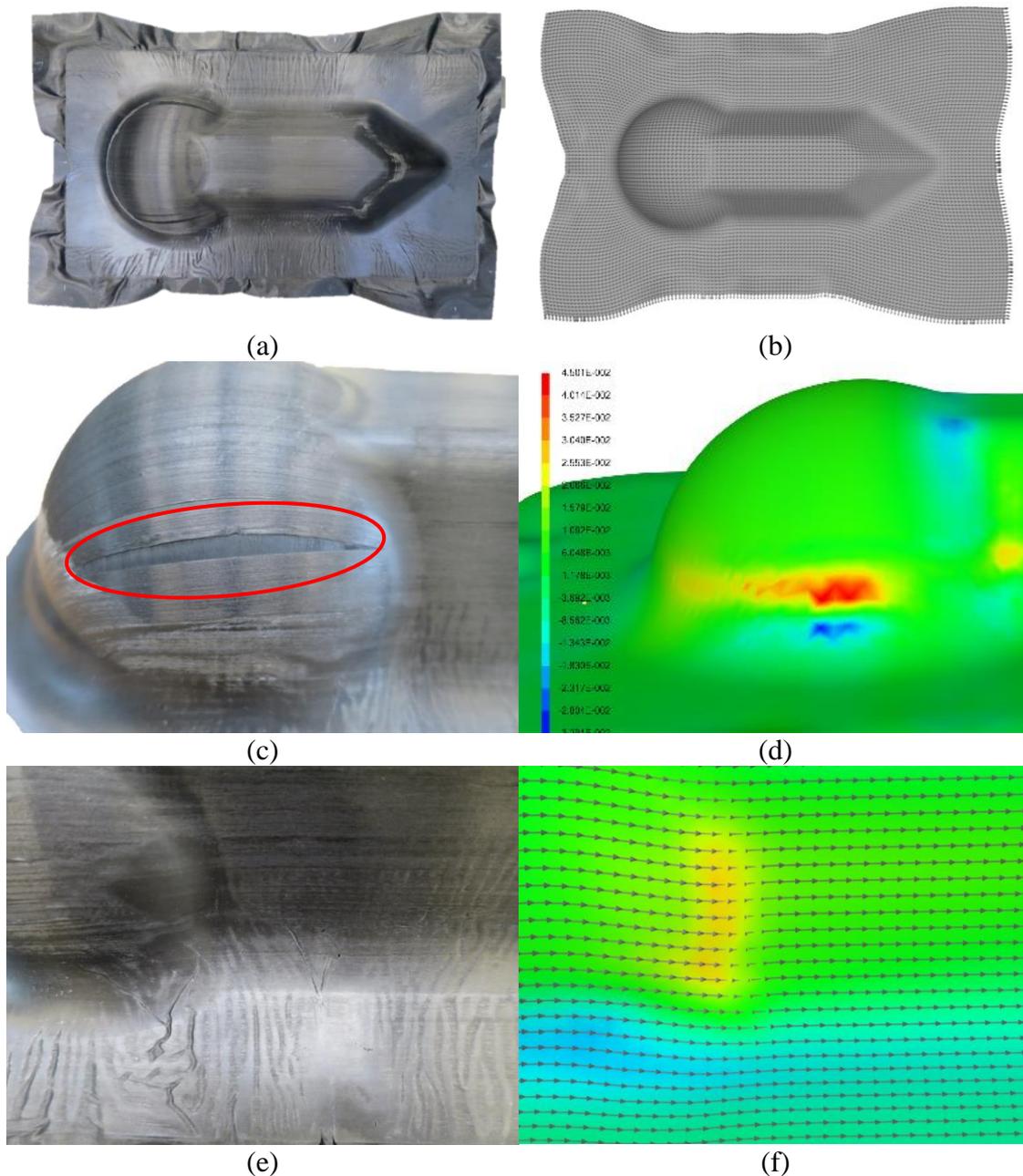
Fig. 4-35.   **CF/PEEK complex geometry experimental and simulation results**
(a) Top view of formed part, (b) top view of simulation model, (c) large gap of the top
ply, (d) high strain transverse to fibre direction indicating possible gap, (e) fibre waviness
and severe folds, (f) fibre strain of the 0° surface ply on the side of the geometry

Comparing the top view of the formed part and the simulation model it can be
determined that the outer contour coincides rather well (see Fig. 4-35a, b). However,
the real part clearly shows a higher number of wrinkles and fibre waviness than the
simulation. In Fig. 4-35c a large gap of the top ply is highlighted (red mark). This gap
is probably caused by transverse sliding of the fibres. At the same spot of the
simulation a high transverse shear strain of the 0° surface ply is displayed indicating a

possible gap. As mentioned above, in the formed part numerous wrinkles and fibre waviness are present. The latter is especially gathered on both sides, closely to the geometry (see Fig. 4-35e). The waviness is not visible in the simulation result and all fibre directions are straight. But examining the fibre strain of the 0° plies, compressive strains are present, which is an indication for fibre waviness.

4.4 Validation of the fibre directions

The validation of the forming simulation results can be performed applying different methods. In the previous chapter the simulation results were visually compared with experimentally formed parts. The focus was on the outer contour and the position, size and number of surface forming defects such as wrinkles, folds or gaps. Even more important is the actual fibre direction after the forming process, given the usage of the forming simulation results for structural analyses. For this purpose, it has to be ensured that the predicted fibre directions match the real fibre directions of the formed part. In this chapter a method using optically measured fibre directions for the validation of the predicted fibre directions of the forming simulation is presented.

The measurements described hereinafter were performed within the scope of [S7]. Parts of this chapter's content (text and figures) are based on [K4]

For validating the simulation results within this work, the fibre directions were captured using an optical measuring system, namely the FScan by the Profactor GmbH. Its functional principle is based on the Photometric Stereo that uses the special reflectional behaviour of fibres for determining the fibre direction. With the help of several images taken from the same point of view under varying illumination directions the orientations can be derived [162, 163]. The CMOS sensor of the camera is surrounded by a ring of 96 LEDs, which enables different illumination patterns. The camera provides a resolution of 1312 x 1024 pixels; depending on the measuring area 40-60 μm per pixel are possible [127]. For automated measurements the sensor can be included in a robot cell (see Fig. 4-36). With the corresponding evaluation software, the measured fibre directions of a 3D geometry can be projected directly on a computer aided design (CAD) surface. The optical measurements were conducted at the Profactor GmbH.

Fig. 4-36.   Measuring setup at the Profactor GmbH

It was planned to scan a GF/PP and CF/PEEK part of the experimental study described in chapter 3.2. Contrary to the expectations, measurement of the GF/PP part was not possible, as due to the pressed and glossy surface the measuring principle could not be applied. Therefore, only the CF/PEEK part could be measured. With the sensor almost the complete top surface of the part could be scanned. Only the bottom radius was not reachable because of the sensor size. Also a measurement of the bottom surface was not possible. Due to the size and geometry of the part, it was necessary to scan it in two steps and merge the results afterwards. The measured fibre orientations were projected on a 3D mesh of the geometry. About 20,000 measuring points over the whole geometry were generated. In Fig. 4-37 the measured fibre directions are shown with a reduced number of measuring points. The coordinates of every mesh point and the corresponding fibre direction as vector were exported to an HDF5-file for further processing. In that way, measured orientations could be used directly for a comparison with the results of the forming simulations.
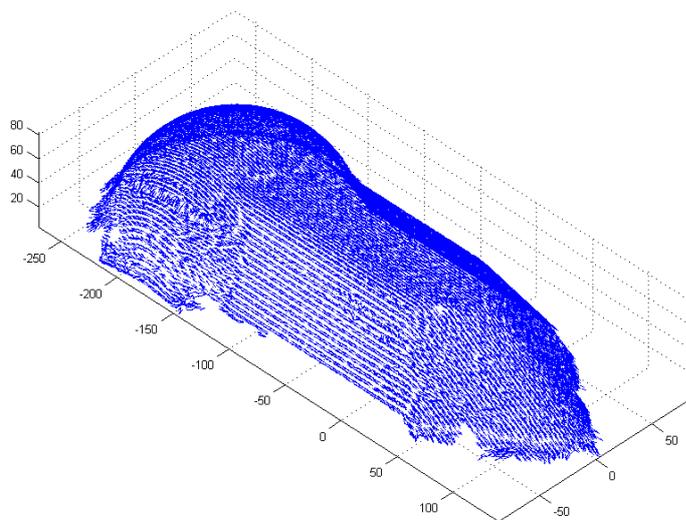
Fig. 4-37.   Measured fibre directions of the CF/PEEK part

For the comparison between simulation data and measured directions a Matlab code was generated. In this programme the measured data and simulation results are loaded first. Then the meshes are positioned accordingly. For every simulation node measuring points within a certain range are searched. For that, a range at least half the size of the simulation mesh should be used. The fibre direction of these measuring points is then averaged and the result is compared to the predicted fibre orientation of the simulation. In doing so an angle characterising the deviation at every simulation node is obtained. The result is then printed as 3D colour plot (see Fig. 4-38). Thereby the prediction accuracy of the forming simulation can be evaluated easily.
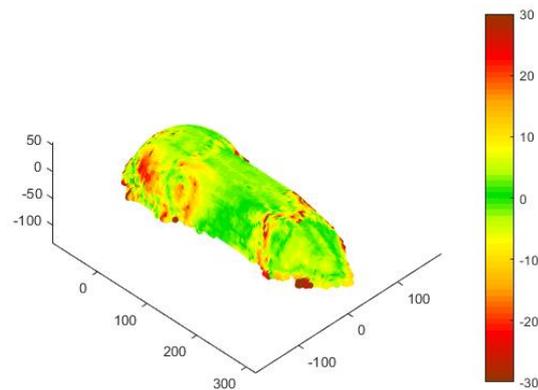
Fig. 4-38.   **3D scatter plot of the fibre direction deviations**

This validation method was applied to the CF/PEEK complex geometry. The simulation results presented in chapter 4.3.3 were compared with the fibre direction that had been measured using the optical sensor of Profactor GmbH. The results are shown in Fig. 4-39.
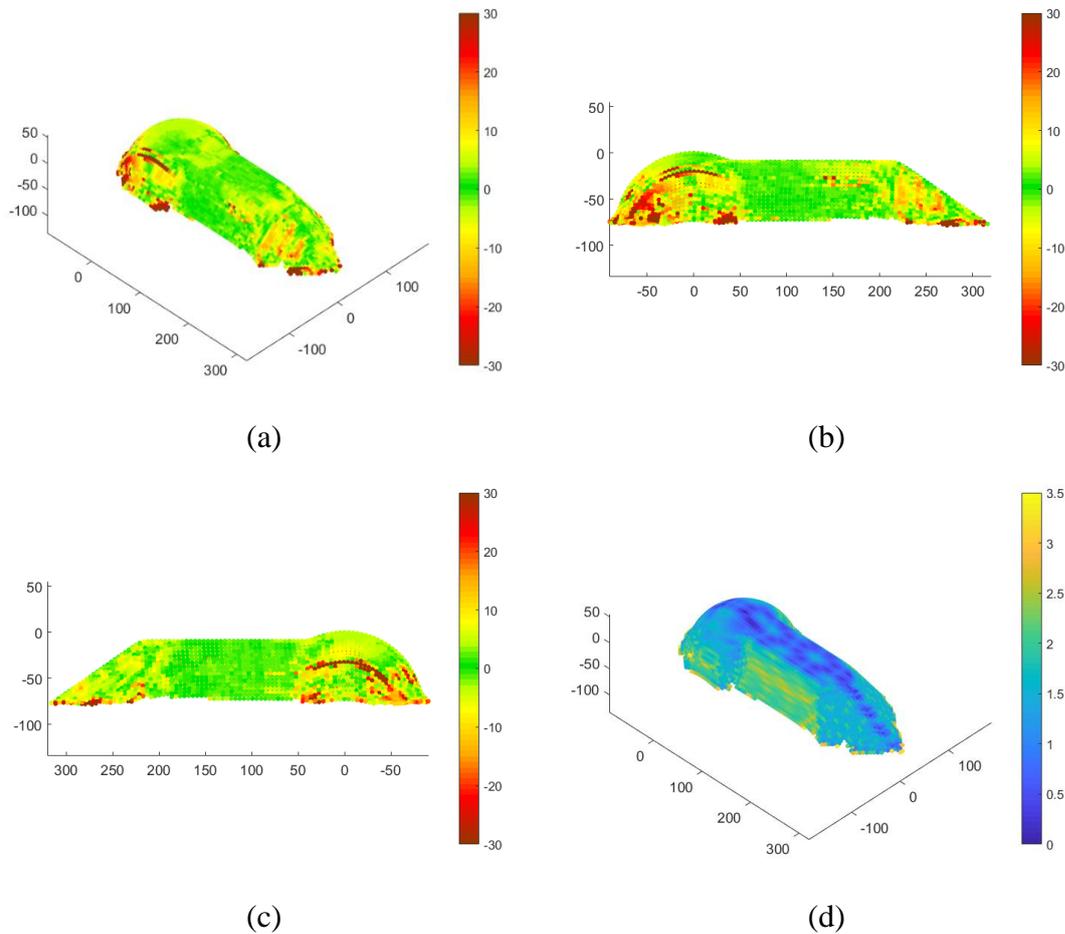
Fig. 4-39.   **3D scatter plot comparison of CF/PEEK part and simulation results**
(a-c) deviation of fibre directions, (d) distance between simulation mesh and measured surface

Evaluating the results, it has to be considered that the measured and simulation mesh are not completely congruent, as there may be some geometry differences. This could influence the accuracy of the comparison. Examining the results in Fig. 4-39, a good conformity between simulation and experiment can be determined. The widespread green colour represents deviations of about ±3°. The lines of high deviations on both sides of the hemisphere and on the right side of the middle part are based on surface gaps on the formed part. Here, the fibre direction of the underlying ply was measured, which is rotated about 90°. There are higher deviations close to the bottom of the hemisphere and on the tip of the geometry. The mismatch between the geometries in these areas (see Fig. 4-39d) could be an explanation. Another reason might be the higher deformation of the material at points, where a high shearing of the material occurs due to the geometry shape. Also it might be possible that the high compaction of the material and the resulting glossy surface caused errors during the optical measurement process in the respective areas.

4.5 Summary and discussion

Within the previous chapters the numerical studies were described, including material characterisation, material data fitting, forming simulations and the validation based on fibre directions.

The focus of the material characterisation was on the ply-ply interface properties, bending and in-plane shear behaviour.

For the friction characterisations a test stand was designed, which was suited for pull-out and pull-through measurements. The experiments showed that the friction measurements are difficult to perform. Due to the loss of stability of the material during heat up, it was challenging to assure stable clamping and prevent deformations. During the experiments fibre orientation, test speed and normal pressure were varied. The friction coefficient was calculated and the peak was used for evaluation. The results revealed that an increasing test speed causes a rise of the friction coefficient. A higher normal pressure, in contrast, decreases it. This behaviour was the same for all tested fibre orientation combinations, but the levels of the values differed. The 0°/0° orientation caused significantly higher friction coefficients than the 0°/90° combination. The reason might be the interlocking of fibres with the same orientation during the measurement. A similar frictional behaviour was observed by other authors [62, 74, 164].

For the bending characterisation a test developed by Margossian et al. [83] was used. The method is based on a quasi-static three-point bending test in a DMA. Tests were performed at three different temperatures and three different deformation rates. They revealed a clear deformation rate dependency, which was less distinct for higher temperatures. The drawback of this method is that only small deformations are possible that do not represent the material behaviour during the formation of wrinkles or folds. Additionally, laminates with a thickness of 1 mm are required for this test. But for the forming simulation the properties of a single ply are necessary. Hence, it would be preferable to characterise a single ply. A different bending test was developed by Sachs et al. [165]. This method bends a single ply specimen with a custom-built device mounted in a rheometer. The necessary torque is recorded depending on the rotational velocity and temperature. With this test the bending properties of a single ply under large deformations can be examined.

The characterisation of the intra-ply shear properties was based on the torsion bar test developed by Haanappel et al. [63]. A bar with rectangular cross-section and fibres oriented in longitudinal direction is twisted using a rheometer. A relation between torque and rotation angle was determined. Due to the specific geometry of the specimens the manufacturing was quite elaborate, and a great amount of material was necessary. Nevertheless, using this test method the testing conditions could be controlled exactly.

After the material characterisation a material data fitting was performed to determine the input parameters for the simulation models. This step is crucial as the constitutive

equations of the material models require many input parameters (e.g. up to ten for the Polymer friction model) that cannot be obtained directly from the characterisation tests. For the friction a self-developed Matlab tool was used, for bending and in-plane shear it was drawn on a Matlab tool provided by AniForm. They both were based on a curve fitting approach and minimise the deviation between measured values and model behaviour. It must be considered that the resulting input parameters do not have any relation to physical parameters. Due to the large number of input parameters several solutions might be possible. For that reason, it was necessary to simulate the characterisation tests with the fitted input parameters to verify the material behaviour. For the friction, bending and in-plane properties it was possible to reproduce the courses of the characterisation tests rather well. So, the fitted parameters could have been used for the forming simulations.

Forming simulations were performed with different geometries and materials based on the described experimental studies. The used input parameters were either characterised and fitted as described above (GF/PP) or provided by AniForm (CF/PA6 and CF/PEEK). All tools were modelled as rigid bodies, which is legitimate as real metal tools are much stiffer than the formed laminates and are not expected to deform during the process. The laminates consisted of shell elements, with every ply being represented by one layer of shell elements. The results of the forming simulations were then compared with the formed parts of the experimental studies. It showed that the outer contour of simulation and real parts coincided well in almost all cases. There were only larger deviations for the GF/PP complex part with QI layup. Also surface gaps resulting of fibre shift were clearly visible in the simulation results as transverse strain of the plies. Despite that, not all effects that were observed during the experimental studies were also directly visible in the simulation results. Especially small in-plane fibre waviness or wrinkles could not be represented correctly as these effects were mostly smaller than the used element size. As a result, the simulations in general showed less wrinkles and folds than the experiments. Nevertheless, by analysing occurring shear or fibre strains of the plies all critical areas could be identified. A localised high shear strain emerged at locations that were prone to wrinkling in the experiments. Such shear localisations were especially present in plies where fibres where oriented 90° to the direction of the wrinkles or folds. By looking for compressive strains in fibre direction, areas critical for in-plane fibre waviness could be identified.

Finally, a validation method for the forming simulations based on fibre orientations was presented. As the resulting fibre directions directly influence the mechanical properties of formed part, it is important to know the changes evoked by the forming process. If the predicted fibre directions of a forming simulation are correct, the orientations can be transferred directly to a structural FE simulation. To ensure that, a validation of the calculated fibre directions is necessary. For that purpose, the fibre courses of the real part have to be measured. The fibre orientations of a complex part

made of CF/PEEK were measured using an optical sensor system of Profactor. The outer surface of the part was recorded, fibre orientations calculated and projected on a CAD geometry. The fibre directions of the outer ply of the simulation model were exported to a txt-file. For comparing the results with the simulation outcome, a Matlab code was generated, with which the measured and simulation data could be loaded and an angle indicating the deviation could be calculated. For evaluation reasons the angles were displayed as coloured 3D scatter plot. Only small deviations (±5°) were detected in most areas. Higher deviations were mainly present in areas of high shear strain or wrinkles. Also, a very glossy surface could distort the optical measurement and therefore cause more differences. A drawback of the optical measurement is that only the surface ply can be analysed and even the inner surface was not reachable due to the sensor size. In a previous study also other measurement methods such as eddy current or computer assisted tomography were considered [K4]. But these systems have not yet been capable of measuring larger parts completely.

5 Conclusion

The subsequent chapter summarizes and discusses the results of this thesis. It compares the outcomes of different chapters and relates the findings. This section provides a comprehensive overview over the entire work and reviews the fulfilment of the defined tasks.

The first half of this work was focused on extensively studying the forming behaviour of UD FRTP materials. Three different studies with increasing part complexity were conducted and knowledge about the influence of various process parameters achieved. Laminates, that were created by ATL and consolidated in a hot-press afterwards, were thermoformed. Prior to forming the laminates were clamped in a support frame and pre-heated in an IR oven.

The experimental tests began with a 90° radius forming of CF/PEEK. The thickness and layup sequence were varied in combination with radius sizes and pre-tension. The results showed that depending on layup and pre-tension, radius thinning and fibre waviness occurred for small radii. Especially UD layups were prone to these effects. To avoid them, higher pre-tensions, orthotropic layups and radius sizes larger than two times the laminate thickness should be chosen.

To further investigate the effect of process parameters on the part quality, a complex tool geometry was designed for the second forming study. The geometry combined different shapes such as flat areas, a hemisphere, radii with different sizes and convex and concave areas. The goal was to generate forming defects and examine the emergence of these defects with respect to process and laminate parameters. The main experiments were performed using GF/PP; then the results were applied to CF/PEEK. For the GF/PP forming experiments the influence of tool temperature, forming speed, forming pressure, support frame configuration, pre-tension and layup on the resulting part quality was investigated. The results were evaluated based on four forming effects: wrinkles, fibre waviness, surface gaps and surface roughness. The influence of each parameter on each forming effect was determined. It could be observed that within the considered range higher forming pressure, forming speed and tool temperature reduced the frequency and number of in-plane undulations and wrinkles and improved the surface quality. Also, a higher number of constant force springs in the support frame was found to improve these effects. In contrast, a higher spring force increased the number of undulations. Finally, the forming behaviour of a QI layup compared to the orthotropic layup under the same forming conditions was studied. It could be stated that the QI layup produced distinctly more wrinkles than the orthotropic layup even though constant force springs in 45°-direction were included to apply tension to the additional fibre directions. Based on the gained findings CF/PEEK

laminates were formed with the complex geometry. Although the parameters functioned well for the radius forming, the pre-heating and tool temperature had to be raised significantly to achieve a satisfying part quality.

During the preparation of the laminates for the forming experiments, a time consuming and effortful consolidation step was always necessary. Depending on the matrix material the ATL layups were either pre-heated in a heating table and then consolidated in the heated press or via a variothermal consolidation cycle with closed mould in the heating press. Both cycles implicated an additional heating of the layups. To avoid that, the third experimental study tested approaches to form spot-welded ATL layups without previous consolidation. For that study CF/PA6 was used, as this technical material is applied in the automotive industry, which always strives for cycle time reductions. Three concepts were tested and the usage of PA6 films for creating a vacuum setup to pre-heat and forming the layups under vacuum showed promising results. A part quality comparable to conventional manufactured parts could be achieved, which was assured by microsections and thermography, FVF and VVC measurements.

The performed experiments enabled gaining a profound understanding of the influence of the most important process parameters on forming effects or defects. By considering the determined coherences, forming results could be influenced purposefully to reduce certain effects and improve the part quality. The last forming study gave perspective on how to improve the forming process and reduce the overall cycle time.

The second half of the thesis was dedicated to numerical studies on the forming behaviour. The basis of a proper FE forming simulation is the material characterisation. For FE simulations on a macroscopic level, in-plane shear, out-of-plane bending and interface properties must be determined. Several publications about this topic can be found. However, so far there are no standardised characterisation tests for UD FRTP materials. As the properties of FRTP are strongly dependant on temperature and shear rate, the characterisation has to be performed under specific environmental conditions that are similar to the forming conditions. Taking that into account, GF/PP tape was characterised.

For the interface characterisation a friction test stand for PO and PT test was developed. The test stand was mounted to a universal testing machine to determine the friction properties under different temperatures, test speeds and normal forces. With this specific setup it was possible to measure the inter-ply slip for different fibre orientations. The results showed that an increase in test speed caused an increase of the CoF. Also, an influence of the normal force could be determined, where higher normal forces produced lower CoFs. It was detected that the CoF of 0°/0° interface is higher than of a 0°/90° interface, probably due to fibre interlocking effects.

The out-of-plane bending tests were performed using the DMA method developed by Margossian et al. [83]. A small UD specimen is deformed in a three-point bending test under controlled environmental conditions in the thermal chamber of the DMA. Tests were performed under different deformation rates and temperatures. The material

showed a clear shear rate dependency especially at lower temperatures. The main drawback of this test method was, that only small deformations and low deformations rates were possible.

For the in-plane shear characterisation it was drawn on the torsion bar test method presented by Haanappel et al. [41, 63]. The properties were measured under a controlled temperature and dynamical testing within the LVE region. Again, a shear rate dependency was found.

To determine the correct input parameters for the material models in AniForm, a material data fitting was performed using a self-developed Matlab routine and one provided by AniForm. The characterisation tests were modelled in AniForm and the material behaviour with the fitted parameters was reviewed.

In AniForm, forming simulation models based on the experimental studies were set up. Simulations were performed, and the results compared to the experimental outcomes with respect to outer contour, wrinkle development or in-plane undulations. There was a high accordance regarding the outer contour. Also wrinkles and undulations were pictured correctly in some cases. Despite that, by analysing the in-plane shear strains, transverse strains and compressive fibre strains, the critical areas prone to wrinkling or undulations could be detected. It could be stated that the macroscopic FE forming simulation is suitable to reveal critical areas during the forming process for all geometries and materials that were considered.

Despite the correct prediction of forming defects, it is also important to know the fibre directions after forming. The predicted fibre directions could be used for subsequent structural analyses. Thus, a validation of the simulation results based on the fibre directions was performed. A CF/PEEK part was measured using an optical sensor by Profactor, with which the top surface plies were traced. The deviations between the measured directions and the ones predicted by the simulation were then compared in a Matlab tool. The deviations were illustrated with a 3D scatter plot. The developed method was found to be suitable to provide a good overview over the deviations. In most areas only small deviations were detected, with higher values in regions with wrinkles or higher shear deformations.

6 Outlook

Based on the acquired findings, the following recommendations can be given for future activities in forming of UD FRTP.

The described experimental forming studies revealed that the process parameters not only depend on the used material but are also strongly influenced by the complexity of the geometry. To improve the part quality and reduce the development time, further efforts should be made to determine guidelines for process parameters resulting of the properties of the geometry such as degree of deformation or minimal radius sizes.

The performed material characterisation tests were limited to minor deformation rates. To characterise the material behaviour based on realistic forming speeds, higher deformation rates must be tested in future studies. In addition to that, with the tests used for bending and in-plane characterisation, only small deformations within the LVE were possible. These test methods must be developed further to be able to perform characterisation tests for high deformations as they occur in real forming processes.

To improve the quality of the forming simulation results and simplify the process, forming simulation software suppliers should provide guidance for the material characterisation used for their material models. At least information regarding the recommended characterisation methods should be available. It is especially necessary to know, how the measured material data can be transferred to the required input parameters for the material models. Currently, an automated fitting process must be performed for that purpose, or the parameters must be adapted iteratively until the desired material behaviour is achieved. This procedure is not satisfying as the resulting input parameters do not correspond to physical quantities.

With the finite element forming simulations on macro level conducted in this thesis, only isothermal forming processes can be simulated. In contrast, the forming experiments are performed on a variothermal basis. As the mould temperature is clearly cooler than the laminate, the cooling already begins during forming. Nevertheless, the isothermal modelling is applicable, because the forming procedure is fast and only little cooling occurs until the mould is fully closed. But to simulate the forming process even more realistically and to consider slow forming procedures, the development of new modelling approaches is essential. In addition to characterisation methods that cover the temperature dependence of the material properties, also new thermo-mechanical material models are crucial and must be developed.

For an enhanced validation of the forming simulation results, measuring methods such as eddy current or computer assisted tomography must be developed further. With these methods it might be possible to also measure the fibre directions of the inner plies. So far it has not been possible to determine the fibre directions of large parts with high resolution using the existing technologies.

Bibliography

[1]   Bundesministerium für Umwelt, Naturschutz, Bau und Reaktorsicherheit (BMUB), "Klimaschutz in Zahlen 2017: Fakten, Trends und Impulse deutscher Klimapolitik," Apr. 2017. [Online] Available: https://www.bmu.de/fileadmin/Daten_BMU/Pools/Broschueren/klimaschutz_in_zahlen_2017_bf.pdf. Accessed on: Sep. 19 2018.

[2]   Bundesministerium für Umwelt, Naturschutz und nukleare Sicherheit (BMU) and www.bmu.de, "Klimaschutz in Zahlen 2018: Fakten, Trends und Impulse deutscher Klimapolitik," May. 2018. [Online] Available: https://www.bmu.de/fileadmin/Daten_BMU/Pools/Broschueren/klimaschutz_in_zahlen_2018_bf.pdf. Accessed on: Oct. 04 2018.

[3]   M. Lienkamp and F. Homm, *Status Elektromobilität 2018: Der Kunde wird es entscheiden*, 2018.

[4]   "The automotive industry and composites as of today," *JEC Composite Magazine*, vol. 55, no. 123, pp. 29–36, 2018.

[5]   J. Komornicki, L. Bax, H. Vasiliadis, I. Magallon, and K. Ong, "Polymer composites for automotive sustainability," 2017. [Online] Available: http://www.suschem.org/files/library/Publications/POLYMERS_Brochure_Web.pdf. Accessed on: Jan. 19 2018.

[6]   P. Vetter, "Leichtbau fällt nicht schwer ins Gewicht," *Welt am Sonntag*, 03 Dec., 2017, https://www.uni-due.de/~hk0378/publikationen/2017/20171203_WAMS.pdf.

[7]   M. Lienkamp, *Status Elektromobilität 2014: Der Ausblick bis 2025 zeigt eine stille Revolution der bisherigen automobilen Welt*, 2014.

[8]   M. Lienkamp, *Status Elektromobilität 2016: Oder wie Tesla nicht gewinnen wird*, 2016.

[9]   M. Effing, "We have to think more and more about multi-material systems," *JEC Composite Magazine*, vol. 55, no. 123, pp. 38–40, 2018.

[10]   H. Eickenbusch and O. Krauss, "Kurzanalyse Nr. 3: Kohlenstofffaserverstärkte Kunststoffe im Fahrzeugbau: Ressourceneffizienz und Technologien," VDI Zentrum Ressourceneffizienz, Mar. 2013. [Online] Available: https://www.ressource-deutschland.de/fileadmin/user_upload/downloads/kurzanalysen/2014-Kurzanalyse-03-VDI-ZRE-CFK.pdf. Accessed on: Dec. 27 2017.

[11]   T. Pfefferkorn, R. Jakobi, and A. Nixdorf, "Vom Laminat zum Bauteil," *Kunststoffe*, no. 12, pp. 94–100, 2013.

[12]   U. K. Vaidya and K. K. Chawla, "Processing of fibre reinforced thermoplastic composites," *International Materials Reviews*, vol. 53, no. 4, pp. 185–218, 2013.

[13]   E. Witten, M. Sauer, and M. Kühnel, "Composites-Marktbericht 2017: Marktentwicklungen, Trends, Ausblicke und Herausforderungen," AVK– Industrievereinigung Verstärkte Kunststoffe e. V. (Hrsg.); CCeV, Sep. 2017. [Online] Available: http://www.avk-tv.de/files/20170919_avkccev__marktbericht_2017.pdf. Accessed on: Dec. 27 2017.

[14]   T. J. Ahmed, D. Stavrov, H.E.N. Bersee, and A. Beukers, "Induction welding of thermoplastic composites—an overview," *Composites Part A: Applied Science and Manufacturing*, vol. 37, no. 10, pp. 1638–1651, 2006.

[15]   A. R. Offringa, "Thermoplastic composites—rapid processing applications," *Composites Part A: Applied Science and Manufacturing*, vol. 27, no. 4, pp. 329–336, 1996.

[16]   A. Yousefpour, M. Hojjati, and J.-P. Immarigeon, "Fusion Bonding/Welding of Thermoplastic Composites," (af), *Journal of Thermoplastic Composite Materials*, vol. 17, no. 4, pp. 303–341, 2004.

[17]   M. Flemming, G. Ziegmann, and S. Roth, *Faserverbundbauweisen: Halbzeuge und Bauweisen*. Berlin, Heidelberg: Springer Berlin Heidelberg, 1996.

[18]   G. Beresheim, M. Latrille, and R. Schledjewski, "Auf dem Weg zur Automation: Neue Entwicklungsstufe der Thermoplast-Tapelegetechnik," (ha), *KU Kunststoffe*, vol. 91, no. 12, pp. 78–81, 2001.

[19]   J. Mondo, S. Wijskamp, and R. Lenferink, "Overview of Thermoplastic Composite ATL and AFP Technologies," in *International Conference & Exhibition on Thermoplastic Composites*, Bremen, 2012.

[20]   J. Verrey, M. D. Wakeman, V. Michaud, and J.-A. E. Manson, "Manufacturing cost comparison of thermoplastic and thermoset RTM for an automotive floor pan," *Composites Part A: Applied Science and Manufacturing*, vol. 37, no. 1, pp. 9–22, 2006.

[21]   H. Lengsfeld, F. Wolff-Fabris, J. Krämer, J. Lacalle, and V. Altstädt, *Faserverbundwerkstoffe: Prepregs und ihre Verarbeitung,* 1st ed. München: Carl Hanser Verlag, 2015.

[22]   Dieffenbacher GmbH, *Tailored blank line with Fiberforge and Fibercon systems*. [Online] Available: http://www.dieffenbacher.de/upload/downloads/Brochure_Fiberforge_Fibercon_2017.pdf. Accessed on: Dec. 19 2017.

[23]   A. Burkhart and D. Cramer, "Continuous-fibre reinforced thermoplastic tailored blanks," *JEC Composite Magazine*, vol. 43, no. 22, pp. 41–43, 2006.

[24]   F.C. Campbell, Ed., *Manufacturing Processes for Advanced Composites*. Amsterdam: Elsevier Science, 2004.

[25]   B. T. Åström, *Manufacturing of Polymer Composites*. London: CRC Press, 1997.

[26]   G. Lebrun, J. Denault, and M. Bureau, "Influence of Consolidation and Forming Parameters in the Molding of Continuous Fibre Reinforced Thermoplastic Composites," in *2nd Annual Automotive Composites Conference*, Troy, MI, USA, 2002.

[27]   M. Neitzel, P. Mitschang, and U. Breuer, Eds., *Handbuch Verbundwerkstoffe: Werkstoffe, Verarbeitung, Anwendung*. München: Carl Hanser Verlag GmbH & Co. KG, 2014.

[28]   M. Hou, "Stamp forming of continuous glass fibre reinforced polypropylene," *Composites Part A: Applied Science and Manufacturing*, vol. 28, no. 8, pp. 695–702, 1997.

[29]   U. Breuer, *Beitrag Zur Umformtechnik Gewebeverstärkter Thermoplaste*. Düsseldorf: VDI-Verl., 1997.

[30]   K. Friedrich, M. Hou, and J. Krebs, "Chapter 4 Thermoforming of Continuous Fibre/Thermoplastic Composite Sheets," in *Composite Sheet Forming*, D. Bhattacharyya, Ed., 1997, pp. 92–162.

[31]   T. G. Gutowski, "Cost, Automation and Design," in *Advanced Composites Manufacturing*, T. G. Gutowski, Ed., New York: John Wiley & Sons, 1997, pp. 513–570.

[32]   D. Leutz, "Forming simulation of AFP material layups: Material characterization, simulation and validation," Ph.D. thesis, Lehrstuhl für Carbon Composites, Technische Universität München, München, 2016.

[33]   P. de Luca, P. Lefébure, and A. K. Pickett, "Numerical and experimental investigation of some press forming parameters of two fibre reinforced thermoplastics: APC2-AS4 and PEI-CETEX," *Composites Part A: Applied Science and Manufacturing*, vol. 29, pp. 101–110, 1998.

[34]   K. Vanclooster, S. V. Lomov, and I. Verpoest, "Simulation of Multi-Layered Composites Forming," 2010.

[35]   P. Boisse, N. Hamila, E. Vidal-Sallé, and F. Dumont, "Simulation of wrinkling during textile composite reinforcement forming. Influence of tensile, in-plane shear and bending stiffnesses," *Composites Science and Technology*, vol. 71, no. 5, pp. 683–692, 2011.

[36]   S. Haanappel, R. H. W. ten Thije, U. Sachs, B. Rietman, and R. Akkerman, "Formability analyses of uni-directional and textile reinforced thermoplastics," *Composites Part A: Applied Science and Manufacturing*, vol. 56, pp. 80–92, 2014.

[37]   E. Guzman-Maldonado, N. Hamila, N. Naouar, G. Moulin, and P. Boisse, "Simulation of thermoplastic prepreg thermoforming based on a visco-hyperelastic model and a thermal homogenization," *Materials & Design*, vol. 93, pp. 431–442, 2016.

[38]   D. Doerr, F. J. Schirmaier, F. Henning, and L. Kärger, "A viscoelastic approach for modeling bending behavior in finite element forming simulation of continuously fiber reinforced composites," *Composites Part A: Applied Science and Manufacturing*, vol. 94, pp. 113–123, 2017.

[39]   R. H. W. ten Thije, "Finite Element Simulations of Laminated Composite Forming Processes," Ph.D. thesis, Universiteit Twente, Twente, 2007.

[40]   D. Doerr *et al.,* "A Benchmark Study of Finite Element Codes for Forming Simulation of Thermoplastic UD-Tapes," *Procedia CIRP*, vol. 66, pp. 101–106, 2017.

[41]   S. Haanappel, "Forming of UD fibre reinforced thermoplastics: A critical evaluation of intra-ply shear," Ph.D. thesis, Universiteit Twente, Twente, 2013.

[42]   AVK–Industrievereinigung Verstärkte Kunststoffe e. V. (Hrsg.), *Handbuch Faserverbundkunststoffe/Composites: Grundlagen - Verarbeitung - Anwendungen,* 4th ed.: Springer, 2014.

[43]   E. Roos and K. Maile, *Werkstoffkunde für Ingenieure*. Berlin, Heidelberg: Springer Berlin Heidelberg, 2015.

[44]   H. Schürmann, *Konstruieren mit Faser-Kunststoff-Verbunden: Mit 39 Tabellen,* 2nd ed. Berlin, Heidelberg, New York, NY: Springer, 2007.

[45]   M. Bitterlich *et al.,* "Tailored to Reactive Polyamide 6," *Kunststoffe international*, pp. 47–51, Mar. 2014.

[46]   C. Cherif, *Textile Werkstoffe für den Leichtbau*. Berlin, Heidelberg: Springer Berlin Heidelberg, 2011.

[47]   M. Bonnet, *Kunststofftechnik: Grundlagen, Verarbeitung, Werkstoffauswahl und Fallbeispiele*. Wiesbaden: Springer Fachmedien Wiesbaden, 2014.

[48]   F. Henning and E. Moeller, *Handbuch Leichtbau: Methoden, Werkstoffe, Fertigung*. München: Hanser, 2011.

[49]   A. C. Long, Ed., *Design and manufacture of textile composites*. Cambridge: Woodhead Publishing Limited, 2005.

[50]   U. Berthold, "Beitrag zur Thermoformung gewebeverstärkter Thermoplaste mittels elastischer Stempel," Ph.D. thesis, Institut für Konstruktion und Verbundbauweisen, TU Chemnitz, Chemnitz, 2001.

[51]   V. Antonelli, "Improvements of thermoforming of thermoplastic composites using a collection of rubber particles as a soft mould half," Ph.D. thesis, Technische Universiteit Delft, Delft, 2014.

[52]   J. Krebs, K. Friedrich, and D. Bhattacharyya, "A direct comparison of matched-die versus diaphragm forming," *Composites Part A: Applied Science and Manufacturing*, vol. 29, no. 1-2, pp. 183–188, 1998.

[53]   TenCate, "Cetex TC1200 PEEK Resin System Datasheet," Jan. 2017. [Online] Available: https://www.tencatecomposites.com/media/7765d981-1f9f-472d-bf24-69a647412e38/XDoW-A/TenCate%20Advanced%20Composites/Documents/Product%20datasheets/Thermoplastic/UD%20tapes,%20prepregs%20and%20laminates/TenCate-Cetex-TC1200_PEEK_PDS.pdf. Accessed on: Jan. 09 2018.

[54]   Celanese, "CELSTRAN CFR-TP PA6 CF60-03 - PA6 Datasheet," Jun. 2016. [Online] Available: http://tools.celanese.com/material/pdf/150991/CELSTRANCFRTPPA6CF6003?rnd=1504695640274. Accessed on: Nov. 10 2017.

[55]   Celanese, "CELSTRAN CFR-TP PP GF70-13 - PP Datasheet," Jan. 2018. [Online] Available: http://tools.celanese.com/material/pdf/150995/CELSTRANCFRTPPPGF7013?rnd=1514978446220. Accessed on: Jan. 03 2018.

[56]   J. A. Sherwood, K. A. Fetfatsidis, J. L. Gorczyca, and L. Berger, "Fabric thermostamping in polymer matrix composites," in *Manufacturing Techniques for Polymer Matrix Composites (PMCs)*: Elsevier, 2012, pp. 139–181.

[57]   T. Joppich *et al.,* "Layup and Process Dependent Wrinkling Behavior of PPS/CF UD Tape-Laminates during Non-Isothermal Press Forming Into a Complex Component," in *ESAFORM 2016: Proceedings of the 19th International ESAFORM Conference on Material Forming*, Nantes, France, 2016.

[58]   H. Lessard, G. Lebrun, A. Benkaddour, and X.-T. Pham, "Influence of process parameters on the thermostamping of a [0/90]12 carbon/polyether ether ketone laminate," *Composites Part A: Applied Science and Manufacturing*, vol. 70, pp. 59–68, 2015.

[59]   P. Han, J. Butterfield, M. Price, S. Buchanan, and A. Murphy, "Experimental investigation of thermoforming carbon fibre-reinforced polyphenylene sulphide composites," *Journal of Thermoplastic Composite Materials*, vol. 28, no. 4, pp. 529–547, 2015.

[60] S. Black, "Thermoplastic composites "clip" time, labor on small but crucial parts: Preconsolidated carbon fiber/PPS and PEEK and automated thermoforming enable six-figure production of connectors for the Airbus A350 XWB," *ComposteWorld*, no. 5, pp. 66–73, 2015.

[61] K. Drechsler, R. Hinterhoelzl, and A. Margossian, "Process Simulation and Material Modeling of Composites SS2015," 2015.

[62] A. Margossian, "Forming of tailored thermoplastic composite blanks: material characterisation, simulation and validation," Ph.D. thesis, LCC, Technische Universität München, München, 2017.

[63] S. Haanappel and R. Akkerman, "Shear characterisation of uni-directional fibre reinforced thermoplastic melts by means of torsion," *Composites Part A: Applied Science and Manufacturing*, vol. 56, pp. 8–26, 2014.

[64] K. Potter, "In-plane and out-of-plane deformation properties of unidirectional preimpregnated reinforcement," *Composites Part A: Applied Science and Manufacturing*, vol. 33, no. 11, pp. 1469–1477, 2002.

[65] W. R. Yu, M. Zampaloni, F. Pourboghrat, K. Chung, and T. J. Kang, "Analysis of flexible bending behavior of woven preform using non-orthogonal constitutive equation," *Composites Part A: Applied Science and Manufacturing*, vol. 36, no. 6, pp. 839–850, 2005.

[66] R. Akkerman, R.H.W. ten Thije, U. Sachs, and M. B. de Rooij, "Friction in textile thermoplastic composites forming," in *Recent Advances in Textile Composites: Proceedings of the 10th International Conference on Textile Composites*, 2010, pp. 271–279.

[67] D. J. Groves, "A characterization of shear flow in continuous fibre thermoplastic laminates," *Composites*, vol. 20, no. 1, pp. 28–32, 1989.

[68] P. Harrison, R. H. W. ten Thije, R. Akkerman, and A. C. Long, "Characterising and Modelling Tool-Ply Friction of Vicsous Textile Composites," *World Journal of Engineering*, pp. 5–22, 2010.

[69] A. M. Murtagh, J. J. Lennon, and P. J. Mallon, "Surface friction effects related to pressforming of continuous fibre thermoplastic composites," *Composites Manufacturing*, vol. 6, no. 3-4, pp. 169–175, 1995.

[70] J. Gorczyca-Cole, J. A. Sherwood, and J. Chen, "A friction model for thermostamping commingled glass-polypropylene woven fabrics," *Composites Part A: Applied Science and Manufacturing*, no. 38, pp. 393–406, 2006.

[71] S. R. Morris and C. T. Sun, "An investigation of interply slip behaviour in AS4/PEEK at forming temperatures," *Composites Manufacturing*, vol. 5, no. 4, pp. 217–224, 1994.

[72]   G. Lebrun, M. N. Bureau, and J. Denault, "Thermoforming-Stamping of
         Continuous Glass Fiber/Polypropylene Composites: Interlaminar and Tool–
         Laminate Shear Properties," *Journal of Thermoplastic Composite Materials*,
         vol. 17, no. 2, pp. 137–165, 2016.

[73]   *DIN EN 14882 - Determination of the static and dynamic coefficient of
         friction*, 2005.

[74]   U. Sachs *et al.,* "A Friction-Test Benchmark with Twintex PP," *KEM*, vol.
         504-506, pp. 307–312, 2012.

[75]   U. Sachs, "Friction and bending in thermoplastic composites forming
         processes," Ph.D. thesis, Universiteit Twente, 2014.

[76]   E. de Bilbao, D. Soulat, G. Hivet, and A. Gasser, "Experimental Study of
         Bending Behaviour of Reinforcements," *Exp Mech*, vol. 50, no. 3, pp. 333–
         351, 2010.

[77]   B. Liang, N. Hamila, M. Peillon, and P. Boisse, "Analysis of thermoplastic
         prepreg bending stiffness during manufacturing and of its influence on
         wrinkling simulations," *Composites Part A: Applied Science and
         Manufacturing*, vol. 67, pp. 111–122, 2014.

[78]   D. Soteropoulos, K. Fetfatsidis, J. A. Sherwood, and J. Langworthy, "Digital
         Method of Analyzing the Bending Stiffness of Non-Crimp Fabrics," in
         *ESAFORM 2011: Proceedings of the 14th International ESAFORM
         Conference on Material Forming*, Belfast, (United Kingdom), 2011, pp. 913–
         917.

[79]   L. M. Dangora, C. Mitchell, K. D. White, J. A. Sherwood, and J. C. Parker,
         "Characterization of temperature-dependent tensile and flexural rigidities of a
         cross-ply thermoplastic lamina with implementation into a forming model,"
         Int J Mater Form, vol. 11, no. 1, pp. 43–52, 2018.

[80]   T. A. Martin, S. J. Mander, and Dykes, R.J., Bhattacharyya, D., "Chapter 9
         Bending of continuous fibre-reinforced thermoplastic sheets," in *Composite
         Sheet Forming*, D. Bhattacharyya, Ed., 1997, pp. 371–401.

[81]   C. H. ten Hove, "Bending of CF/PEEK prepregs," University of Twente,
         Enschede, 2012.

[82]   S. Ropers, M. Kardos, and T. A. Osswald, "A thermo-viscoelastic approach
         for the characterization and modeling of the bending behavior of thermoplastic
         composites," *Composites Part A: Applied Science and Manufacturing*, vol. 90,
         pp. 22–32, 2016.

[83]   A. Margossian, S. Bel, and R. Hinterhoelzl, "Bending characterisation of a
         molten unidirectional carbon fibre reinforced thermoplastic composite using a

Dynamic Mechanical Analysis system," *Composites Part A: Applied Science and Manufacturing*, vol. 77, pp. 154–163, 2015.

[84]   F. T. Peirce, "26—THE "HANDLE" OF CLOTH AS A MEASURABLE QUANTITY," *Journal of the Textile Institute Transactions*, vol. 21, no. 9, T377-T416, 1930.

[85]   S.V. Lomov, I. Verpoest, M. Barburski, and J. Laperre, "Carbon composites based on multiaxial multiply stitched preforms. Part 2. KES-F characterisation of the deformability of the preforms at low loads," *Composites Part A: Applied Science and Manufacturing*, vol. 34, no. 4, pp. 359–370, 2003.

[86]   J. Wang, A. C. Long, and M. J. Clifford, "Experimental measurement and predictive modelling of bending behaviour for viscous unidirectional composite materials," *Int J Mater Form*, vol. 3, no. S2, pp. 1253–1266, 2010.

[87]   H. Alshahrani and M. Hojjati, "A new test method for the characterization of the bending behavior of textile prepregs," *Composites Part A: Applied Science and Manufacturing*, vol. 97, pp. 128–140, 2017.

[88]   H. Alshahrani and M. Hojjati, "Bending behavior of multilayered textile composite prepregs: Experiment and finite element modeling," *Materials & Design*, vol. 124, pp. 211–224, 2017.

[89]   P. Boisse, "Simulations of Composite Reinforcement Forming," in *Woven fabric engineering*, P. D. Dubrovski, Ed., Rijeka, Croatia: Sciyo, 2010, pp. 387–414.

[90]   G. B. McGuinness and C. M. ÓBrádaigh, "Characterisation of thermoplastic composite melts in rhombus-shear: The picture-frame experiment," *Composites Part A: Applied Science and Manufacturing*, vol. 29, no. 1-2, pp. 115–132, 1998.

[91]   P. Harrison, M. J. Clifford, and A. C. Long, "Shear characterisation of viscous woven textile composites: A comparison between picture frame and bias extension experiments," *Composites Science and Technology*, vol. 64, no. 10-11, pp. 1453–1465, 2004.

[92]   K. Potter, "Bias extension measurements on cross-plied unidirectional prepreg," *Composites Part A: Applied Science and Manufacturing*, vol. 33, no. 1, pp. 63–73, 2002.

[93]   Y. R. Larberg, M. Åkermo, and M. Norrby, "On the in-plane deformability of cross-plied unidirectional prepreg," *Journal of Composite Materials*, vol. 46, no. 8, pp. 929–939, 2012.

[94]   C. Mack and H. M. Taylor, "39—The Fitting of Woven Cloth to Surfaces," *Journal of the Textile Institute Transactions*, vol. 47, no. 9, T477-T488, 1956.

[95]   R. Akkerman, S. P. Haanappel, and U. Sachs, "History and future of composites forming analysis," *IOP Conf. Ser.: Mater. Sci. Eng.*, vol. 406, p. 12003, 2018.

[96]   J. W. Klintworth and A. C. Long, "The use of draping simulation in composite design," in *Composites forming technologies*, A. C. Long, Ed., Cambridge, Boca Raton: Woodhead; CRC, 2007, pp. 277–292.

[97]   N. Hamila, P. Boisse, F. Sabourin, and M. Brunet, "A semi-discrete shell finite element for textile composite reinforcement forming simulation," *Int. J. Numer. Meth. Engng*, vol. 79, no. 12, pp. 1443–1466, 2009.

[98]   R.H.W. ten Thije, R. Akkerman, and J. Huétink, "Large deformation simulation of anisotropic material using an updated Lagrangian finite element method," *Computer Methods in Applied Mechanics and Engineering*, vol. 196, no. 33-34, pp. 3141–3150, 2007.

[99]   M. Nishi and T. Hirashima, "Approach for Dry Textile Composite Forming Simulation," in *Proc. 19th International Conference on Composite Materials 2013: ICCM 2013*, Montreal, Canada, 2013.

[100]   D. Durville, "Simulation of the mechanical behaviour of woven fabrics at the scale of fibers," *Int J Mater Form*, vol. 3, no. S2, pp. 1241–1251, 2010.

[101]   P. Boisse, "Finite element analysis of composite forming," in *Composites forming technologies*, A. C. Long, Ed., Cambridge, Boca Raton: Woodhead; CRC, 2007, pp. 46–79.

[102]   Y. Aimène, E. Vidal-Sallé, B. Hagège, F. Sidoroff, and P. Boisse, "A Hyperelastic Approach for Composite Reinforcement Large Deformation Analysis," *Journal of Composite Materials*, vol. 44, no. 1, pp. 5–26, 2009.

[103]   P. Badel, S. Gauthier, E. Vidal-Sallé, and P. Boisse, "Rate constitutive equations for computational analyses of textile composite reinforcement mechanical behaviour during forming," *Composites Part A: Applied Science and Manufacturing*, vol. 40, no. 8, pp. 997–1007, 2009.

[104]   P. Harrison, R. Gomes, and N. Correia, "Press Forming a 0/90 Cross-Ply Advanced Thermoplastic Composite Using The Double-Dome Benchmark Geometry," *Composites Part A: Applied Science and Manufacturing*, pp. 56–69, 2013.

[105]   L. Liu, J. Chen, X. Li, and J. A. Sherwood, "Two-dimensional macro-mechanics shear models of woven fabrics," *Composites Part A: Applied Science and Manufacturing*, vol. 36, no. 1, pp. 105–114, 2005.

[106]   X. Q. Peng and J. Cao, "A continuum mechanics-based non-orthogonal constitutive model for woven composite fabrics," *Composites Part A: Applied Science and Manufacturing*, vol. 36, no. 6, pp. 859–874, 2005.

[107]   D. Doerr, F. Henning, and L. Kärger, "Nonlinear hyperviscoelastic modelling of intra-ply deformation behaviour in finite element forming simulation of continuously fibre-reinforced thermoplastics," *Composites Part A: Applied Science and Manufacturing*, vol. 109, pp. 585–596, 2018.

[108]   L. Dong, C. Lekakou, and M. G. Bader, "Processing of Composites: Simulations of the Draping of Fabrics with Updated Material Behaviour Law," *Journal of Composite Materials*, vol. 35, no. 2, pp. 138–163, 2016.

[109]   R.H.W. ten Thije and R. Akkerman, "A multi-layer triangular membrane finite element for the forming simulation of laminated composites," *Composites Part A: Applied Science and Manufacturing*, vol. 40, no. 6-7, pp. 739–753, 2009.

[110]   S. Haanappel, R. H. W. ten Thije, and R. Akkerman, "Forming Predictions of UD Reinforced Thermoplastic Laminates," in *Proc. 14th European Conference on Composite Materials ECCM14*, Budapest, 2010.

[111]   H. Alshahrani and M. Hojjati, "Experimental and numerical investigations on formability of out-of-autoclave thermoset prepreg using a double diaphragm process," *Composites Part A: Applied Science and Manufacturing*, vol. 101, pp. 199–214, 2017.

[112]   K. Kouwonou, X.-T. Pham, and G. Lebrun, "Modeling and Characterization of Thermoplastic Composites PEEK/Carbon," in *Proc. 19th International Conference on Composite Materials 2013: ICCM 2013*, Montreal, Canada, 2013, pp. 1188–1195.

[113]   Y. R. Larberg and M. Åkermo, "In-plane deformation of multi-layered unidirectional thermoset prepreg – Modelling and experimental verification," *Composites Part A: Applied Science and Manufacturing*, vol. 56, pp. 203–212, 2014.

[114]   J. Sjölander, P. Hallander, and M. Åkermo, "Forming induced wrinkling of composite laminates: A numerical study on wrinkling mechanisms," *Composites Part A: Applied Science and Manufacturing*, vol. 81, pp. 41–51, 2016.

[115]   A. Margossian *et al.,* "Finite element forming simulation of locally stitched non-crimp fabrics," *Composites Part A: Applied Science and Manufacturing*, vol. 61, pp. 152–162, 2014.

[116]   D. Jauffrès, J. A. Sherwood, C. D. Morris, and J. Chen, "Discrete mesoscopic modeling for the simulation of woven-fabric reinforcement forming," *Int J Mater Form*, vol. 3, no. S2, pp. 1205–1216, 2010.

[117]   P. Badel, E. Vidal-Sallé, E. Maire, and P. Boisse, "Simulation and tomography analysis of textile composite reinforcement deformation at the mesoscopic scale," *Int J Mater Form*, vol. 2, no. S1, pp. 189–192, 2009.

[118]   A. Hosseini, M. H. Kashani, F. Sassani, A. S. Milani, and F. Ko, "A Mesoscopic Analytical Model to Predict the Onset of Wrinkling in Plain Woven Preforms under Bias Extension Shear Deformation," (eng), *Materials (Basel, Switzerland)*, vol. 10, no. 10, 2017.

[119]   A. Cherouat and J. L. Billoët, "Mechanical and numerical modelling of composite manufacturing processes deep-drawing and laying-up of thin pre-impregnated woven fabrics," *Journal of Materials Processing Technology*, vol. 118, no. 1-3, pp. 460–471, 2001.

[120]   G. Zhou, X. Sun, and Y. Wang, "Multi-chain digital element analysis in textile mechanics," *Composites Science and Technology*, vol. 64, no. 2, pp. 239–244, 2004.

[121]   N. Moustaghfir, S. El-Ghezal Jeguirim, D. Durville, S. Fontaine, and C. Wagner-Kocher, "Transverse compression behavior of textile rovings: Finite element simulation and experimental study," *J Mater Sci*, vol. 48, no. 1, pp. 462–472, 2013.

[122]   S. D. Green, A. C. Long, B.S.F. El Said, and S. R. Hallett, "Numerical modelling of 3D woven preform deformations," *Composite Structures*, vol. 108, pp. 747–756, 2014.

[123]   D. Colin, S. Bel, T. Hans, and M. Hartmann, "Towards a Virtual Characterization of a Biaxial Non-Crimp Fabric," in *Proc. 18th European Conference on Composite Materials ECCM18*, Athens, Greece, 2018.

[124]   *AniForm Virtual Forming*. [Online] Available: https://aniform.com/.

[125]   AniForm Engineering B.V., "AniForm Suite manual," 2014.

[126]   D. Doerr *et al.,* "A Method for Validation of Finite Element Forming Simulation On Basis of a Pointwise Comparison of Distance and Curvature," in *ESAFORM 2016: Proceedings of the 19th International ESAFORM Conference on Material Forming*, Nantes, France, 2016.

[127]   C. Eitzinger, "Integrated robotic system for 3D part scanning: Automated Mapping of Fibre Orientation for Draping of Carbon Fibre Parts," Deliverable D3.4 of FibreMap 608768, Jun. 2016.

[128]   A. Dereims *et al.,* "Inverse Characterization Method for Draping Simulation Based on Automatic Measurement of Fiber Orientation," in *Proc. 17th European Conference on Composite Materials ECCM17*, Munich, Germany, 2016.

[129]   G. Bardl *et al.,* "Automated detection of yarn orientation in 3D-draped carbon fiber fabrics and preforms from eddy current data," *Composites Part B: Engineering*, vol. 96, pp. 312–324, 2016.

[130]   H. Heuer *et al.,* "Review on quality assurance along the CFRP value chain – Non-destructive testing of fabrics, preforms and CFRP by HF radio wave techniques," *Composites Part B: Engineering*, vol. 77, pp. 494–501, 2015.

[131]   A. Mallach *et al.,* "Experimental comparison of a macroscopic draping simulation for dry non-crimp fabric preforming on a complex geometry by means of optical measurement," *Journal of Composite Materials*, 2016.

[132]   C. Bonten, Ed., *Kunststofftechnik: Einführung und Grundlagen*. München: Carl Hanser Verlag GmbH & Co. KG, 2014.

[133]   P. Hubert and A. Poursartip, "Aspects of the Compaction of Composite Angle Laminates: An Experimental Investigation," *Journal of Composite Materials*, vol. 35, no. 1, pp. 2–26, 2001.

[134]   R. McCool *et al.,* "Thermoforming carbon fibre-reinforced thermoplastic composites," *Proceedings of the Institution of Mechanical Engineers, Part L: Journal of Materials: Design and Applications*, vol. 226, no. 2, pp. 91–102, 2012.

[135]   *ASTM D 6415 - Measuring the Curved Beam Strength of a Fiber-Reinforced Polymer-Matrix Composite*, 2006.

[136]   T. Jamin, M. Dube, and L. Laberge Lebel, "Effect of stamp-forming parameters and bend radius on the mechanical performance of curved beam carbon fiber/polyphenylene sulfide specimens," *Journal of Composite Materials*, vol. 50, no. 9, pp. 1213–1225, 2016.

[137]   S. C. Avalon and S. L. Donaldson, "Strength of composite angle brackets with multiple geometries and nanofiber-enhanced resins," *Journal of Composite Materials*, vol. 45, no. 9, pp. 1017–1030, 2010.

[138]   K. Vanclooster, "Forming of Multilayered Fabric Reinforced Thermoplastic Composites," Ph.D. thesis, Katholieke Universiteit Leuven, Leuven, 2009.

[139]   S. Isogawa, H. Aoki, and M. Tejima, "Isothermal Forming of CFRTP Sheet by Penetration of Hemispherical Punch," *Procedia Engineering*, vol. 81, pp. 1620–1626, 2014.

[140]   M. R. Monaghan, P. J. Mallon, C. M. O'Brádaigh, and R. B. Pipes, "The effect of diaphragm stiffness on the quality of diaphragm formed thermoplastic composite components," *Journal of Thermoplastic Composite Materials*, no. 3, pp. 202–215, 1990.

[141] C. M. O'Brádaigh and R. B. Pipes, "Issues in diaphragm forming of continuous fibre reinforced thermoplastic composites," *Polymer Composites*, vol. 12, no. 4, pp. 246–256, 1991.

[142] A. Hohmann *et al., Recommendations for resource efficient and environmentally responsible manufacturing of CFRP products: Results of the Research Study MAI Enviro 2.0*. Augsburg: Carbon Composites e.V., 2018.

[143] O. de Almeida, E. Bessard, and G. Bernhart, "Influence of Processing Parameters and Semi-Finished Product on Consolidation of Carbon/PEEK Laminates," in *Proc. 15th European Conference on Composite Materials ECCM15*, Venice, Italy, 2012.

[144] V. Radlmaier, C. Heckel, M. Winnacker, A. Erber, and H. Koerber, "Effects of thermal cycling on polyamides during processing," *Thermochimica Acta*, vol. 648, pp. 44–51, 2017.

[145] Ostgathe, M., U. Breuer, Mayer C., and M. Neitzel, "Fabric Reinforced Thermopalstic Composites: Manufacturing and Processing," in *Proc. 7th European Conference on Composite Materials ECCM7*, London, United Kingdom, 1996, pp. 195–200.

[146] M. D. Wakeman, T. A. Cain, C. D. Rudd, R. Brooks, and A. C. Long, "Compression moulding of glass and polypropylene composites for optimised macro- and micro- mechanical properties—1 commingled glass and polypropylene," *Composites Science and Technology*, vol. 58, no. 12, pp. 1879–1898, 1998.

[147] D. Trudel-Boucher, B. Fisa, J. Denault, and P. Gagnon, "Thermoforming Complex Parts from Unconsolidated and Consolidated Polypropylene/Glass Fibre Fabrics," *Polymers & Polymer Composites*, vol. 13, no. 6, pp. 543–558, 2005.

[148] D. Trudel-Boucher, B. Fisa, J. Denault, and P. Gagnon, "Experimental investigation of stamp forming of unconsolidated commingled E-glass/polypropylene fabrics," *Composites Science and Technology*, vol. 66, no. 3-4, pp. 555–570, 2006.

[149] A. C. Long, C. E. Wilks, and C. D. Rudd, "Experimental characterisation of the consolidation of a commingled glass/polypropylene composite," *Composites Science and Technology*, vol. 61, no. 11, pp. 1591–1603, 2001.

[150] N. Svensson and R. Shishoo, "Manufactoring of Thermoplastic Composites from Commingled Yarns - A Review," *Journal of Thermoplastic Composite Materials*, vol. 11, pp. 22–56, 1998.

[151] T. K. Slange, L. Warnet, W. J. B. Grouve, and R. Akkerman, "Influence of Preconsolidation on Consolidation Quality after Stamp Forming of C/PEEK

Composites," in *ESAFORM 2016: Proceedings of the 19th International ESAFORM Conference on Material Forming*, Nantes, France, 2016.

[152] *DIN EN 2564 - Determination of the fibre-, resin- and void contents*, 1998.

[153] O. Breitenstein, W. Warta, and M. Langenkamp, *Lock-in thermography: Basics and applications to functional diagnostics of electronic components*. Berlin, London: Springer, 2011.

[154] M. Perterer, "Schadenidentifikation und -bewertung von CFK-Bauteilen mittels phasenmodulierter Thermographie," Ph.D. thesis, Technische Universität München, München, 2012.

[155] Edevis GmbH, *Testing of CFRP Components.* [Online] Available: https://www.edevis.com/download/AppNote_OTvis_CFRP_EN.pdf. Accessed on: Mar. 15 2018.

[156] F. Yüksel, R. Hinterhoelzl, and K. Drechsler, "Experimental Investigation of Direct Adhesion of CFR-Thermoplast on Steel," in *Proc. Euro Hybrid Materials and Structures 2016*, Kaiserslautern, 2016.

[157] Sturm Präzision GmbH, *Keramik-Rillenkugellager 6001-KER-ZRO2-F.* [Online] Available: https://www.sturm-kugellager-shop.de/keramik-rillenkugellager/keramiklager-zro2/60.-ker-zro2-f/1783/keramik-rillenkugellager-6001-ker-zro2-f?c=146. Accessed on: Jan. 03 2018.

[158] U. Sachs, R. Akkerman, S. Haanappel, R. H. W. ten Thije, and M. B. de Rooij, "Friction in Forming of UD Composites," in *ESAFORM 2011: Proceedings of the 14th International ESAFORM Conference on Material Forming*, Belfast, (United Kingdom), 2011, pp. 984–989.

[159] *DIN EN ISO 14125 - Fibre-reinforced plastic composites – Determination of flexural properties*, 2011.

[160] TA Instruments, *Rheology solutions: Determining the linear viscoelastic region in polymers.* [Online] Available: http://www.tainstruments.com/pdf/literature/RS23.pdf. Accessed on: Jan. 05 2018.

[161] U. Sachs and R. Akkerman, "Viscoelastic bending model for continuous fiber-reinforced thermoplastic composites in melt," *Composites Part A: Applied Science and Manufacturing*, 2017.

[162] W. Palfinger, S. Thumfart, and C. Eitzinger, "Photometric stereo on carbon fiber surfaces," in *35th Workshop of the Austrian Association for Pattern Recognition*, 2011.

[163] S. Zambal, W. Palfinger, M. Stöger, and C. Eitzinger, "Accurate fibre orientation measurement for carbon fibre surfaces," *Pattern Recognition*, vol. 48, no. 11, pp. 3324–3332, 2015.

[164] U. Sachs, S. Haanappel, B. Rietman, and R. Akkerman, "Friction Testing of Thermoplastic Composites," *SEICO 11 – Paris: SAMPE Europe's 32nd International Technical Conference and Forum*, Mar. 2011.

[165] U. Sachs, R. Akkerman, and S. P. Haanappel, "Bending Characterization of UD Composites," *KEM*, vol. 611-612, pp. 399–406, 2014.

A Appendix

a Simulation input parameters

Tab. A-1.   **Fitted input parameters for PO0/0 friction configuration for GF/PP (selected: grey)**

	Polymer friction + Coulomb fiction	Viscous friction + Coulomb friction
C	88.081	-
Eta0	5.7673	-
Film Thickness	0.0366	0.6585
N	1.2096	-
Ap	92.0001	-
Bp	4.3195	-
P0	0.021	-
μ	2.5963	2.8881
η	-	0.00074611

Tab. A-2.   **Fitted input parameters for PT0/90 friction configuration for GF/PP (selected: grey)**

	Viscous friction + Coulomb friction V1	Viscous friction + Coulomb friction V2
Film Thickness	0.5921	1.5896
η	0.00021203	0.00103017
μ	1.0026	0.887236

Tab. A-3.   **Fitted bending input parameters for GF/PP (selected: grey)**

	Isotropic elastic + Cross Viscosity Fluid V1	Isotropic elastic + Cross Viscosity Fluid V2	Isotropic elastic + Cross Viscosity Fluid V3
Young	41.90048	58.3165	30.5805
η0	630.1208	33.5515	31384.5564
ηInf	6928.664	65298.145	322.5409
M	5.53792E-06	1.4512E-05	137504.98
N	23.44648	2.0469	-0.23103

Tab. A-4.   **Fitted in-plane input parameters for GF/PP (selected: grey)**

	Isotropic elastic + Newtonian Fluid	Isotropic elastic + Cross Viscosity Fluid
Young	2.43935	2.16127
$\eta 0$	-	0.00739367
ηInf	-	0.000001
M	-	1402790
N	-	-1.64464
η	0.00496485	-

b Friction simulation diagram
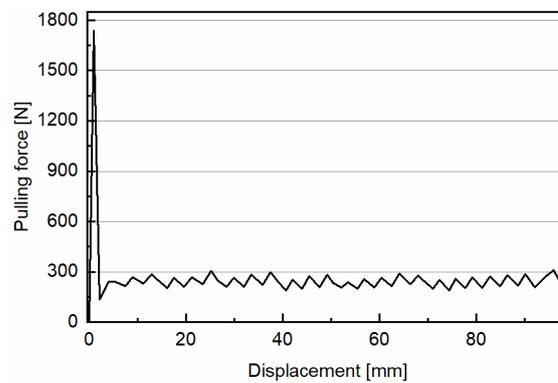
Fig. A-1.   **Force displacement diagram of PT0/90 simulation**
1200 mm/min, 0.76 kg normal weight, Polymer & Coulomb friction model causing high force peak at the beginning.

B Publications

Scientific journal papers

[P1]   A. Schug, D. Rinker, R. Hinterhoelzl, K. Drechsler, "Evaluating the potential of forming spot-welded layups out of fibre reinforced thermoplastic tape without previous consolidation", *International Journal of Material Forming*, 2018. https://doi.org/10.1007/s12289-018-1416-5.

Conferences

[K1]   A. Schug, R. Hinterhoelzl, and K. Drechsler, "Experimental Investigation of the Radius Forming Behavior of Fiber Reinforced Thermoplastics", in *17th European Conference on Composite Materials ECCM17*, Munich, Germany, 2016.

[K2]   A. Schug, J. Winkelbauer, R. Hinterhoelzl, and K. Drechsler, "Thermoforming of Glass Fibre Reinforced Polypropylene: A Study on the Influence of Different Process Parameters", in *The 20th International ESAFORM Conference on Material Forming: ESAFORM2017*, Dublin, Ireland, 2017.

[K3]   A. Schug, M. Popp, A. Margossian, R. Hinterhoelzl, K. Drechsler, "Forming behaviour and achievable part quality of thermosetting AFP-towpreg-laminates", in *SAMPE*, Stuttgart, Germany, 2017.

[K4]   A. Schug, G. Kapphan, G. Bardl, R. Hinterhoelzl, K. Drechsler, "Comparison of Validation Methods for Forming Simulations", in *The 21st International ESAFORM Conference on Material Forming: ESAFORM2018*, Palermo, Italy, 2018.

C List of supervised students

In the following all student works are listed, which had been advised by the author.

[S1]   M. Hofner, „Entwicklung und Konstruktion eines Reibungsprüfstandes für faserverstärkte Thermoplaste", Masterarbeit, HS Augsburg, 2015.

[S2]   H. Ahmad, „Konstruktion und Auslegung eines Infrarotheizfelds für das Themoformen von faserverstärkten Thermoplasten", Bachelorarbeit, TH Nürnberg, 2015.

[S3]   J. Winkelbauer, „Untersuchung des Einflusses verschiedener Prozessparameter auf das Umformergebnis von Faserverstärkten Thermoplasten", Bachelorarbeit, HS Augsburg, 2016.

[S4]   M. Popp, „Experimentelle Untersuchung des Umformverhaltens und der erzielbaren Bauteilqualität von duroplastischem AFP-Towpreg-Gelege", Masterarbeit, Lehrstuhl für Carbon Composites, TU München, 2016.

[S5]   S. Lizak, „Interlaminare Reibung von faserverstärkten Thermoplast-Tapes Optimierung eines Reibungsprüfstandes", Laboratory project, Universität Augsburg, 2016.

[S6]   D. Rinker, „Entwicklung eines Verfahrens zum Umformen unkonsolidierter thermoplastischer Gelege", Masterarbeit, Universität Augsburg, 2017.

[S7]   G. Kapphan, „Bewertung von Verfahren zur Faserwinkelbestimmung in faserverstärkten Kunststoffen", Bachelorarbeit, Universität Augsburg, 2017.

Parts of above listed theses contributed to the underlying doctoral dissertation, as indicated within the text.